LAPPEENRANTA
UNIVERSITY OF TECHNOLOGY

Antti Häkkinen

THE INFLUENCE OF CRYSTALLIZATION CONDITIONS ON THE FILTRATION CHARACTERISTICS OF SULPHATHIAZOLE SUSPENSIONS

Thesis for the degree of Doctor of Science (Technology) to be presented with due permission for public examination and criticism in the Auditorium 1383 at Lappeenranta University of Technology, Lappeenranta, Finland on the 22nd of December, 2009, at noon.

Acta Universitatis
Lappeenrantaensis
380

Supervisors Professor Emeritus Lars Nyström
Department of Chemical Technology
Lappeenranta University of Technology
Finland

Professor Marjatta Louhi-Kultanen
Department of Chemical Technology
Lappeenranta University of Technology
Finland

Reviewers Professor Emeritus Kohei Ogawa
Department of Chemical Engineering
Tokyo Institute of Technology
Japan

Ph.D. Matthew Jones
AstraZeneca Process R&D
Södertälje
Sweden

Opponent Professor Ville Alopaeus
Department of Chemical Technology
Helsinki University of Technology
Finland

Custos Professor Emeritus Lars Nyström
Department of Chemical Technology
Lappeenranta University of Technology
Finland

ISBN 978-952-214-896-4

ISBN 978-952-214-897-1 (PDF)

ISSN 1456-4491

Lappeenrannan teknillinen yliopisto

Digipaino 2009

ABSTRACT

Antti Häkkinen

The influence of crystallization conditions on the filtration characteristics of sulphathiazole suspensions

Lappeenranta 2009
156 p.

Acta Universitatis Lappeenrantaensis 380
Diss. Lappeenranta University of Technology

ISBN 978-952-214-896-4, ISBN 978-952-214-897-1 (PDF), ISSN 1456-4491

Cooling crystallization is one of the most important purification and separation techniques in the chemical and pharmaceutical industry. The product of the cooling crystallization process is always a suspension that contains both the mother liquor and the product crystals, and therefore the first process step following crystallization is usually solid-liquid separation. The properties of the produced crystals, such as their size and shape, can be affected by modifying the conditions during the crystallization process. The filtration characteristics of solid/liquid suspensions, on the other hand, are strongly influenced by the particle properties, as well as the properties of the liquid phase. It is thus obvious that the effect of the changes made to the crystallization parameters can also be seen in the course of the filtration process. Although the relationship between crystallization and filtration is widely recognized, the number of publications where these unit operations have been considered in the same context seems to be surprisingly small.

This thesis explores the influence of different crystallization parameters in an unseeded batch cooling crystallization process on the external appearance of the product crystals and on the pressure filtration characteristics of the obtained product suspensions. Crystallization experiments are performed by crystallizing sulphathiazole ($C_9H_9N_3O_2S_2$), which is a well-known antibiotic agent, from different mixtures of water and *n*-propanol in an unseeded batch crystallizer. The different crystallization parameters that are studied are the composition of the solvent, the cooling rate during the crystallization experiments carried out by using a constant cooling rate throughout the whole batch, the cooling profile, as well as the mixing intensity during the batch. The obtained crystals are characterized by using an automated image analyzer and the crystals are separated from the solvent through constant pressure batch filtration experiments. Separation characteristics of the suspensions are described by means of average specific cake resistance and average filter cake porosity, and the compressibilities of the cakes are also determined.

The results show that fairly large differences can be observed between the size and shape of the crystals, and it is also shown experimentally that the changes in the crystal size and shape have a direct impact on the pressure filtration characteristics of the crystal suspensions. The experimental results are utilized to create a procedure that can be used for estimating the filtration characteristics of solid-liquid suspensions according to the particle size and shape data obtained by image analysis. Multilinear partial least squares regression (*N-PLS*) models are created between the filtration parameters and the particle size and shape data, and the results presented in this thesis show that relatively obvious correlations can be detected with the obtained models.

Keywords: Crystallization, crystal characterization, filtration, mixing, image analysis, multilinear partial least squares regression

UDC 66.065.5 : 66.067.11 : 519.237 : 544.778.3

ACKNOWLEDGEMENTS

This study has been carried out at Lappeenranta University of Technology in the Laboratory of Separation Technology.

I wish to thank my supervisors Professor Emeritus Lars Nyström and Professor Marjatta Louhi-Kultanen for their guidance, advices and patience during this study. I am also thankful for the reviewers of this manuscript, Professor Emeritus Kohei Ogawa and Ph.D Matthew Jones, for their valuable and helpful comments which significantly helped me to improve the thesis. Mrs. Sinikka Talonpoika is thanked for revising the language of this thesis.

I am deeply indebted to all of my co-workers at the LUT Laboratory of Separation Technology. Dr. Kati Pöllänen and M.Sc. Mikko Huhtanen deserve special appreciation for their friendship and encouragement and for all of those fruitful conversations that we have had during these years. Additionally, I wish to thank Emeritus Professor Juha Kallas for his support in all issues, and Markku Maijanen and Päivi Hovila for their valuable help. Dr. Satu-Pia Reinikainen and Dr. Tuomas Koiranen are acknowledged for the expertise and advices that they have provided me during this study. I am also grateful to my industrial partners, especially at Larox, for their trust and support.

The financial support from the Research Foundation of Lappeenranta University of Technology, South Carelian Cultural Foundation, Kemira Foundation, Danisco Foundation, Gust. Komppa Foundation and The Finnish Foundation for Economic and Technology Sciences is gratefully acknowledged.

My warmest gratitude goes to my family, Sari, Aleksi and Ville, for all of their understanding, patience and encouragement during these years. I would also like to thank my mother, brother and Sari's parents for the endless support and help that I have received from them.

Lappeenranta, December 2009

Antti Häkkinen

LIST OF PUBLICATIONS

Some of the results presented in this thesis have been previously published in the following papers:

I *Häkkinen, A.*, Pöllänen, K., Louhi-Kultanen, M., Nyström, L.,* Pressure filtration of sulphathiazole crystallized by batch cooling crystallization: the influence of solvent composition, *Chemical Engineering Transactions,* 2003, 3(2): 931-936; Proceedings of the *6th Italian Conference on Chemical and Process Engineering,* Pisa, Italy, June 8 – 11, 2003.

II *Häkkinen, A.*, Pöllänen, K., Louhi-Kultanen, M., Nyström, L.,* Pressure filtration of crystallized sulphathiazole: the influence of cooling rate used in batch cooling crystallization, *Advances in Filtration and Separation Technology,* 2003, 16: 354-374; Proceedings of the *16th Annual AFS Conference and Expo*, Reno, USA, June 17 - 20, 2003.

III *Häkkinen, A.*, Pöllänen, K., Koiranen, T., Louhi-Kultanen, M., Nyström, L.,* Pressure filtration of sulphathiazole crystallized by batch cooling crystallization: the influence of mixing conditions, Proceedings of *Filtech Europa 2003*, Düsseldorf, Germany, October 21 - 23, 2003: L120-L127.

IV *Häkkinen, A.*, Pöllänen, K., Louhi-Kultanen, M., Nyström, L.,* Pressure filtration of crystallized sulphathiazole: the influence of cooling policy used in batch cooling crystallization, Proceedings of the *9th World Filtration Congress*, New Orleans, USA, April 18 - 22, 2004: 309-327.

V *Häkkinen, A.*, Pöllänen, K., Karjalainen, M., Rantanen, J., Louhi-Kultanen, M., Nyström, L.,* Batch cooling crystallization and pressure filtration of sulphathiazole: the influence of solvent composition, *Biotechnology and Applied Biochemistry,* 2005, 41(1): 17-28.

VI *Häkkinen, A.*, Pöllänen, K., Reinikainen, S-P., Louhi-Kultanen, M., Nyström, L.*, A method for predicting filtration characteristics from particle size and shape data, Proceedings of *Filtech Europa 2005*, Wiesbaden, Germany, October 11 - 13, 2005: L521-L527.

VII *Pöllänen, K., Häkkinen, A.*, Reinikainen, S-P., Louhi-Kultanen, M., Nyström, L.,* A study on batch cooling crystallization of sulphathiazole: process monitoring using ATR-FTIR and product characterization by automated image analysis, *Chemical Engineering Research and Design,* 2006, 84(A1): 47-59.

VIII *Häkkinen, A.*, Pöllänen, K., Reinikainen, S-P., Louhi-Kultanen, M., Nyström, L.*, Prediction of filtration characteristics by means of multivariate data analysis, Proceedings of the *20th Annual AFS Conference*, Orlando, USA, March 26 - 30, 2007.

IX *Häkkinen, A.*, Pöllänen, K., Reinikainen, S-P., Louhi-Kultanen, M., Nyström, L.*, Prediction of filtration characteristics by multivariate data analysis, *Filtration*, 2008, 8(2): 144 – 153.

Contribution of the author

The author was responsible for the preparation of papers I – IV and VIII – IX. In paper VII, the parts concerning crystallization and crystal characterization were under the responsibility of the author. All experiments, as well as the crystal size and shape analyses in all papers have been performed by the author.

LIST OF RELATED PUBLICATIONS

1. *Pöllänen, K.*, Häkkinen, A., Reinikainen, S-P., Louhi-Kultanen, M., Nyström, L.,* ATR-FTIR in monitoring of crystallization processes: comparison of indirect and direct OSC methods, *Chemometrics and Intelligent Laboratory Systems*, 2005, 76(1): 25-35.

2. *Pöllänen, K.*, Häkkinen, A., Reinikainen, S-P., Rantanen, J., Karjalainen, M., Louhi-Kultanen, M., Nyström, L.,* IR spectroscopy together with multivariate data analysis as a process analytical tool for in-line monitoring of crystallization process and solid state analysis of crystalline product, *Journal of Pharmaceutical and Biomedical Analysis*, 2005, 38(2): 275-284.

3. *Pöllänen, K.*, Häkkinen, A., Huhtanen, M., Reinikainen, S-P., Karjalainen, M., Rantanen, J., Louhi-Kultanen, M., Nyström, L.,* DRIFT-IR for quantitative characterization of polymorphic composition of sulphathiazole, *Analytica Chimica Acta*, 2005, 544(1-2): 108-117.

4. *Pöllänen, K.*, Häkkinen, A., Reinikainen, S-P., Rantanen, J., Minkkinen, P.*, Dynamic PCA-based MSPC charts for nucleation prediction in batch cooling crystallization processes, *Chemometrics and Intelligent Laboratory Systems*, 2006, 84(1-2): 126-133.

Although these papers do not directly concern the exact topic of this thesis, and have not been written primarily by the author, they are related to the experiments introduced in this thesis. All crystallization experiments of sulphathiazole presented in these papers have been carried out by the author.

TABLE OF CONTENTS

Abstract
Acknowledgements
List of publications
Table of contents
Symbols

1 INTRODUCTION 17

2 BATCH COOLING CRYSTALLIZATION 21

2.1 CRYSTALLINE SOLIDS 24
2.1.1 Polymorphism 26
2.2 NUCLEATION 28
2.2.1 Primary nucleation 28
2.2.2 Secondary nucleation 30
2.3 CRYSTAL GROWTH 31
2.4 CRYSTAL BREAKAGE 33
2.5 AGGLOMERATION 34
2.6 SEEDING 35
2.7 CRYSTALLIZATION CONDITIONS 36
2.7.1 The role of the solvent composition in crystallization 37
2.7.2 Cooling policies in batch cooling crystallization 38
2.7.2.1 Natural cooling 39
2.7.2.2 Linear cooling 40
2.7.2.3 Programmed cooling 42
2.8 TAILOR-MADE ADDITIVES AND IMPURITIES 45

3 MIXING IN BATCH CRYSTALLIZERS 47

4 CHARACTERIZATION OF CRYSTALS 50

4.1 CRYSTAL SIZE 51
4.2 CRYSTAL SHAPE 51
4.3 TECHNIQUES FOR PARTICLE SIZING AND CHARACTERIZATION 53
4.4 AUTOMATED IMAGE ANALYSIS 54

5 FILTRATION 55

5.1 FILTRATION FUNDAMENTALS 55
5.1.1 The filtration process 55
5.1.2 Pre-treatment techniques 56
5.1.3 Post-treatment processes 56
5.2 FILTRATION PARAMETERS 56
5.2.1 Cake resistance 57
5.2.2 Cake porosity 57
5.2.3 Filter cake compressibility 59

5.3 FACTORS AFFECTING THE FILTERABILITY OF SUSPENSIONS 61
5.3.1 Particle size 63
5.3.2 Particle shape 64
5.3.3 Particle size distribution 64
5.3.4 Properties of the liquid phase 64
5.4 FILTRATION OF CRYSTAL SUSPENSIONS 65

6 EXPERIMENTAL WORK 66
6.1 MATERIALS 67
6.1.1 Sulphathiazole 67
6.2 SOLUBILITY MEASUREMENTS 68
6.3 CRYSTALLIZATION EXPERIMENTS 69
6.3.1 Crystallization experiments for defining the influence of solvent composition 71
6.3.2 Crystallization experiments for defining the influence of cooling rate 71
6.3.3 Crystallization experiments for defining the influence of cooling profile 72
6.3.4 Crystallization experiments for defining the influence of mixing conditions 74
6.4 CHARACTERIZATION OF THE CRYSTAL SUSPENSIONS 75
6.4.1 Solid concentration 76
6.4.2 Solvent properties 76
6.4.3 Analysis of crystal size and shape 77
6.5 FILTRATION EXPERIMENTS 80

7 RESULTS 83
7.1 INFLUENCE OF THE SOLVENT COMPOSITION 84
7.1.1 Crystal size and shape 84
7.1.1.1 Short cooling time 84
7.1.1.2 Long cooling time 86
7.1.2 Filtration characteristics 89
7.1.2.1 Short cooling time 89
7.1.2.1 Long cooling time 91
7.2 INFLUENCE OF THE COOLING RATE 93
7.2.1 Crystal size and shape 93
7.2.1.1 3:1 water:n-propanol mixture 93
7.2.1.2 1:1 water:n-propanol mixture 95
7.2.1.3 1:3 water:n-propanol mixture 97
7.2.2 Filtration characteristics 98
7.2.2.1 3:1 water:n-propanol mixture 98
7.2.2.2 1:1 water:n-propanol mixture 100
7.2.2.3 1:3 water:n-propanol mixture 102
7.3 INFLUENCE OF THE COOLING PROFILE 105
7.3.1 Crystal size and shape 105
7.3.1.1 3:1 water:n-propanol mixture 105
7.3.1.2 1:1 water:n-propanol mixture 106
7.3.1.3 1:3 water:n-propanol mixture 108
7.3.2 Filtration characteristics 109
7.3.2.1 3:1 water:n-propanol mixture 109
7.3.2.2 1:1 water:n-propanol mixture 111
7.3.2.3 1:3 water:n-propanol mixture 113

7.4 INFLUENCE OF THE MIXING CONDITIONS 115
7.4.1 Crystal size and shape 116
7.4.1.1 Curved Blade Turbine 116
7.4.1.2 Pitched Blade Turbine 117
7.4.1.3 Bar Turbine 119
7.4.1.4 Anchor Impeller 120
7.4.2 Filtration characteristics 122
7.4.2.1 Curved Blade Turbine 122
7.4.2.2 Pitched Blade Turbine 124
7.4.2.3 Bar Turbine 126
7.4.1.4 Anchor Impeller 127

8 MULTIVARIATE MODELLING 130

8.1 MULTILINEAR PARTIAL LEAST SQUARES REGRESSION 134

8.2 MODELLING RESULTS 135

9 CONCLUSIONS 139

10 REFERENCES 142

SYMBOLS

A	area of the particle image	, m^2
A_B	heat transfer area	, m^2
A_F	filtration area	, m^2
A_p	external surface area of a particle	, m^2
B	secondary nucleation rate	, # m^{-3} s^{-1}
c	effective concentration of solids in the suspension	, kg m^{-3}
C	circularity	, -
c^*	saturation concentration	, kg m^{-3}
Δc	concentration driving force	, kg m^{-3}
c_I	interface concentration	, kg m^{-3}
c_s	concentration of solution	, kg m^{-3}
c_p	perimeter of a circle of the same area as the particle image	, m
C_p	specific heat of the solution	, J $kg^{-1}K^{-1}$
C_{per}	perimeter of the particle image	, m
d	particle diameter	, m
$d_{F\,(min)}$	minimum Feret diameter measured for all particle orientations	, m
$d_{F\,(max)}$	maximum Feret diameter measured for all particle orientations	, m
$d_{F\,(mean)}$	mean of Feret diameters measured for all particle orientations	, m
d_p	perimeter diameter of the particle	, m
D	stirrer diameter	, m
f_s	surface shape factor	, -
f_v	volume shape factor	, -
g	empirical coefficient (Eq. 6)	, -
h	thickness of the filter cake	, m
k_b	nucleation rate coefficient	, -
k_d	mass transfer coefficient	, m s^{-1}
k_g	growth rate coefficient	, $kg^{1-g}m^{3g-2}s^{-1}$
k_r	reaction rate constant	, var.
K	Kozeny constant	, -
K_1	bed permeability	, m^{-1}
L	characteristic dimension of a particle	, m
L_{50}	median crystal size	, m
m_c	mass of the dry filter cake	, kg
m_{max}	maximum crystal mass	, kg
m_s	solvent mass	, kg
M_s	mass of the solution	, kg
M_T	suspension density	, kg m^{-3}
n	cake compressibility coefficient related to cake resistance	, -

N	agitator speed	, s^{-1}
Δp	pressure difference	, Pa
r	order of integration reaction	, -
R_m	filter medium resistance	, m^{-1}
s_p	surface area of a sphere of the same volume as the particle	, m^2
S	supersaturation ratio	, -
S_0	specific surface area of particles	, $m^2\ m^{-3}$
S_m	constant in Eq. 13	, -
S_p	actual particle surface	, m^2
t	time	, s
T	the solution temperature at time t	, K
T_0	the initial solution temperature	, K
T_f	the final solution temperature	, K
U	flow rate of filtrate per unit cross-sectional area of the cake	, $m^3\ m^{-2}\ s^{-1}$
U	overall heat transfer coefficient	, $J\ K^{-1}m^{-2}s^{-1}$
V	filtrate volume	, m^3
V_p	volume of a particle	, m^3
x	fraction of solids in the vessel	, -
x_i	concentration at the beginning of the batch	, $kg\ m^{-3}$
x_f	solubility at the final temperature of the batch	, $kg\ m^{-3}$
x_p	equivalent spherical particle size	, m
α	local cake resistance	, $m\ kg^{-1}$
α_0	cake resistance at pressure of one unit	, $m\ kg^{-1}\ bar^{-n}$
α_{av}	average specific filter cake resistance	, $m\ kg^{-1}$
ε	local cake porosity	, -
ε_0	cake porosity at pressure of one unit	, $bar^{-\lambda}$
ε_{av}	average filter cake porosity	, -
λ	cake compressibility coefficient related to cake porosity	, -
v	kinematic viscosity of the solution	, m^2s^{-1}
ρ_l	liquid density	, $kg\ m^{-3}$
ρ_s	density of the solids	, $kg\ m^{-3}$
$\Delta\rho$	difference in density between the crystals and the liquid	, $kg\ m^{-3}$
σ	relative supersaturation	, -
θ_i	the initial temperature	, K
θ_0	the final temperature	, K
μ	dynamic viscosity of the filtrate	, Pa s
τ_B	batch time constant	, s
ψ	sphericity	, -

1 INTRODUCTION

Crystallization is an important separation process that purifies liquids by forming solids. Crystallization is also a particle formation process by which molecules in a solution or vapour are transformed into a solid phase of a regular lattice structure, which is reflected on the external faces. Well-established examples of crystalline materials include bulk and fine chemicals and their intermediates, such as common salt, sodium carbonate, zeolite catalysts and absorbents, ceramic and polyester precursors, detergents, fertilizers, foodstuffs, pharmaceuticals and pigments. More recent applications include crystalline materials and substances for electronic devices, healthcare products, and a wide variety of special applications. Thus, the tonnage and variety of particulate crystals worldwide is enormous, amounting to about half the output of the modern chemical industry.

In the manufacturing processes of organic fine chemicals, and especially in those of pharmaceutical substances, crystallization processes are mostly carried out in batch-wise cooling crystallizers. Since the outcome of a batch crystallization process is a suspension that contains both the mother liquor and the product crystals, the first process step following crystallization is usually solid-liquid separation. Thus, the unit operation of crystallization is normally only one part of a wider processing system. These systems should preferably be designed and optimized as a whole – problems detected in one part of the plant (poor filtration, for example) may in fact arise in another process step (inadequate crystallizer control). The requirements concerning the physical characteristics of crystalline materials are usually strictly predetermined, which is why the crystallization processes need to be accurately controlled in order to meet the desired product characteristics. Typical examples of these product properties are crystal size distribution, crystal shape, and crystal purity (Mersmann, 1996). A crucial factor, particularly in the crystallization processes of pharmaceutical compounds may also be the ability to control the crystal modification and the stability of the product crystals (Davey and Garside, 2000).

As most batch crystallizers are used for a wide variety of different substances, the possibilities of affecting the crystal properties by modifying the design features of equipment are often limited. This is why batch crystallization processes are typically controlled by modifying the mode of operation which specifies the batch time, the

cooling policy employed, the solvent used, the possible addition of seed crystals, and the type and level of agitation employed (Myerson *et al.*, 1986; Davey and Garside, 2000). If the operating conditions of a batch cooling crystallizer can be controlled accurately enough, the properties of the crystal product, such as the crystal size distribution and crystal shape, can be significantly modified by altering the crystallization parameters.

One of the main targets of the study presented in this thesis is to optimize the crystallization stage, but the separation of a crystalline product from the suspension also plays an important role. The filtration characteristics of a solid/liquid-suspension, and the properties of a filter cake, are typically governed by the primary particle properties, together with the primary properties of the liquid, and also with the concentration and the state of dispersion in the suspension (Svarovsky, 2000a). As the primary properties of the crystal product depend strongly on the operating conditions of the crystallizer, it is obvious that the changes made to the crystallization parameters can also be seen in the course of the filtration process. Besides the changes that can be observed in the actual filtration process, the variations in the structure of the obtained filter cake can also affect filtration post-treatment operations, such as cake washing and cake drying, which are exceptionally important in the pharmaceutical industry, where the requirements for the purity of the product are typically strict.

Traditionally, quality control in pharmaceutical production focuses on the analysis of the end product. Obtaining information through deeper process understanding of different pharmaceutical unit operations opens new perspectives for safer manufacture of pharmaceutics. However, getting relevant information of these multicomponent systems, such as crystallization, is not a straightforward task. The U.S. Food and Drug Administration (FDA) has introduced an initiative to address this issue. Process analytical technology (PAT) is a system for developing and implementing new efficient tools for use during pharmaceutical development, manufacturing, and quality assurance, while maintaining or improving the current level of product quality assurance (FDA, 2003). The relationships between the different unit operations in pharmaceutical processes can result in long-lasting impacts, and they should therefore be taken into account when optimizing and developing these processes.

The existing literature contains a large number of articles on different aspects of filtration and crystallization, but these two processes have seldom been discussed in

the same context. Although some work in this field has been conducted for example by Matthews and Rawlings (1998), Togkalidou *et al.* (2001), and Wibowo *et al.* (2001), the influences of crystallization conditions on the filtration processes have often been considered mainly from the theoretical point of view, and the verification of theoretical predictions by experimentally obtained data has received fairly little attention. Despite this, the results introduced in the abovementioned articles inevitably show that significant improvements in the performance of the solid-liquid separation processes can be achieved by optimizing the operation of the crystallizer.

The main objective of this study is to explore the influence of different crystallization parameters in an unseeded batch cooling crystallization process on the external appearance of the product crystals and on the pressure filtration characteristics of the obtained product suspensions. Crystallization experiments have been performed by crystallizing sulphathiazole ($C_9H_9N_3O_2S_2$), which is a well-known antibiotic agent with multiple crystal modifications, from different mixtures of water and *n*-propanol in a batch crystallizer. After the obtained crystal suspensions were characterized, the crystals were separated from the solvent through constant pressure batch filtration experiments. Separation characteristics of different crystal suspensions are described by means of average specific filter cake resistance and average filter cake porosity, obtained from the data collected during the filtration experiments. Also the compressibilities of the filter cakes were determined on the basis of the cake resistances and the cake porosities.

The experimental results obtained during this study have been utilized in creating a procedure that can be used for predicting the filtration characteristics of solid-liquid suspensions according to the particle size and shape data obtained by image analysis. Chemometrical multivariate modeling techniques have been applied to create empirical models between the filtration parameters and the crystal size and shape data. The parameters used for characterizing the filterability of the test suspensions in this study are the average filter cake resistance and porosity, as well as two different cake compressibility coefficients. The crystal size and shape data for each test suspension consists of seven different distributions describing some of the chosen crystal properties. A 3-dimensional data set has been analyzed by a modern multivariate modeling technique called multilinear partial least squares regression (*N-PLS*), and empirical models for predicting each of the four filtration parameters from the particle

properties have been created. The results presented in this thesis show that the filtration characteristics of the model suspensions can be correlated relatively well by using the obtained models.

2 BATCH COOLING CRYSTALLIZATION

Crystallization is one of the most common purification and separation techniques in the chemical industry. It can be defined as a phase-change operation, during which a group of randomly organized molecules, ions or atoms in a fluid come together to form an ordered solid structure called a crystal (Davey and Garside, 2000). The formation of crystals always takes place in unstable solutions and is induced by the natural tendency of the solutions to reach the equilibrium state. Thus the actual driving force of crystallization is the difference between the chemical potential of the solute in the liquid phase and in the solid phase (Klein and David, 1995). Due to the fact that the absolute chemical potential is not easy to measure, the driving force of crystallization is typically expressed as the concentration of solute in excess of its equilibrium concentration, i.e. solubility (Jones, 2002). This quantity is commonly termed as supersaturation and can be expressed as:

$$\Delta c = c_s - c^* \tag{1}$$

where c_s is the concentration of the solution, c^* is the saturation concentration, and Δc is the concentration driving force. Alternatively, the driving force may also be given as relative supersaturation:

$$S = \frac{c_s}{c^*} \tag{2}$$

or

$$\sigma = \frac{\Delta c}{c^*} = S - 1 \tag{3}$$

where S is the supersaturation ratio and σ is the relative supersaturation (Mersmann, 1995). Crystals can be born and grow only in supersaturated solutions, and therefore the generation of supersaturation is a prerequisite for all crystallization processes. Depending on the method used for creating the supersaturated environment, crystallization techniques can be divided into cooling crystallization, evaporative crystallization, drowning-out crystallization, freeze crystallization, reaction crystallization (i.e. precipitation), and vacuum crystallization (Mersmann, 1995; Jones, 2002). The selection of the most suitable crystallization technique depends largely on the phase diagram of the considered solution and on the yield required.

When the solubility of the substance to be crystallized increases considerably with temperature, cooling crystallization is likely to be a suitable method, as a good crystal yield can be obtained by a modest temperature decrease (Davey and Garside, 2000). The solubility of a substance represents the equilibrium saturation concentration of that substance in the specified solution environment. If the concentration of the substance in a solution is lower than its solubility, all the crystals existing in the solution will dissolve. When the solution is cooled down, the solubility typically decreases, and the solution eventually becomes supersaturated, because the amount of dissolved substance in the solution becomes larger than its saturation value. The solubility curve is therefore the most important information required for designing and controlling cooling crystallization processes. Theoretical prediction of solubility for most systems is still unreliable, and that is why solubility curves are typically determined experimentally (Jones, 2002; Mersmann, 1995).

Cooling crystallization processes can be carried out either continuously or batchwise. When the production rates are comparatively low, such as in the manufacturing processes of specialty chemicals and pharmaceuticals, batch crystallizers are typically preferred (Mersmann, 1996; Davey and Garside, 2000; Beckmann, 2000; Jones, 2002). Batch cooling crystallizers are usually relatively simple vessels which are cooled either with an external jacket or a cooler installed inside the crystallizer. In order to ensure uniform distribution of temperature and concentrations of all components in different parts of the vessel, and to prevent the sedimentation of crystals, some kind of a mixer is always required. In general, batch crystallizers are more flexible and require less capital investment than continuous units, but the main drawback of them is the difficulty to operate them at constant conditions (Mersmann and Rennie, 2001; Lang *et al.*, 1999).

The maximum theoretical crystal mass that can be obtained from a batch cooling crystallization process can be expressed as

$$m_{\max} = m_s\left(x_i - x_f\right) \tag{4}$$

where m_{max} is the maximum crystal mass, m_s is the solvent mass, x_i is the concentration of the crystallized substance at the beginning of the batch, and x_f is the solubility of the substance at the final temperature of the batch. Once a saturated solution is cooled, a solid crystal phase is formed into the solution through two

different mechanisms, which are nucleation and crystal growth. Nucleation refers to a process where a new solid phase appears from a supersaturated homogeneous mother phase (Davey and Garside 2000), and it typically occurs at rather high supersaturation levels. Crystal growth, on the other hand, refers to the expansion of existing nuclei into larger crystals, and it can occur and proceed at considerably lower levels of supersaturated than nucleation. These two processes can be regarded as competitors when the crystallization process proceeds, as they both consume the available mass of the dissolved material (Lang *et al*., 1999). In addition to nucleation and crystal growth, important secondary processes, such as agglomeration and breakage of crystals, also occur during crystallization (Jones, 2002). Although these secondary processes do not directly contribute to converting the crystallized substance from dissolved to solid phase, they often have a significant influence on the quality of the final crystal product.

Typical requirements for the properties of a crystalline material include certain average crystal size, narrow size distribution, desired crystal shape, adequate crystal purity, correct crystal structure, and good stability of the product crystals (Mersmann, 1996; Davey and Garside, 2000; Togkalidou *et al.*, 2001). Depending on the nature of the produced substances, some of the properties mentioned above are typically more crucial than the others. There may also be some important secondary characteristics, such as the dissolution rate of the crystals, the behavior of the crystals during the crystallization downstream processes, powder flow properties, etc. These secondary characteristics are mainly governed by the primary crystal properties.

The properties of the products obtained from crystallization processes are strongly influenced by the geometry and type of the crystallizer, by the operating conditions applied during the process, and by the chemical and physical properties of the liquid and the solid phases (Mersmann, 1995). When considering batch processes, crystallization is often carried out in multipurpose reactors designed to be used for the production of a wide variety of different materials (Jones, 2002; Myerson, 1986). In addition, the same vessel is frequently used as a reactor, crystallizer, mixer, blender, etc., and therefore the geometry of the crystallizer can only rarely be optimized for a certain single compound (Davey and Garside, 2000). This is why the batch cooling crystallization processes are typically controlled by modifying the operation conditions of the crystallizer. Operation conditions are defined by such variables as

the batch time, the cooling policy employed, the composition of the solvent, the type and amount of possible seed crystals or additives, as well as the mixing conditions applied during the crystallization (Myerson *et al.* 1986; Davey and Garside, 2000). The optimization of crystallization conditions principally aims at controlling the level of supersaturation throughout the whole batch, due to the fact that supersaturation is the most important process parameter influencing the properties of the crystals produced (Mersmann, 1995). The significance of supersaturation has been confirmed experimentally by several authors, such as Myerson *et al.* (1986), Jagadesh *et al.* (1996), Matthews and Rawlings (1998), Togkalidou *et al.* (2001), Srinivasakannan *et al.* (2002), Ulrich and Strege (2002), and Lewiner *et al.* (2002). In order to produce crystals with controllable properties, it is typically advisable to avoid excessive nucleation and to maximize the role of crystal growth, so that most of the material that is dissolved in the solution can accumulate on the surfaces of a small number of crystals. This means that the supersaturation level should be kept at a relatively low level throughout the whole crystallization process. In some cases, it is also equally important to optimize the mixing conditions during the crystallization, so that most of the crystal breakage can be avoided while still ensuring homogeneous solution environment in all parts of the crystallizer. This chapter contains a description of the different phenomena affecting the formation of crystals from a solution, and introduces the principles of some typically applied methods for controlling the level of supersaturation during the batch cooling crystallization processes. The influence of mixing characteristics on crystallization are considered in Chapter 3.

2.1 Crystalline solids

Crystalline solids are highly structured compounds that are constructed of identical structural elements. In the simplest case, these elements can consist of only a single atom, or as in the case of most organic pharmaceutical compounds, they are constructed of one or more molecules (Brittain and Byrn, 1999). In general, the structural elements can be thought of as a three-dimensional building blocks characterized by the lengths of the three edges and by the angles between these edges (Mersmann, 1995). The characteristic dimensions and angles of these elements are different for different compounds.

Crystals are formed when the growth elements are attached to a crystal lattice, which can be defined as a set of points arranged so that each point has identical surroundings. In other words, a crystal structure is generated only when the growth units are attached identically to each lattice point and extended along each crystal axis, so that a regular repetition of identical units in three dimensions is formed. The existence of identical long-range order of growth units is considered as an indication of crystalline structure; otherwise the material is classified as amorphous (Davey and Garside, 2000).

An important consequence of ordered internal structure is that the crystal surfaces are highly selective, thus allowing only similar molecular-scale components to attach themselves. For this reason, crystallization can be utilized for producing products with very high purity, which also explains its predominant use in the pharmaceuticals industry (Togkalidou *et al.*, 2001). Another significant consequence of the organized structure is that the shape of an ideal crystal is completely regular and characteristic of the material in question (Mersmann, 1995; Davey and Garside, 2000; Jones, 2002). This means that if the crystal structure of a material is known, it is in principle possible to predict the shape of an ideal crystal by calculating the strengths of bonds that form when the growth units join different surfaces (Davey and Garside, 2000).

Real crystals are never exactly ideal, however, and that is why their external appearance is not determined only by the crystal structure, but is also influenced by several other variables. It is known that due to the variations in the interaction energies between the crystallizing units and different crystal surfaces, the growth rates of individual crystal faces are different (Davey and Garside, 2000; Jones, 2002). The relative growth rates of different faces often depend strongly on the prevailing growth conditions, such as the level of supersaturation, temperature, solvent, and solution purity. For these reasons, the relative sizes of individual crystal surfaces become different, and that directly influences the overall shape that the crystal eventually adopts. In general, the final shape of the crystal is primarily governed by the slowest growing faces while the very fast growing faces have little or no effect (Davey and Garside, 2000). The growth of certain crystal surfaces may also be hindered or completely blocked due to the adsorption of impurities or deliberately used additives, which affect the overall crystal shape (Mersmann *et al.*, 2001). In addition to crystal growth, the differences between the properties of individual surfaces may cause the

behavior of crystals to be directionally dependent. This means that the dissolution rates, mechanical properties, refractive indices, etc. often vary between the different crystal faces (Davey and Garside, 2000).

Most cooling crystallization processes are carried out in agitated vessels, and therefore the actual shape of the crystals produced is often affected also by the crystal breakage. The role of breakage becomes more important with increasing crystal size, suspension density, batch time, and mixing intensity. As a consequence of breakage, the crystals typically become more rounded and their shape therefore begins to deviate from the characteristic shape of ideal crystals of the same material. Crystal shape is thus a complex function of a vast variety of different process parameters, and it is therefore obvious that predicting the shape of real crystals produced in industrial crystallizers is extremely difficult (Mersmann, 1995).

2.1.1 Polymorphism

When considering the research work made in the area of crystallization and in pharmaceutical sciences in recent years, the keyword of considerable importance is polymorphism, which can be defined as the ability of a substance to exist in more than one crystal structure (Khoshkhoo and Anwar, 1993). In other words, polymorphs are different crystal modifications of the same pure substance, which have the same chemical composition but different internal crystal structures. Several authors (e.g. Davey and Garside, 2000) have concluded that it is possible for almost every crystalline substance to exist in two or more solid structures if the crystallization environment is suitable. It has also been found that a majority of all organic and inorganic compounds of pharmaceutical relevance are capable of crystallizing in more than one solid modification, being either polymorphs or solvates (Vippagunta *et al.*, 2001). Solvates are crystals that contain solvent molecules within the crystal structure. If the solvent is water, the solvate is called a hydrate (Vippagunta *et al.*, 2001).

The existence of different crystal modifications is a reflection of the alternative ways the molecules or ions can pack to form a unit cell. Variations in the dimensions, shape, symmetry, capacity (number of molecules) and void volumes of the unit cells cause different crystal modifications of a given substance to have different physical, chemical and pharmaceutical properties (Grant, 1999). Among others, these include solubility, hardness, melting point, and density. These primary properties typically

determine the secondary characteristics of the produced material, including the processing properties, such as compressibility, powder flow and filtration behavior, as well as the bioavailability of a drug product for its intended therapeutic use (Guillory, 1999; Brittain and Grant, 1999). It is therefore crucial in terms of quality, stability and safety to ensure that the selected crystal modification can be reproducibly produced (Bauer *et al.*, 1998; Beckmann, 2000). Although it is often the most stable crystal modification that is chosen for production, also thermodynamically unstable modifications are sometimes produced because of their enhanced material properties, higher yields, or higher production rates (Bugay, 2001; Davey and Garside, 2000).

Different crystal modifications of a substance constitute different homogenous phases. Under defined conditions of temperature and pressure, only one of the crystal modifications can be stable and all the others are unstable. The most stable modification always has the lowest solubility, and that is why the relative solubilities of different crystal modifications are often used as a convenient measure of the thermodynamical stability of crystal modifications (Guillory, 1999). It is important to notice that this relationship is completely independent of the solvent (Davey and Garside, 2000).

Although the thermodynamical factors favor the formation of the most stable crystal modification, it is also possible to crystallize unstable crystal modifications by carefully controlling the crystallization conditions, such as supersaturation, temperature and concentrations of various components, throughout the whole process (Grant, 1999). The composition of the solvent is one of the most crucial factors in defining the modification of the crystals produced (Khoshkhoo and Anwar, 1993). According to Guillory (1999), some solvents can favor the crystallization of certain crystal modifications, because they adsorb to particular faces of some modifications selectively, thereby either inhibiting their nucleation or retarding their growth to the advantage of others. It has also been shown that certain additives may have an influence on the modification of crystals (Davey and Garside, 2000).

The production of unstable crystal modifications is further complicated by the fact that the formation of unstable crystal modifications will eventually be followed by the phase transition of them to the most stable structure. This is due to the tendency of all systems to reach the equilibrium state, and means that a polymorphic system would move to the state where the crystals of the most stable phase appear through each

possible crystal modification (Blagden *et al.* 1998b). The transformation from one modification to another may be solvent-mediated or occur in the solid state (Davey and Garside, 2000). Although the crystallization process is the most critical part in the manufacturing of different crystal modifications, attention must also be paid to controlling the processes that follow crystallization. These processes typically involve filtration of the crystal slurry, drying of the solids, grinding, granulation, compaction, etc. During these processes, a variety of phase conversions are possible when the crystals are exposed to several processing stresses (Grant, 1999).

2.2 Nucleation

The process where a new solid phase is created from a homogenous solution is generally called nucleation. Several different nucleation mechanisms exist, and they can be roughly divided into two main categories, namely primary and secondary nucleation (Jones, 2002). Primary nucleation refers to a process where nuclei are formed in the absence of solid crystal material, whereas secondary nucleation results from the presence of crystals in the solution.

2.2.1 Primary nucleation

As soon as a supersaturated solution environment has been created, the solution attempts to achieve thermodynamic equilibrium either through birth of new crystals by nucleation or through growth of the existing nuclei. If the solution contains neither solid foreign particles nor crystals of its own type, nuclei can only be formed by homogeneous nucleation. If the solution contains foreign particles, such as dust particles or solid impurities, the nucleation process is facilitated and the process is known as heterogeneous nucleation. Both homogenous and heterogeneous nucleation take place in the absence of solution-own crystals and are collectively known as primary nucleation (Mersmann, 1995).

Primary nucleation typically requires a fairly high supersaturation level, and it therefore occurs mainly only during unseeded crystallization or precipitation processes. When a saturated solution is cooled during the cooling crystallization, the supersaturation of the solution increases until it reaches the maximum value which cannot be exceeded without the solution becoming unstable. This maximum value is commonly known as the metastable supersaturation. The zone between the solubility curve and metastable supersaturation is called the metastable zone, and that is where

all crystallization operations occur. The width of the metastable zone depends on a number of parameters, such as the temperature level, the rate of generating the supersaturation, the solution history, impurities, fluid dynamics, etc. (Ulrich and Strege, 2002). In addition, the width of the metastable zone can also depend on the thermal history of the solution, that is, how long and how high it has been heated above the saturation temperature (Beckmann, 2000).

Metastable supersaturation is the supersaturation level that is required for the primary nucleation to occur. When considering unseeded cooling crystallization processes, primary homogeneous nucleation typically occurs only at the beginning of them. However, the rate of primary homogeneous nucleation is usually highly nonlinear. Its kinetics are extremely low for small values of the supersaturation, but become very high for values corresponding to the metastable zone limit (Klein and David, 1995). Primary homogeneous nucleation can therefore have a detrimental impact on the properties of the final crystal product. It has been reported, for example by Beckmann (2000) that it is common for organic systems that up to 30 – 50 % of the solute dissolved can crash out of the solution rapidly during spontaneous nucleation.

As soon as the crystals become present in the solution, nucleation by heterogeneous and secondary mechanisms will begin to dominate in most cases (Mersmann, 1995). In heterogeneous nucleation, foreign particles present in a supersaturated solution act like catalysts for nucleation. The presence of foreign particles is generally known to reduce the energy required for nucleation, which is the reason why the width of the metastable zone in a heterogeneous system is smaller than it is in a homogenous system. When considering industrial crystallizers, various foreign surfaces usually exist in the system and therefore the primary nucleation cannot be considered as homogeneous but arises essentially from a heterogeneous mechanism (Klein and David, 1995).

When the solution is brought into the supersaturated state, the molecules or ions of the dissolved substance begin to form clusters that are held together by relatively weak intermolecular forces and packed in a regular way. The destiny of these clusters depends on their size, because the system always aims at the lower level of free energy. This can be achieved only through the dissolution or the growth of the nuclei. If the size of the formed crystal is smaller than the size of a critical nucleus, it will dissolve. Similarly, if the size of the cluster is sufficient to create a stable nucleus, it

will continue to grow (Klein and David, 1995). The size of the critical nucleus depends mainly on the supersaturation. When the supersaturation increases, the size of the critical nucleus decreases and eventually becomes small enough for nucleation to become spontaneous. The rate of nucleation is therefore defined as the rate at which clusters grow through this critical size to become crystals (Davey and Garside, 2000). The rate of nucleation cannot be reliably predicted yet, and therefore it has to be determined experimentally for each system. Furthermore, as the crystallization conditions, such as supersaturation, temperature and concentrations, typically fluctuate considerably during the process, the nucleation rate is usually not constant.

2.2.2 Secondary nucleation

Secondary nucleation refers to a phenomenon where the formation of nuclei is induced by the presence of crystals of the material being crystallized. Several different secondary nucleation mechanisms have been reported to exist, but as proposed by Mersmann (1996), these mechanisms can be roughly divided into attrition nucleation and surface nucleation. Attrition nucleation is the formation of nuclei as a result of crystal collisions with the walls of the crystallizer, a stirrer or pump impeller or other crystals in the suspension (Klein and David, 1995), whereas surface nucleation refers to formation of new nuclei on the surface of crystals present in the solution or in the immediate vicinity of such crystals, and it depends on the level of supersaturation.

Secondary nucleation generally occurs at much lower supersaturations than primary nucleation, which implies that secondary nucleation is likely to take place immediately after the first crystals have appeared in an unseeded solution by primary nucleation processes. Attrition nucleation can, in principle, occur also in solutions that are not supersaturated at all, because it is mainly caused by the mixing and fluid flow characteristics of the crystallizer. The process of secondary nucleation is, however, not simply an attrition event alone but is also related to the level of supersaturation at which the parent crystals are growing.

The occurrence of secondary nucleation might set some limits to the size distribution that can be achieved with controlled crystallization, because it creates new crystal surfaces on which the available mass of the dissolved material can deposit. In addition, attrition nucleation also decreases the size of already formed crystals. A good example of this phenomenon is given by Mersmann (1999), who demonstrates

the influence of residence time and specific mixing power input on the median size of KNO_3-crystals produced in a continuously operated crystallizer. The overall conclusion that can be drawn from the results of this example is that the median crystal size clearly decreases as the specific mixing power input is increased. Davey and Garside (2000) state that attrition nucleation is nowadays recognized as the most significant nucleation mechanism for materials of high or moderate solubility. The importance of attrition nucleation is also remarked on by Mersmann and Löffelmann (2000), who propose that the final product size can be strongly determined by attrition if the mean size of the crystals is above 100 μm.

Many experiments have shown that the nucleation rate in crystallizers depends not only on supersaturation, but also on the concentration of crystals in suspension, M_T, and on some measure of the hydrodynamic interactions between the crystals and the solution, for example stirrer speed, N, or average power input to the solution. The effect of these variables can be expressed empirically as a power law function:

$$B = k_b M_T^j N^k \Delta c^b \tag{5}$$

where the symbol B is used to represent the secondary nucleation rate. Parameter k_b is a specific function of the vessel geometry (Davey and Garside, 2000). Equation (5) clearly shows the variables that influence the secondary nucleation process, but the problem is that the values for these variables are very difficult to predict and therefore need to be determined experimentally. Some of the parameters, such as the supersaturation and concentration of crystals, typically vary during the crystallization process, therefore also changing the rate of secondary nucleation with time.

2.3 Crystal growth

As soon as crystals larger than the critical size have been created into a supersaturated solution, they begin to grow. The flux of growth units (atoms, ions or molecules) to the newly created crystal surface in the supersaturated solution exceeds the equilibrium flux, which results in the growth of the crystal surface. The ability of a surface to capture arriving growth units and integrate them into the crystal lattice depends, among other things, upon the strength and number of interactions that can form between the surface and the growth unit. Crystal growth is a diffusion and integration process that occurs in such a way that the growth units are first transported

by diffusion and/or convection near the crystal surface and then attached onto the surface by integration, supersaturation being the driving force. Neither the diffusion nor the integration step will proceed unless the solution is supersaturated. As these kinetic processes occur consecutively, the solution concentration adjusts itself so that the rates of the two steps are equal at steady the state. If the different mechanisms take place in parallel, then the overall growth rate is controlled by the mechanism resulting in the faster growth. On the other hand, if the processes take place in series, as in the case of bulk diffusion followed by surface reaction, then the slower mechanism will control the overall rate (Jones, 2002).

The growth rate of crystals may be expressed either as a rate of linear increase of characteristic dimension or as a mass deposition rate. Different crystallographic faces of a crystal usually have different linear growth rates, which causes variations to occur in the shape of the crystals. The overall crystal shape is determined by the slowest growing face (Mullin, 1997). In addition to the structure of the crystal-solution interface, the growth process may be influenced by several other factors as well. Temperature has a strong impact on the crystal growth rate, as it can affect the relative rates of the diffusion and surface integration steps significantly. The growth rate may also be influenced by the liquid velocity around the crystals, because an increase in the solution velocity past the crystal results in reduction of the mass transfer resistance. The crystal growth rate may thus be subject to changes during scale-up if the local solution velocities vary. Experimental results of several authors also indicate that the crystal growth of a number of substances is a function of crystal size in such a way that large crystals grow at a higher rate than small ones (Mersmann, 1995). The real supersaturation for a given crystal is thus a function of its size and increases as the crystal grows. Sensible differences are, however, observed only for very small crystals (< 10 μm), and therefore the influence of size dependent growth rate is typically assumed to be fairly small when considering cooling crystallization processes (Klein and David, 1995). Another phenomenon that is suggested to influence the fluctuation in the growth rates is the growth rate dispersion, which describes the variation in the growth rate among crystals of the same size while they grow under constant microscopic conditions (Berglund and Murphy, 1986). A clear distinction between the size-dependent growth and growth rate dispersion is, however, very difficult to make (Mersmann, 1995)

The overall mass flux density may be described by the following equation (Mersmann, 1995):

$$\dot{m} = k_g (c_s - c^*)^g \tag{6}$$

where k_g is the growth rate constant and g is an empirical coefficient that typically varies between 1 and 2. If the growth is limited only by convection and bulk diffusion, the mass flux may be described by

$$\dot{m}_{dif} = k_d (c_s - c_l) \tag{7}$$

where k_d is the mass transfer coefficient and c_l the interface concentration. If the growth is limited only by integration, the mass flux $\dot{m}_{\text{int}}$ is usually expressed as

$$\dot{m}_{\text{int}} = k_r (c_l - c^*)^r \tag{8}$$

where k_r is the reaction rate constant and r the order of integration reaction.

2.4 Crystal breakage

Particle formation can also occur via breakage processes that start with existing particles and form new, smaller ones, of varying sizes. Attrition is the generic name for particle size reduction and generation, whilst secondary nucleation occurs due to the presence of existing crystals in supersaturated solutions. These both processes may occur simultaneously in crystallizers, giving rise to the more complex process of secondary nucleation.

Particle break-up may occur by two general modes which are collisional break-up and fluid mechanical break-up. Collisional break-up is a result of crystal-crystal, crystal-impeller or crystal-vessel collisions whereas fluid mechanical break-up is the breakage of crystals due to due to turbulent fluid flow. It is typically assumed that the collisional breakage rate is a function of the stirring intensity, the impact probability between a crystal of given size and an impeller or other crystals, the material properties of the crystals and the stirrer, and the total number of crystals in the vessel.

For particles to break up in a turbulent flow field, the fluid eddies responsible for the break-up have to be less than the critical size and possess sufficient disruptive energy. Eddies that are larger than the critical size tend to entrain particles, thus causing little surface stress whereas eddies that are smaller than the size of a crystal will flow over

the crystals providing crystal shear, surface drag and pressure forces. This means that the turbulent break-up rate of the crystals depends on the frequency of eddies, the relation between the turbulent energy component and unit energy required to generate an attrition particle, and the total number of parent crystals (Jones, 2002).

The attrition of large crystals causes the median crystal size L_{50} plotted against the residence time to pass through a maximum value. The greater the mean specific power input in the crystallizer, the higher will be the attrition rate, especially for crystal products that tend to abrade easily, and therefore the smaller the residence time at which the maximum value occurs. (Mersmann *et al.*, 2001)

Crystallizers should be designed and operated in such a way that only a small amount of large attrition fragments have the chance to grow into the size range of the crystalline product that is significantly suffered from attrition. This means that low impeller-tip speeds, low specific power inputs, and low suspension densities should be applied to obtain low attrition rates.

2.5 Agglomeration

In addition to nucleation, growth and breakage of crystals, the size distribution of the product crystals is also influenced by a process called agglomeration. Agglomeration means a particle size enlargement process by which fine particles are joined together during a suspension crystallization process. Agglomeration occurs in many kinds of crystallization systems and especially in those where fairly small crystals are produced. As a consequence of agglomeration, the distribution will contain more crystals of larger sizes than would be found normally.

Agglomeration can proceed vie two different mechanisms. Primary agglomeration refers to the mal-growth of crystalline particles to form polycrystals, dentrites, and twins. Secondary agglomeration, on the other hand, is mainly a result of crystal-crystal collisions in supersaturated solutions which causes them to join together. Secondary agglomeration takes place in suspended particle systems and depends on the mechanical and fluid dynamic processes, such as the movement of particles and liquid, on particle collisions, and on kinetic processes, mainly crystal growth in supersaturated solutions. Both types of agglomeration may occur simultaneously. Agglomeration is dominant in the submicron and micron range of primary species and is less important or negligible for particles larger than 50 μm. (Mersmann, 1995)

Agglomeration normally takes place after the formation of small primary particles by primary nucleation. Two steps are essential for secondary agglomeration: primary particles must collide and they must grow together to form a crystalline bridge. The collision rate of primary crystals depends on particle concentration (suspension density) and fluid dynamics (specific power input). The growth is governed mainly by supersaturation, which depends on macromixing. (Jones, 2002; Mersmann, 1995)

Unlike nucleation and growth, agglomeration does not occur in all crystallization processes. The existence of agglomeration depends on the properties of the crystallizing system and the key parameters affecting agglomeration are normally the hydrodynamic conditions prevailing in the crystallizer, the nature of the solvent, the size and shape of the crystals, the population density of the crystals, supersaturation, and the related growth rate and cohesion forces between the solvent, impurities, and the crystals. (Klein and David, 1995)

2.6 Seeding

Seeding is a technique that can be utilized to control the properties of product crystals efficiently. In seeding, a small amount of solution-own crystals are added into the supersaturated solution before the before spontaneous nucleation occurs. If the seeding process is performed correctly, spontaneous nucleation can be avoided completely. If, despite seeding, spontaneous nucleation still occurs, it means that the kinetics of crystallization are too fast, the seeds have been added too late, the amount of seeds has been insufficient, or the seeds have been inactive. Typical values for the amount of seed crystals are given as $m_{seed} / m_{product} \leq 10$ % (Beckmann, 2000).

Crystallization processes in the pharmaceutical industry are normally carried out as unseeded crystallization, which means that crystals are formed from a solution by spontaneous nucleation. This often leads to formation of unstable crystal modifications and rapid spontaneous nucleation. The crystallization kinetics can have a major impact on the process, especially when organic crystals are manufactured, since according to Beckmann (2000), it is common for organic systems that during spontaneous nucleation up to 30 – 50 % of the solute dissolved can crash out of the solution rapidly, having a detrimental impact on the entire crystallization process. It is therefore very important to accurately select the moment in time when the seeds are added (Davey and Garside, 2000; Jones, 2001). In order to achieve the optimal results,

the seeding should be performed within the “window of seeding” that has limits, which depend mainly on the supersaturation of the solution. The lower limit is at low supersaturations, while the upper limit is determined by the metastable zone.

Controlling the crystal modification of the newly created crystals born through primary nucleation is difficult and almost impossible to verify during the crystallization process. Instead of relying on the ability of the system to form crystal modifications of the desired type, the nucleation process can be influenced by seeding. This is a highly effective method to control the crystal modification, because the best match between the substrate and the crystallizing solute exists when the substrate is in fact a seed crystal of the solute. This means that if seed crystals consisting of only one crystal modification are available, the crystallization of pure crystal modifications can be facilitated. Further on, it means that seeding can also be used to create pure crystals of unstable crystal modifications, although seeding and crystallizing of stable forms is by far the easier task (Beckmann, 2000).

2.7 Crystallization conditions

Batch crystallizers are widely used in the chemical industry and allied industries. They are normally relatively simple vessels, which are usually provided with some kind of agitation and have often artificial aids to heat exchange or evaporation. Batch crystallizers are generally quite labour intensive and are therefore preferred for production rates of up to 10 000 tonnes per year, above which continuous operation often becomes more favourable. Batch crystallizers are the most commonly applied equipment in the crystallization of fine chemicals, pharmaceutical components and specialty products. Whereas continuous crystallizers are usually purpose-built for a specific application, batch crystallization operations tend to be carried out in multipurpose units, the same vessel serving as a reactor, crystallizer, mixer and blender, as well as handling many different products. The optimization of batch crystallization processes is therefore normally performed by modifying the mode of operation rather than the design of a specific piece of equipment.

All batch crystallization processes take place under unsteady-state conditions. Central to their successful operation is the control of supersaturation during the batch. This depends on the operating policy, which specifies the batch time, the rate at which supersaturation is generated, the possible addition of seed crystals, and the type and

level of agitation. Cooling can be provided via a jacket, hollow internal shroud or coil, or externally via recirculation of liquor through a heat exchanger. In order to improve the crystal size distribution in a batch crystallizer further, the creation of supersaturation (i.e. cooling) may in some cases be programmed. A 'fines destruction loop' in which tiny crystals are dissolved and the solute liquor returned to the crystallizer may also be added to the vessel.

A simple operating method for controlling a batch crystallization process consists of cooling the solution at a constant cooling rate. This is typically not optimal, however, as at the beginning of cooling no seed surface or, after seeding, only a small seed surface is available, which creates very high supersaturations followed by extensive nucleation. At the end of the cooling process, the crystal product may have a large surface, but it still grows very slowly due to low supersaturations. Therefore, it is beneficial to set the cooling rate so that the supersaturation remains almost constant during the cooling period.

2.7.1 The role of the solvent composition in crystallization

Solvents are used for a number of different purposes in various unit operations in the pharmaceutical manufacturing processes. As these unit operations are related to each other, the solvents used in a certain unit operation can considerably affect the characteristics of the downstream processing steps and also the properties of the final product. Therefore, the selection of appropriate solvents for different process steps may become a complex task, and the effects of different solvents need to be considered from a wide perspective. The role of solvents in different parts of pharmaceutical processes and some of the limitations and difficulties related to them have been described comprehensively by Kolář et al. (2002), who have also proposed a systematic approach to aid the solvent selection procedure. The work introduced in this thesis focuses on considering the solvent effects only from the viewpoint of crystallization and filtration.

In discussions of the crystallization of different crystal modifications, the effect of the solvent used in the experiments has been definitely one of the most important factors. Guillory (1999) states that some solvents can favor the crystallization of particular crystal modifications because they selectively adsorb to certain faces of some modifications, thereby either inhibiting their nucleation or retarding their growth to

the advantage of others. This same observation has been made by Khoshkhoo and Anwar (1993) who also claim that according to their experiments, the effect of the solvent is not thermodynamic by nature. Khoshkhoo and Anwar (1993) also state that although supersaturation is an important factor in the crystallization of crystal modifications, its effect can be dominated by the effect of the solvent. This last claim has been partly overruled by Threlfall (2000), who says that the widespread belief that the solvent is the unique determinant of the crystal modification is erroneous, and this is the reason why other essential parameters such as the concentration, cooling rate, and temperature of nucleation are often not recorded and reported. The influence of the solvent composition on the crystal shape and crystal growth characteristics has been also been recognized and examined by several researchers (Wang *et al.* 1999, Myerson *et al.* 1986, Lahav and Leiserowitz 2001, and Winn and Docherty 2002). According to these studies, it seems obvious that the solvent composition can have a significant influence on the overall crystallization process, as well as on the characteristics of the final product.

2.7.2 Cooling policies in batch cooling crystallization

In cooling crystallization, a hot, saturated solution is cooled which causes the supersaturation to generate and nucleation to occur. In the simplest case, the solution is allowed to cool naturally when the cooling rate is faster at the beginning of the process and slower at the end. A more commonly used crystallization method involves controlled (or 'programmed') temperature change. The cooling rate can be adjusted to be constant during the whole process, or it can be programmed to follow the solubility curve of the solute. By using programmed cooling, the supersaturation of the solution can be maintained at a constant level throughout the process. Theoretical and mathematical descriptions, as well as experimental verification of the improvements achieved by using the programmed cooling method have been presented rather comprehensively by Mullin and Nývlt (1971) and Jones and Mullin (1974). The experimental results presented in these studies show that the quality of crystalline product can be significantly improved by using programmed instead of uncontrolled cooling. However, also opposite results can be found in the literature. It therefore seems that the suitability of a certain cooling policy depends significantly on the characteristics of the material that is crystallized, as well as on the features of the crystallization equipment.

The general form of some of the different cooling profiles that can be applied to influence the level of supersaturation, is illustrated schematically in Figure 1.

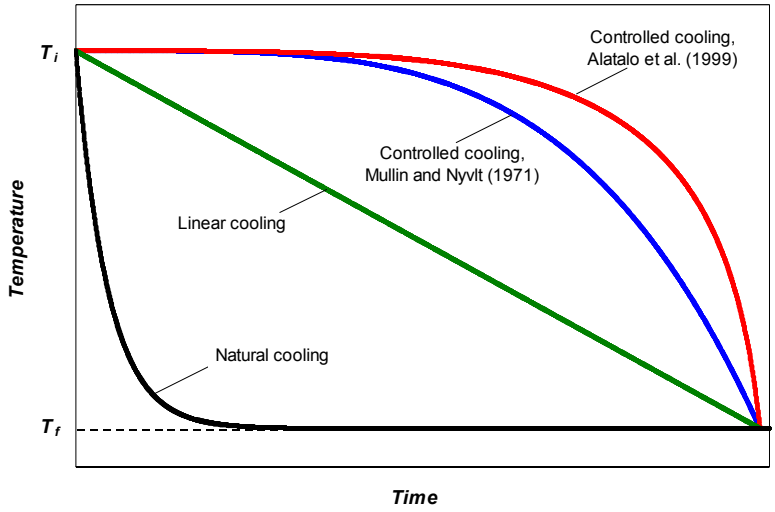

Figure 1 Schematic description of different types of cooling profiles.

2.7.2.1 Natural cooling

Natural cooling refers to a cooling method where the crystallizer is cooled by allowing a constant temperature coolant to flow at a constant rate through the cooling jacket of the crystallizer, which normally results in very high cooling rates at the early parts of the batch. Rapid cooling will inevitably cause the solution to cross the boundary of the metastable zone, resulting in uncontrolled nucleation. The very large number of nuclei so produced sets a limit to the size to which they can grow, as the available solute resources must be distributed over this large number of particles. This kind of cooling is therefore exactly what is typically not desired if the aim is to minimize nucleation by maintaining the supersaturation at a constant value within some appropriate limits. Rapid initial cooling will definitely produce uncontrolled crystallization resulting in massive nucleation (Davey and Garside 2000), and the crystal product obtained with this kind of a cooling policy would most likely consist of a large amount of small, irregularly shaped crystals.

If a crystallizing batch is cooled naturally for example by allowing constant temperature cooling water to flow at a constant rate through the cooling jacket of the

crystallizer, the temperature/time-profile can be calculated as

$$\frac{(\theta - \theta_0)}{(\theta_i - \theta_0)} = \exp\left(-\frac{t}{\tau_B}\right) \tag{9}$$

where θ_i is the initial temperature and θ_0 is the final and hence the cooling water temperature. The batch time constant τ_B is given by

$$\tau_B = \frac{M_s C_p}{U A_B} \tag{10}$$

where U is the overall heat transfer coefficient, A_B the heat transfer area, and M_s the mass of solution that has specific heat C_p. As Figure 1 shows, a cooling curve of this type gives very high cooling rates initially when the temperature driving force is the greatest. The rapid initial cooling will cause the solution inevitably crossing the metastability limit, causing producing massive primary nucleation.

2.7.2.2 Linear cooling

When the crystallizer is cooled by using a linear cooling profile, the cooling rate is maintained constant throughout the whole duration of the cooling, as can be seen in the example presented in Figure 1. Depending on the chosen cooling rate, it is possible to reduce the high initial supersaturation peak associated with natural cooling significantly with this method. This should typically lead to an increase in the average crystal size, as also reported by Jones and Mullin (1974), who calculated the theoretical size distributions of potassium sulphate crystals obtained from a seeded batch cooling crystallizer operated with four different cooling profiles.

Theoretical illustrations shown in Figure 2 demonstrate solute concentration profiles during an unseeded batch cooling crystallization process, where the only nucleation mechanism occurring is assumed to be primary homogenous nucleation. Examples are given for both slow and rapid cooling, assuming a constant cooling rate throughout the whole duration of the batch.

Figure 2a) demonstrates a process where a batch having initial concentration and temperature, as marked by point A, is cooled at a slow constant cooling rate. The solution is initially undersaturated, as the solute concentration lies below the solubility curve, which is represented by the solid line. When the temperature of the batch is

decreased, the solution becomes supersaturated and spontaneous nucleation finally takes place at point B, which lies at the boundary of the metastable zone represented by the dashed line. Spontaneous nucleation is associated with a sudden collapse in the solute concentration as the solid crystal phase bursts into the solution. This is illustrated as a drop in solute concentration from point B to point C, which lies in the metastable region. Spontaneous nucleation is not likely to occur within the metastable zone, but since the solution is at the supersaturated state, the nuclei existing in the solution are able to grow as the batch is cooled further. If the growth rate of the crystals is high enough and the cooling rate is sufficiently low, supersaturation is released via the growth process causing the solute concentration to remain within the metastable zone. This kind of a process would most likely produce crystals with large mean size and narrow size distribution.

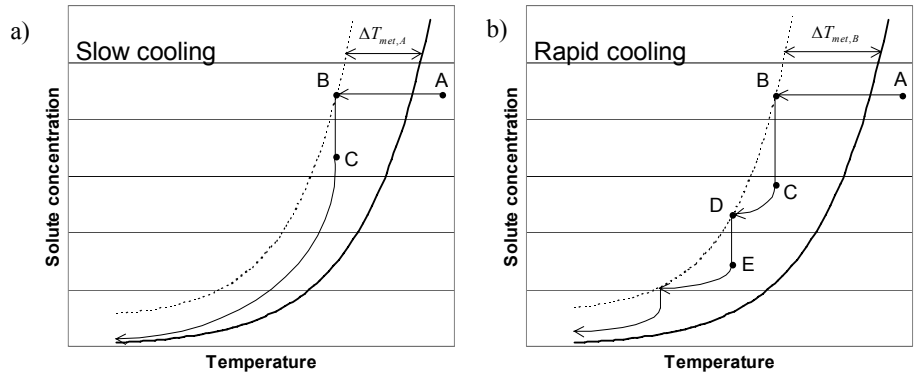

Figure 2 Theoretical illustrations describing the influence of cooling rate on the solute concentration profiles during an unseeded batch cooling crystallization process with a) slow cooling and b) rapid cooling. It is assumed that only primary homogeneous nucleation occurs and that the cooling rate is constant throughout the whole process. The solid lines represent the solubility curves, whereas the dashed lines symbolize the boundaries of the metastable region.

Figure 2b) shows the theoretical concentration profile if the same batch as in Figure 2a) is cooled with a much higher cooling rate. As stated by Ulrich and Strege (2002), the width of the metastable zone depends on a number of parameters, such as the temperature level, the rate of generating supersaturation, solution history, impurities, fluid dynamics, etc. When the cooling rate is increased, the metastable zone has been detected to become broader (Mersmann and Löffelmann 2000, and Ulrich and Strege 2002). Referring to the notations in Figure 2, the preceding assumption implies that

$T_{met,B} > T_{met,A}$. An important consequence of a wider metastable zone is that spontaneous nucleation now takes place at higher supersaturation in point B than with the lower cooling rate. This again causes a larger number of nuclei to form and the collapse in concentration to become larger, as shown by the drop in solute concentration from point B to point C. When the batch is further cooled from point C with the same high cooling rate, the formed nuclei begin to grow again. If the growth rate of crystals is not high enough, the large supersaturation generated by the high cooling rate cannot be released completely via crystal growth. As a result, the solute concentration crosses the boundary of the metastable zone for the second time, as marked by point D, causing a new nucleation event to take place. Therefore the number of nucleation events during the batch depends mainly on the kinetic parameters of crystal growth and nucleation, which are both influenced by the cooling rate. Uncontrolled nucleation caused by rapid cooling results in very large numbers of nuclei, which sets a limit to the size to which they can grow, as the available solute resources must be distributed over a large number of particles (Davey and Garside 2000). Consequently, the crystal product of this kind of an uncontrolled process would probably have a small mean size and wide size distribution.

The theoretical considerations presented above are only applicable for unseeded batch cooling crystallization processes, where it is assumed that the only form of nucleation is primary homogeneous nucleation. However, this assumption never holds true in the actual crystallization processes, as the formation of new nuclei through primary heterogeneous nucleation and secondary nucleation always occurs. As has been demonstrated by Mersmann (2001), metastable supersaturation for secondary nucleation is lower than it is for primary nucleation, which implies that secondary nucleation is likely to take place immediately after the first crystals have appeared in an unseeded solution by the primary nucleation process. The importance of secondary nucleation in crystallization processes should not be underestimated, as especially attrition nucleation can impact the size distribution of the crystals considerably.

2.7.2.3 Programmed cooling

Utilization of the so-called programmed cooling profiles during batch cooling crystallization processes is commonly accepted as one of the most effective methods of controlling the properties of the product crystals. Numerous articles (Mullin and

Nývlt (1971) and Jones and Mullin (1974), for example) in the literature deal with different aspects of these programmed cooling profiles and with the improvements that can be achieved by using them.

Some of the typically required properties for the crystalline material are large crystal size, narrow crystal size distribution, and desired crystal shape. As demonstrated above, these properties can be achieved only if the nucleation is minimized and the available solute resources are consumed by the crystal growth process. Primary nucleation can be minimized by maintaining the solute concentration below the metastable boundary by using for example slow cooling rates. However, long batch times are not desirable for economic reasons (Ulrich and Strege 2002), and on the other hand, longer batch times also lead to an increased amount of attrition nucleation thus widening the size distribution through the development of crystals in the smaller size range (Davey and Garside 2000). It has also been shown in various studies that the physical crystal properties can be effectively controlled by using so-called programmed cooling profiles. These profiles take into account the nonlinearity of the solubility curve in such a way that the supersaturation is maintained approximately constant throughout the whole duration of the batch.

The main principle behind the controlled cooling policies is to make certain that the generation rate of supersaturation always matches the available crystal surface area on which the formed crystal mass is to be deposited (Davey and Garside 2000). This means that at the early stages of the batch when the surface area of the crystals existing in the solution is small, the rate of supersaturation production has to be slow, and therefore also the applied cooling rates need to be extremely low. When the crystallization then proceeds and the surface area of the crystals increases, also the cooling rate increases towards the end of the batch, as can be observed also in Figure 1, which shows examples of two different programmed (or ‘controlled’) cooling profiles. A lot of work has been done in this field by numerous authors who have tried to calculate the optimal temperature-time profiles that should be followed to achieve such controlled crystallization. In practice, it is not usually important that the exact form of theoretical equations is followed, but rather that a reasonable approximation to the appropriate time profile is achieved. The final optimization of the process is invariably achieved through subsequent experimentation.

Mullin and Nývlt (1971) have derived an exact theoretical equation that represents the

ideal cooling curve based on constant nucleation and growth rates in a seeded solution. This equation, however, was too complex for general use and it was therefore simplified by making some appropriate assumptions. For an unseeded batch cooling crystallization process of a substance with solubility depending linearly on the temperature, the simplified cooling curve that should be followed in order to maintain approximately constant supersaturation throughout the whole batch is:

$$(T_0 - T)/(T_0 - T_f) = (t/\tau)^4 \tag{11}$$

where T_0 is the initial solution temperature, T is the solution temperature at time t, T_f is the final solution temperature, t is time and τ is the batch time. The obtained simplified profiles were utilized by Mullin and Nývlt (1971) in crystallization experiments made with aqueous solutions of potassium sulphate and ammonium sulphate, and it could be shown in both cases that the mean crystal size was slightly increased when the cooling profile was changed from natural to programmed cooling. Their results, however, also showed that the programmed cooling profile was not very effective in eliminating the occurrence of nucleation during the crystallization, as all the obtained crystal products contained a significant amount of fine crystals.

The programmed cooling curves are almost mirror images of the natural cooling curve, giving the required very low initial cooling rate that then gradually increases as the batch proceeds. In most of cases, the experimental results confirm the advantages that can be gained through the increase in product crystal size and the narrowing of the size distribution by following a controlled crystallization, but also opposite results can be found in the literature. It therefore seems that the suitability of a certain cooling policy depends significantly on the characteristics of the material that is crystallized, as well as on the features of the crystallization equipment.

The occurrence of secondary nucleation sets some limits on the size distribution that can be achieved with controlled crystallization. As soon as crystals appear in the solution, secondary nucleation is likely to take place, and the number of nuclei that are produced by this mechanism will increase with the increasing mass of crystals in the solution. The longer the batch time, therefore, the greater the number of secondary nuclei, and the more their presence will widen the size distribution by the development of a population of crystals in the smaller size range. A bimodal distribution frequently results. If a large product size and narrow distribution are

required, it is important to minimize the secondary nucleation, and the most effective way of doing this is usually to minimize the stirrer power input. (Mersmann, 2001)

It is very typical, especially with many organic compounds, that their solubility grows exponentially with respect to temperature and not linearly, as was assumed in the approximations concerning the cooling profile described by equation (11). Alatalo *et al.* (1999) have modified equation (11) further and concluded that the theoretical cooling profiles for unseeded systems having solubility curves that follow the exponential function form, $w = ae^{bT}$, can be calculated from equation

$$T(t) = \frac{1}{b}\ln\left[e^{bT_0} - \left(\left(e^{bT_0} - e^{bT_f}\right)\left(\frac{t}{\tau}\right)^4\right)\right] \tag{12}$$

An example of this kind of programmed cooling profile is also illustrated in Figure 1.

2.8 Tailor-made additives and impurities

Crystal shape and modification can be markedly affected by the properties of the solvent or by the presence of some impurities. Impurities or 'additives', which change the properties of the interface between the solvent and the crystal surface, are often used deliberatively industrially to modify the characteristics of the product crystals. Impurities or additives may effect in a different manner on different crystal faces and therefore cause them to grow at different rates (Guillory 1999).

Impurities influence the shape and purity of the product crystals because they alter the kinetic parameters, such as the rates of nucleation and growth. Nuclei and attrition fragments covered by impurity molecules change their growth behavior, and therefore the induction time period is different from that of pure systems. The width of the metastable zone is also influenced by the presence of impurities. (Mersmann, 1995)

Some preselected additives can be used to inhibit the nucleation and growth of the undesired crystal modifications. The additives can also be "tailor-made", i.e. the additive can have the same structure as the host molecule but for an altered moiety. This moiety is designed so that the additive can be adsorbed only on a symmetry subset of crystallographic surface sites on specific faces. This way the adsorbed additive, which essentially replaces a host molecule, is oriented so that the altered moiety emerges from the crystal surface. Such an adsorbed additive, therefore, would hinder regular deposition of oncoming molecular layers and so inhibit the crystal

growth at that face (Lahav and Leiserowitz, 2001). Industrial crystallization processes take place in multicomponent systems in which not only the crystallizing component, but also several other solutes are always present in considerable amounts. Additional components can change the solution properties, such as density, viscosity, the diffusion coefficient, and the structure of the solution. These components may also be adsorbed on certain faces of the crystals, thus modifying the crystal habit.

Other solvents or impurities can also have unpredictable effects on the solubility of the crystallized material. For example, addition of a miscible second solvent, sometimes called a co-solvent or diluent, often reduces solubility and is a common method to induce crystallization. The second solvent can be thought of as an impurity, and some impurities can affect the solubility even at very low concentrations. This means that even a slight contamination of the feed solution may have serious effects on the outcome of the crystallization process.

3 MIXING IN BATCH CRYSTALLIZERS

As mentioned in the previous chapter, batch crystallizers are usually simple vessels equipped with some kind of mechanical agitation device for particulate fluidization. These have the effect of reducing the temperature and concentration gradients, and of maintaining the crystals in suspension. Stirred tanks are the most common form of crystallizers, but due to the high local gradients of the energy dissipation, the fluid dynamics are not well understood and depend to a large extent on the geometry of the vessel. Different kinds of impellers, baffles and draft tubes can also produce very different flow fields. Baffles are typically added to improve mixing and heat exchange, and therefore also the structure and size of the baffles plays an important role in defining the flow conditions within the crystallizers.

Local supersaturation levels and consequent crystallizer performance is often very sensitive to mixing conditions, particularly when the supersaturation generation is fast and the vessel size is large. Such local variations in supersaturation can give rise to varying rates of all particle formation kinetic processes, in addition to the fluid mechanical effects on secondary nucleation during crystallization. Crystallization systems frequently exhibit high levels of supersaturation around the points where it is generated, such as at cooling surfaces, evaporation interfaces and locations where two or more liquid reactants are brought into contact. Attainment of uniform conditions throughout the reactor volume therefore becomes difficult, and this mixing problem becomes more important when the scale of operation increases.

Agitation of slurry to create a suspension in a low tonnage batch crystallizer can be provided in several ways. An impeller is typically mounted centrally in the vessel and wall baffles are added to prevent swirling flow. The agitator can also be shrouded with a draft-tube to provide circulation from the base up to the top surface of the crystal suspension. Such agitation improves heat transfer, reduces scale formation, smoothes out supersaturation profiles, suspends crystals, and generally gives rise to a more uniform product and reduced batch time. As has already been mentioned, it is also very important to design the crystallization equipment in such a way that secondary nucleation can be minimized. Best way to achieve this is to use a large slow-moving stirrer rather than a small high-speed device. Whatever the stirrer type employed, it is crucial to ensure that the crystals are kept in suspension; crystals that

settle to the base of the vessel are no longer exposed to fresh supersaturated solution and tend to agglomerate. One way of calculating minimum stirrer speed required to 'just suspend' the particles, N_{JS}, is to use the semi-empirical equation presented by Zwietering (1958):

$$N_{JS} = \frac{S_m \, d_p^{0.2} \left[\frac{\Delta\rho}{\rho_L} \right]^{0.45} \upsilon^{0.1} \, x^{0.13}}{D^{0.85}} \tag{13}$$

where v is the kinematic viscosity of the solution, x is the fraction of solids in the vessel, D is the stirrer diameter, ρ_l is the liquid density, and $\Delta\rho$ the difference in density between the crystals and the liquid. The value of the dimensionless constant S_m depends on the vessel geometry.

Use of the 'just suspended' agitator speed given by equation (13), however, results in a far from homogeneous suspension with axial distribution of the solids volume fraction occurring. In practice, therefore, somewhat higher speeds than N_{JS} are adopted. According to Nienow (1985), it is difficult to achieve solid phase suspension homogeneity in large vessels at economic power inputs. Care must also be taken to avoid excessive particle attrition due to collision with vessel walls or impellers, due to the use of too high agitation rates.

When considering the state of solid/liquid-suspensions in stirred vessels, it is possible to distinguish between several different conditions:

Incomplete suspension means that part of the solid phase is deposited at the bottom of the vessel or carries out a rolling movement on the bottom surface. This situation is observed quite often especially in flat-bottomed tanks, where the solid phase has a tendency to build up as corner deposits or layered zones at the vessel edges or at the center of the vessel bottom, where only stagnant fluid flow exists.

Complete suspension refers to the state where the suspension is complete with no particles remaining at the bottom of the vessel for more than 1 to 2 s. Under this condition, the total surface area of the crystals is suspended in the solution and is available for crystal growth. However, the crystals are not distributed homogeneously throughout the contents of the entire crystallization vessel.

Homogeneous suspension exists when the local particle concentration and also the particle size distribution in the vessel is constant throughout the entire vessel contents.

In the case of large particles L, large density differences (ρ_c - ρ_L) and small viscosities (η_L) of the solution, it is often very difficult to obtain a homogeneous suspension. (Mersmann and Rennie, 1995)

One of the most important issues that should be considered when designing the mixing devices for batch crystallizers is the attrition of the formed crystals due to mixing. Attrition reduces the size of the product crystals and it should therefore be minimized. Favorable stirrers to be used in crystallizers with respect to attrition are those which have a fairly small power number and a large pumping capacity, and those that can be operated at the minimum specific suspension power with respect to mixing and suspending (Mersmann and Rennie, 1995). Mersmann (1995) has summarized the most important actions that should be considered in order to obtain large median crystal sizes L_{50}, as follows:

Selecting an appropriate crystallizer (fluidized-bed is superior to stirred-vessel, which is, in turn, superior to forced-circulation)

- restricting the specific power input to < 0.3 W/kg
- restricting the circumferential impeller velocities to 6 to 8 m/s
- limiting the suspensions densities to < 200 kg/m^3 or volumetric holdup < 0.1
- choosing the optimum residence time

4 CHARACTERIZATION OF CRYSTALS

Crystal size distribution and crystal shape are important indicators of crystal product quality, and they have normally a significant effect on downstream processing, such as solid-liquid separation. Larger particles separate out from the fluids more quickly than fine ones, and they are less prone to dust formation whilst smaller particles dissolve more rapidly. An interesting feature of industrial crystallization systems is the relatively wide range of particle sizes encountered. The particle sizes range over several orders of magnitude from the sub-micron (nanometer) scale to several millimeters or more.

Solid particles have a distinct form, which can strongly affect their appearance, product quality and processing behavior. Thus, in addition to chemical composition, particulate solids have to be additionally characterized by particle size and shape. A common feature of crystallization process systems is the formation of particle populations with a range of characteristics. Real particles, however, are rarely exactly similar to each other, and irregular particles have many individual dimensions – they are in fact multi-dimensional, with several angles and faces giving rise to the corresponding problem of mathematical dimensionality. In order to analyze such particulate populations it is first necessary to define what is meant by ‘particle-size’, ‘size distribution’ and ‘particle shape’. This normally starts with a consideration of the simplest single particles and trying to relate real particles to them.

In the view of product quality, the operation of a crystallizer requires sampling and particle characterization. Sampling has to be carried out representatively to obtain an overall picture of the operating conditions of the crystallizer and to avoid accidental results. The sample mass necessary for measurement depends on the method of analysis and the particular instrument to be employed, the average size of the particles, and their size spread. Size characterization includes the measurement of crystal size distributions, median crystal sizes, and shape factors that are most suitable to describe the variety of shapes of crystals. (Mersmann and Rennie, 1995)

4.1 Crystal size

The dimensions of particles are expressed in terms of length, and micrometer is probably the most commonly unit used in practice. Irregular particles have a unique maximum characteristic length and this, or a mean value of several different lengths, is sometimes used as a characteristic dimension. Normally, however, irregular particles are characterized by some form of 'equivalent dimension'.

The sphere is unique. It is the only particle whose form can be totally described by a single dimension: its diameter d: volume = $\pi d^3/6$; area = πd^2. Because of the uniqueness and simplicity of the sphere, the characteristics of non-spherical particles are often related back in some way to the size of an 'equivalent' sphere which has some shared characteristic, such as the same volume or surface area.

4.2 Crystal shape

Crystal shape can be described qualitatively using standard terms such as granular, flaky, needle, etc. Quantitative description, however, requires use of 'shape factors' that enable the surface area and volume of the particle to be calculated by knowing its 'size'. Shape factors relate the characteristic dimension of a particle to its surface area or volume, respectively. Any characteristic dimension can be chosen, but the corresponding shape factor belongs to the characteristic dimension selected and should not be used with any other dimension.

For example, the surface shape factor f_s relates the external surface area A_p of a particle to its characteristic dimension L:

$$A_p = f_s L^2 \tag{14}$$

For a sphere of characteristic diameter $L = d$, $f_s = \pi$. For all other particles $f_s > \pi$. For example, for a cube of characteristic side length L then $f_s = 6$. Similarly, the volume shape factor f_v relates the particle solid volume V_p to its characteristic dimension L:

$$V_p = f_v L^3 \tag{15}$$

For a sphere: $f_v = \pi/6$. For all other particles $f_v > \pi/6$. For example, for a cube of characteristic side length L then $f_v = 1.0$. The selection of an appropriate shape factor for different applications is fairly complicated, because the number of different shape factors presented in the literature is huge and nobody really seems to know which of

those shape factors should be used for different purposes. Usually the shape factor gives the connection between two different measures or between two different methods of measuring the size or size distribution. Therefore there are no general definitions for the shape factor and shape factors are always developed for some special purpose (Oja 1996). Some of the commonly used particle shape factors are for example (Oja, 1996; Hentschel and Page, 2003):

$$C = \frac{c_p}{C_{per}} \qquad \psi = \frac{s_p}{S_p} \qquad \phi_1 = \frac{4\,\pi\,A}{C_{per}^2} \qquad \phi_2 = \frac{d_{F(\min)}}{d_{F(\max)}}$$

$$\phi_3 = \frac{d_{F(mean)}}{d_{F(\max)}} \qquad \phi_4 = \frac{d_{F(mean)}}{d_p} \qquad \phi_5 = \frac{d}{d_{F(mean)}} \qquad \phi_6 = \frac{d}{d_{F(\max)}}$$

$$\phi_7 = \frac{d_{F(\min)}}{d_{F(mean)}} \qquad \phi_8 = \frac{2\sqrt{A}}{d_{F(mean)}\sqrt{\pi}} \qquad \phi_9 = \frac{\pi\,d_{F(mean)}}{C_{per}} \qquad \phi_{10} = \frac{2\sqrt{A}}{d_{F(\max)}\sqrt{\pi}}$$

$$\phi_{11} = \frac{C_{per}}{\pi\,d_{F(\max)}} \qquad \phi_{12} = \frac{d_{F(\min)}\sqrt{\pi}}{2\sqrt{A}} \qquad \phi_{13} = \frac{\pi\,d_{F(\min)}}{C_{per}} \qquad \phi_{14} = \frac{2\sqrt{\pi\,A}}{C_{per}}$$

where

A	area of the particle image
c_p	perimeter of a circle of the same area as the particle image
C	circularity
C_{per}	perimeter of the particle image
$d_{F\,(min)}$	minimum Feret diameter measured for all particle orientations
$d_{F\,(max)}$	maximum Feret diameter measured for all particle orientations
$d_{F\,(mean)}$	mean of Feret diameters measured for all particle orientations
d_p	perimeter diameter of the particle
d	particle diameter
s_p	surface area of a sphere of the same volume as the particle
S_p	actual particle surface
ψ	sphericity

4.3 Techniques for particle sizing and characterization

The size of the crystals that have been produced can be measured by a number of techniques. Numerous methods exist for determining crystal size characteristics, and some of them are listed in Table I.

Table 1 Some particle sizing techniques

Technique	Approximate size range (μm)	'Size' measured
Sieving	50 – 5000	aperture
Microscope	1 – 2000	projected area
Electron microscope	0.001 – 5	projected area
Sedimentation	3 – 100	hydrodynamic
Gas adsorption	0.001 – 10	surface area
Zone sensing (Coulter®)	1 – 100	volume
Laser light scattering	0.04 – 2500	mean projected area

The most commonly applied techniques for measuring the size distributions of crystalline product today are laser diffraction and sieving. Laser diffraction is a very popular technique mainly due to its simplicity of operation and good quality of results. The principle of this technique is based on the fact that small particles scatter light further than larger ones. Therefore, though the mathematics is complex, it is possible to determine the size distribution of the analyzed particles by using the light intensities scattered from the sample to detectors installed at different angles. Analysis of the crystals by using sieves is probably the most simple and therefore the most widely used sizing technique both to characterize particulate distributions and to separate them into different size fractions. Test sieves are made to great precision and are subject to various national and international standards.

4.4 Automated image analysis

Changes in the crystallization conditions typically affect not only the size but also the shape of the crystals produced. An ideal technique for characterizing crystalline solids would therefore be one, that could simultaneously provide information on the size and the shape of the analyzed crystals. Currently the only methods that are capable of separating different crystal dimensions from each other and thus generating appropriate shape factors are ones that are based on imaging techniques. The use of different kinds of image analysis techniques for characterizing crystalline solids has been recently reported for example by Lewiner *et al.* (2001a, 2001b, 2002), Bernard-Michel *et al.* (2002), Pons *et al.* (2002), Ålander *et al.* (2003), Faria *et al.* (2003), Hurley *et al.* (2004), Calderon De Anda *et al.* (2005a, 2005b, 2005c) and Ferreira *et al.* (2005). Traditionally image analysis has been carried out using manual microscopy, which is such an arduous method that its utilization in practical applications is rather difficult. Manual microscopy measurements are very time-consuming and for that reason the number of particles that can be analyzed in a reasonable period of time is often not sufficient to ensure that the statistical significance of the obtained results is high enough. The results obtained from microscopy measurements also suffer from operator to operator variability due to the fact that the human operator needs to constantly make selections regarding the examined particles and measured particle dimensions. Most of the difficulties related to manual microscopy can, however, be overcome by using automated image analysis techniques.

5 FILTRATION

The process step following crystallization in suspension is often that of solid-liquid separation. The behaviour of a solid-liquid suspension during the filtration process is mainly determined by the external appearance of the solid particles and also by the material properties of the liquid. Since the external appearance of a crystalline product depends strongly on the applied crystallization conditions, it is obvious that the changes made to the operating parameters of the crystallizer also affect the course of the filtration process. In addition to the changes that occur during the actual filtration process, the variations in the internal structure of the filter cake may also affect the further processing of it. Filtration post-treatment operations, such as cake washing and cake drying, are often exceptionally important in the pharmaceutical industry, where the requirements concerning the purity of the final product are typically strictly predefined. Even though the relationship between crystallization and filtration is widely recognized, the number of publications where both these unit operations have been considered in the same context seems to be surprisingly small.

Although the filtration processes in the pharmaceutical industry are often carried out by using filtration centrifuges, this study focuses only on pressure filtration of crystal suspensions. The main reason for this is that laboratory-scale equipment for studying centrifugal filtration is rarely available and very expensive.

5.1 Filtration Fundamentals

5.1.1 The filtration process

Svarovsky (1993) has defined filtration as a unit process where two phases are separated from a mixture by passing the mixture through a porous medium. The most suitable filtration technique for the separation of a crystalline product from crystallization slurry is cake filtration, because the solids contents of the slurries are usually rather high and the recovered phase of the suspension is solids instead of liquid. The driving force in cake filtration is always the pressure difference over the medium, which can be applied by using a vacuum, gravity, pressure or centrifugal force. The equipment for cake filtration is commonly divided according to the driving force into vacuum, pressure and centrifugal filters.

Similarly to all other unit operations in chemical engineering, filtration is never complete, because perfect separation of two phases is impossible. Some solids may leave with the liquid stream, and some amount of liquid will always stay in the filter cake. The imperfection of the separation can be measured for example as mass fraction of the solids recovered or as dryness of the cake.

5.1.2 Pre-treatment techniques

If the suspension is difficult to filter, it can be pre-treated before the filtration. Pre-treatment usually involves changing the nature of the suspension by either chemical or physical means. Commonly used pre-treatment techniques are for example coagulation, flocculation, pH-adjustment of the suspension and magnetic, electric or acoustic treatment.

5.1.3 Post-treatment processes

After the filtration, the obtained filter cake can also be post-treated. Post-treatment processes are operations by which the solid content of the cake is increased or the contaminant level in the cake is decreased. Typical post-treatment techniques are mechanical squeezing, washing of the cake with wash liquid, and drying of the cake with air or steam.

5.2 Filtration parameters

The filtration characteristics of different kinds of solid-liquid suspensions are often described by means of filter cake resistance, cake porosity and cake compressibility. All these parameters are known to depend, among other factors, on the properties of the solid particles as well as on the material properties of the liquid phase. The most significant particle properties influencing the filtration characteristics are typically assumed to be the particle size and particle shape, as well as the type of size and shape factor distributions. Prediction of the filtration characteristics based on completely theoretical aspects has proven to be very difficult, mainly due to the fact that the number of parameters that influence the filtration process is large and all those parameters should therefore be taken into account simultaneously.

5.2.1 Cake resistance

In filters, the particles become static in a 'bed' or 'filter cake', and in such cases the fluid needs to pass through a fixed array of particles or porous solid and experience drag as it does so. The particles resist the flow, reduce the velocity and give rise to an enhanced pressure drop compared with that in open channel flow. Darcy's law (Darcy, 1856) relates the fluid flow rate to bed pressure drop, depth and permeability

$$u = \frac{1}{A_F}\frac{dV}{dt} = \frac{K_1 \Delta p}{h} \tag{17}$$

where A_F is the filtration area, h the thickness of the filter cake V is the fluid volume collected in time t. Parameter K_1 is the bed permeability – a measure of the total drag force which is a function of both fluid and particle characteristics.

In calculations related to solid/liquid separation processes, the difficulty with which a fluid flows through the pores of a filter cake is usually characterized by the specific cake resistance. According to Svarovsky (2000b), the average specific cake resistance can be determined from the collected experimental data by using equation

$$\frac{dt}{dV} = \frac{\mu c \alpha_{av}}{A_F{}^2 \Delta p} V + \frac{\mu R_m}{A \Delta p} \tag{18}$$

where μ dynamic viscosity of the filtrate

c effective concentration of solids in the suspension

α_{av} average specific filter cake resistance

R_m filter medium resistance

5.2.2 Cake porosity

The volume fraction of pores inside the cake obviously affects the resistance, which leads to another important filtration parameter called porosity (Rushton *et al.,* 2000):

$$\varepsilon = \frac{\text{Volume of particulate voids}}{(\text{Volume of voids} + \text{volume of solids, i.e. total bed volume})}$$

The average porosity of a filter cake is thus defined as the volume fraction of voids in the cake and can be calculated from equation

$$\varepsilon_{av} = \frac{A_F\, h - \dfrac{m_c}{\rho_s}}{A_F\, h} \tag{19}$$

where ε_{av} is the average filter cake porosity, m_c the mass of the dry filter cake, and ρ_s the density of the solids.

The porosity of a packed bed is determined largely by the packing structure of the particles, which means the position of the particles relative to one another in the bed (Wakeman and Tarleton, 1999). Efforts to relate particle characteristics to packing characteristics have been made by several authors (Wakeman, 1975; Yu and Standish, 1993; Hwang *et al.*, 1996; Zou and Yu, 1996; Hwang *et al.*, 1997; Yu *et al.*, 1997; Mota *et al.,* 2001; Abreu *et al.*, 2003; Sorrentino and Anlauf, 2004; Ni *et al.*, 2006). Some fairly accurate models have been derived, but they are mostly suitable only for particles which are homogeneous in size and completely spherical in shape. The porosities of filter cakes consisting of irregular particles therefore need to be determined experimentally.

As mentioned above, the porosity of a filter cake typically depends on the properties of the solid particles and on the pressure that is applied on the cake. Grace (1953a, 1953b) has studied the characteristics of filter cakes obtained from constant-pressure filtration experiments with ten different materials (particle size < 10 μm) in the pressure range from 0.1 to 32.3 bar. The average cake porosities varied from 0.64 to 0.98. A similar study has also been conducted by Tiller (1953) who presented average cake porosities in the range from 0.36 to 0.87. These results were obtained with a simple consolidometer for several different materials in the pressure range from 0.1 to about 6.2 bar. The materials that Tiller used had a larger particle size than the materials studied by Grace, which is perhaps the main reason for the lower porosity values. It is known that the particle size itself does not directly affect the average cake porosity, but when the particles are smaller than approximately 10 μm, they tend to exist mainly as aggregates which have a porous structure and are more complex in shape than the individual primary particles. The influence of particle size on porosity is therefore mostly caused by the porosity of the particle aggregates.

5.2.3 Filter cake compressibility

At the early stages of the filtration process, solid particles form loosely packed layers. When the filtration proceeds, the cake that is formed above these bottom layers begins to compress the particles tighter together. If the cake is incompressible, this compression does not affect the porosity of the cake. This means that the porosity of an incompressible cake is constant at all parts of the cake. If the porosity of a filter cake depends on the stress applied to its particle matrix, it is conventionally described as compressible (Meeten 2000). The porosity of a compressible filter cake is always the smallest close to the filter medium and largest at the upper surface of the cake.

The average specific cake resistance of an incompressible cake is always independent of the applied filtration pressure, because pressure has no effect on the internal structure of the cake. In the case of compressible cakes, the cake resistance becomes a function of the applied pressure in a similar manner as cake porosity. When the pressure is increased, the solid content of a compressible cake increases, which means that lower average porosity and higher average specific cake resistance are observed (Rushton *et al.* 2000). Highest local cake resistances for compressible cakes are always observed in the vicinity of the filter medium (where the local porosity is the lowest), and lowest cake resistances are found at the upper surface of the filter cake (where the local porosities are the highest).

Coarse particles ($d > 50$ μm) are quite incompressible, and usually the compressibility of filter cakes increases with decreasing particle size. Compressibility depends on:

- average particle size
- shape of the particle size distribution
- shape of the particles
- surface properties of the particles

Most real filter cakes are compressible to some extent, which means that an increase in the filtration pressure leads to a decrease in the average cake porosity and an increase in the average cake resistance. Compression of a filter cake is typically a consequence of one or more of three mechanisms, which are:

- rearrangement of solid particles in such a way that the distances between the particles get shorter
- movement of small particles into the gaps between larger particles
- breakage or formation of particles in such a way that the volume of the pores decrease

As a result of compressibility, the internal structure of a compressible filter cake is not homogenous, as it is in the case of an incompressible cake. For compressible cakes, the local cake porosity and local specific cake resistance become functions of the cake thickness in such a manner that the porosity decreases and resistance increases as the distance from the surface of the cake increases. Wakeman and Tarleton (1999) have proposed that the variations of the cake porosity and resistance with pressure can be evaluated by using the simplified empirical equations

$$\alpha = \alpha_0 \Delta p^n \tag{20}$$

$$\varepsilon = \varepsilon_0 \Delta p^{-\lambda} \tag{21}$$

Equations (20) and (21) define four different cake constants that are characteristic for the material in question in the specified pressure range. Constants α_0 and ε_0 are the average cake resistance and the average cake porosity at the pressure of one unit. Constants n and λ are the cake compressibility indices that are related to the cake resistance and cake porosity, respectively. The numerical values of both indices are 0 for totally incompressible cakes and increase as the compressibility of the cake increases. All four constants can be determined by plotting the average cake resistances and average cake porosities as a function of filtration pressure and by fitting typical power curves into the data points.

Some reference values for the cake characteristics have been presented for example by Tiller (1953), Shirato *et al.* (1987) and Wakeman and Tarleton (1999), who have given the values of ε_0 and λ presented for a wide variety of different materials. Tiller (1953) also found out that the porosities of the filter cakes did not increase significantly after the loads were removed from above the cake, and reached an important conclusion that the compression process is essentially irreversible.

5.3 Factors affecting the filterability of suspensions

It is well known that all the parameters most commonly used for describing the properties of filter cakes, i.e. the specific cake resistance, cake porosity and cake compressibility, depend strongly on the properties of the particles (Grace, 1953; Tiller, 1953; Jones *et al.*, 1987; Matthews and Rawlings, 1998; Besra *et al.*, 2000; Iritani *et al.*, 2002; Lee *et al.*, 2003) and of the liquid phase. Therefore a lot of research has been carried out to determine the relationships between the particle properties and the characteristics of packed beds (Wakeman, 1975; Hwang *et al.*, 1996; Zou and Yu, 1996; Hwang *et al.*, 1997; Yu *et al.*, 1997; Mota *et al.,* 2001; Abreu *et al.*, 2003; Sorrentino and Anlauf, 2004; Ni *et al.*, 2006). The most widely applied model for relating the flow velocity of fluid through a bed of solids with the properties of the bed is the well-known Kozeny-Carman equation:

$$u = \frac{\varepsilon^3}{(1-\varepsilon)^2 K S_0^2} \cdot \frac{\Delta p}{\mu h} \tag{22}$$

where K is the Kozeny constant, S_0 is the specific surface area of particles. The Kozeny constant K depends on the structure of the bed and is typically assumed to be 5.0 for randomly packed incompressible beds (Grace, 1953; Tiller, 1953; Coulson and Richardson, 1978). When estimating the effects of particle size and porosity, equation (22) is often modified further and written in terms of specific cake resistance α and equivalent spherical particle size x_p, ($x_p = 6/S_0$), to give:

$$\alpha = \frac{180}{\rho_s x_p^2} \frac{1-\varepsilon}{\varepsilon^3} \tag{23}$$

where ρ_s is the density of solids. Equation (23) now clearly shows the strong influence that porosity and particle size have on the specific cake resistance. The equation assumes that the filter cake consists of monosized spherical or cubical particles, but it is quite obvious that this assumption can only rarely be justified when considering complex real-life suspensions containing particles that vary both in size and shape. Although the use of equations (22) and (23) to actually predict the values of u or α is strictly limited to incompressible filter cakes, these equations are practical for demonstrating the complexity of estimating the properties of compressible cakes.

Due to the differences in the local porosities of compressible filter cakes, the effective surface area of the particles in different parts of the cake is not constant, which means that an accurate value for effective S_0 becomes difficult to estimate. Physical compression of the filter cake often changes the orientation of the particles, influencing also the flow path of the fluid through the cake. Therefore also the value of the Kozeny constant varies as a consequence of compressibility (Grace, 1953). These compression effects cause the local specific cake resistance to vary at different depths of the cake, being lowest at the cake surface and increasing towards the medium.

It now becomes clear that if equations (22) and (23) are applied to predict the flow through compressible cakes, parameters ε, S_0 and K need to be replaced by their average values, which invariably depend on the pressure applied on the cake. Due to the considerable difficulties related to predicting appropriate average values for these parameters without experimental filtration data, the Kozeny-Carman relationship typically fails to provide satisfactory estimates when applied to compressible filter cakes. Even for incompressible cakes that have a constant packing structure throughout the cake, the predictions obtained using equations (22) and (23) with independently determined particle properties are often highly inaccurate. While the specific surface area of particles can be routinely obtained by standard measurement techniques, and relatively accurate estimates for constant K for various particle shapes can be found in the literature (Coulson *et al.* 1978), estimation of the cake porosity from particle characteristics is, however, much more challenging.

The influence of particle properties on the structure of packed beds has been investigated extensively by several authors (Wakeman, 1975; Hwang *et al.*, 1996; Zou and Yu, 1996; Hwang *et al.*, 1997; Yu *et al.*, 1997; Mota *et al.,* 2001; Abreu *et al.*, 2003; Sorrentino and Anlauf, 2004; Ni *et al.*, 2006). The research in this field has been especially active since the last decade due to the new possibilities offered by modern simulation techniques that have become widely available as a result of the rapid development of computers. Most of the experimental, as well as simulated, results that have been presented in the literature clearly indicate that the major factors influencing the porosity of packed beds are the size distribution and the shape of the particles. The distribution of particle shapes within individual suspensions or the existence of size-dependent variations in particle shape most likely also play an

important role in defining the cake porosity, but research papers dealing with these topics do not seem to exist. Despite the significant progress that has been achieved in modelling the relationships between porosity and particle properties, the introduced procedures are still relatively complicated to apply, and it therefore appears that straightforward methods suitable for complex suspensions are not yet available.

In addition to modelling difficulties, the prediction of filter cake properties from particle characteristics is further complicated by the fact that statistically reliable characterization of particle shape is laborious. Complete characterization of particle samples requires the use of image analysis which has traditionally been performed by manual microscopy. This technique, however, is so time-consuming that its utilization as a routine characterization method is rarely possible in practice. The recent development of automatic image analyzers offers a solution for this problem, enabling a large number of particles to be characterized in a reliable and repeatable manner.

The short review presented above implies that the prediction of filter cake properties directly from particle properties using a purely theoretical approach is not yet possible. The main reason is that the growth and structure of filter cakes depend on a numerous variables that should be simultaneously taken into account in the models.

5.3.1 Particle size

Particles to be separated by filtration processes may vary in size from very fine or colloidal matter or molecular aggregates to coarse granular solids. Knowledge of the size of the solid particles in the suspension is vital, because particle size is the most important factor affecting the selection of separation equipment. It can be said in general that the finer the particle size, the more difficult the separation (Svarovsky, 1981a). For example, an increase in particle size by a factor of two leads to a four-fold reduction in cake resistance (Wakeman and Tarleton, 1999), as can also be seen directly in equation (23). The reason for this is the increase of surface area inside the cake. It is also worth mentioning that when the particle size decreases under a few microns, the repulsive forces acting between particles may become significant. Particle size does not have a significant effect on the porosity of the cake.

5.3.2 Particle shape

The importance of particle shape on the behaviour of slurries is well known, but there are no general methods for shape characterization, and therefore the influence of the shape is often neglected (Oja, 1996). The most commonly used method for describing particle shape is to use some of the many different shape factors. Solid particles are seldom either spherical or uniform, and it is rare that the particles to be handled can be defined precisely (Wakeman and Tarleton, 1999). Hwang *et al.* (1996) have studied the effect of particle shape on the structure of the filter cake and found out that the porosity of the cake increases when the particle shape departs from spherical. They have also presented some examples obtained by performing computer simulations. Verification of the simulation results by experiments in their study was, however, insufficient to estimate the reliability of the results.

5.3.3 Particle size distribution

The porosity of a filter cake is strongly dependent also on the particle size distribution of the solids. It has been shown for example by Hwang *et al.* (1997) that the cake porosity decreases with increasing standard deviation of the particle size. The reason for this is that small particles fill the pores between larger particles. This phenomenon also increases the resistance of the cake. Thus the fine particles are particularly important in determining the filtration characteristics of solid-liquid suspensions.

Generalized methods for calculating random packing fractions and co-ordination number from size distributions have been proposed, but they are very complex and usually apply only to spheres having a regular size distribution. Unfortunately, the products of industrial crystallizers frequently contain a wide variety of shapes and sizes, which makes them unsuitable for conventional theories.

5.3.4 Properties of the liquid phase

The most important liquid property that affects the filterability of a suspension is viscosity. The flow of the liquid through the filter cake becomes easier when the viscosity decreases. The viscosity of liquids can usually be lowered quite easily by increasing the temperature of the suspension before it is filtered.

5.4 Filtration of crystal suspensions

Even if the relationship between crystallization and filtration is well recognized, the number of research papers that take both of these processes into account is relatively low in the existing literature. Matthews and Rawlings (1998) have studied the influence of operation conditions of a seeded batch cooling crystallizer on the filterability of a photochemical crystallized from a heptane solvent, and conclude that filter cake resistances could be significantly lowered by optimizing the seeding and cooling policy of the crystallizer. Togkalidou *et al.* (2001) have investigated the relative effects of operating conditions on the filtration process of a suspension produced in a pharmaceutical semicontinuous batch crystallizer. They related the filtration time with six different crystallization variables and generated an empirical main-effects model by using first-order multivariate ordinary least-square regression. By using the operating procedure recommended by this model, the filtration time in the laboratory scale pressure filter was shortened from 57 to 23 minutes, whereas the centrifugation time in a factory-scale perforated basket centrifuge was reduced from 110 h to 30 h. Wibowo *et al.* (2001) have examined crystallization based systems from the perspective of process system engineering and introduced a systematic design procedure for synthesizing crystallization process with the solid-liquid stage downstream of the crystallizer. The two example cases used to illustrate this procedure, which is based entirely on theoretical models, show that the procedure can be successfully used at least to point out the direction of changes caused by certain actions and to identify the need for more accurate experimental data. This procedure has been extended also to take into account the possible bulk solids processing equipment following the solid-liquid separation process, such as crushers, blenders, granulators and dryers (Wibowo and Ng, 2002).

The results introduced in the articles mentioned above inevitably show that significant improvements in the performance of the solid-liquid separation processes can be achieved by optimizing the operation of the crystallizer. However, the presented conclusions are mostly based on theoretical considerations, and the verification of these assumptions by a broad set of experimental filtration data seems to be missing.

6 EXPERIMENTAL WORK

The objective of the experimental work introduced in this thesis was to determine the influence of several different crystallization conditions on the size and shape of the crystals produced, and further, on the pressure filtration characteristics of the crystal suspensions obtained from an unseeded batch cooling crystallizer. The model compound that was used in all experiments was sulphathiazole, which is a well-known antibiotic agent that exists in several crystal modifications.

The different crystallization conditions that were considered in the experiments were:

1) the composition of the solvent
2) the cooling rate applied during the experiments which were carried out by using linear cooling profiles
3) the type of the cooling profile
4) the type of the mixer and mixing intensity

All crystallization experiments were performed in a laboratory-scale cooling crystallizer without seed crystals. The produced crystal suspensions were thoroughly characterized, after which the crystals were separated from the solvents through constant pressure batch filtration experiments. The filtration characteristics of different suspensions were evaluated from some commonly used filtration parameters, which were calculated from the experimentally obtained data. The main stages of the experimental work are summarized in Figure 3, and more detailed descriptions of each stage are given in the following chapters. The experimental design regarding all the experiments and analyses carried out in this project is presented in Appendix I.

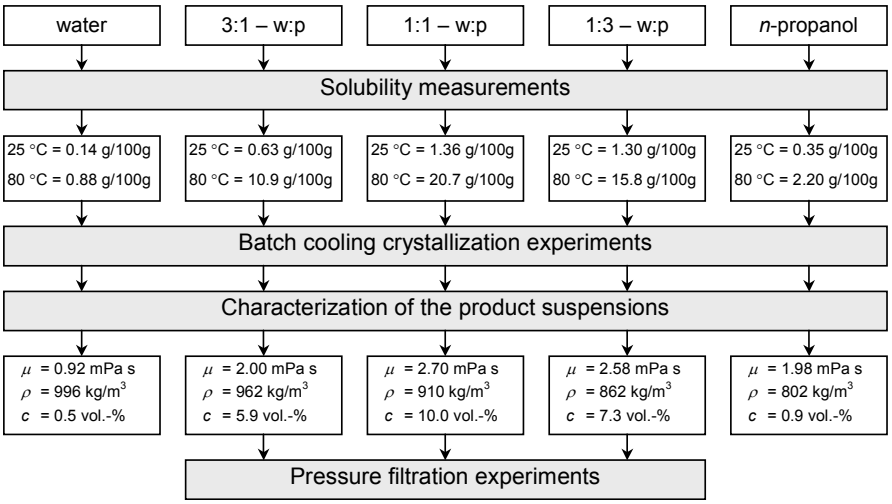

Figure 3 Schematic illustration of the experimental procedure

6.1 Materials

The crystallized material in all experiments was pharmaceutical grade (European Pharmacopoeia/United States Pharmacopoeia) sulphathiazole ($C_9H_9N_3O_2S_2$) supplied by Industrias GMB S.A., Castellbisbal, Barcelona, Spain, and the solvents used in the experiments were different mixtures of deionized water and GC-grade *n*-propanol [purity > 99.7 % (w/w); Aspokem Oy, Helsinki, Finland].

6.1.1 Sulphathiazole

Sulphathiazole, which is a well-known antibiotic agent, has been the subject of numerous investigations concerning organic polymorphism and crystal growth. The molecular structure of sulphathiazole enables it to form a large variety of hydrogen-bonded networks, which makes it an interesting compound for crystallographic studies (Aaltonen *et al.*, 2003). In the works reported in the literature, there appears to be some discrepancies over the number of crystal modifications that exist and the nomenclature regarding the said modifications (Apperley *et al.*, 1999). The reported number of different modifications ranges from two to five with habits including hexagons, plates, rods, and squares (Anderson *et al.,* 2001). Despite the differences between the earlier works, the common opinion currently is that the number of different crystal modifications of sulphathiazole is at least four. The behavior and properties of the different crystal modifications of sulphathiazole have been reported

for example by Khoshkhoo and Anwar (1993), Byrn *et al.* (1999), Anwar *et al.* (1989), Chan *et al.* (1999), Blagden *et al.* (1998a and 1998b), Threlfall (2000), Apperley *et al.* (1999), Bladgen (2001), Anderson *et al.* (2001), and Aaltonen *et al.* (2003). All these papers consider the crystallization process in a very small scale only (mostly in laboratory test tubes), and the crystal properties and filtration characteristics of sulphathiazole have not been presented anywhere.

As mentioned, sulphathiazole is capable of existing as several different crystal modifications. One of the aims in this project was to determine the effect of crystallization conditions on the resulting crystal modification. This part of the study is, however, not considered in this thesis because it was mainly performed by the other members of the research group. Some of the results regarding the observed crystal modifications have already been published earlier (Pöllänen *et al.* 2005b, 2005c). Based on these results, it was concluded that neither the raw material used in the experiments, nor any of the obtained products consisted of only one crystal modification but were mixtures of several different modifications.

6.2 Solubility measurements

Accurate control over any cooling crystallization process requires knowledge on the solubility data of the crystallized substance in the chosen solvent. This is why the solubility of sulphathiazole at different temperatures and in different solvents had to be determined before any crystallization experiments could be performed. The solubilities were determined in pure water, in pure *n*-propanol and in three different binary mixtures, wherein the weight fractions of water and *n*-propanol were 1:3, 1:1 and 3:1. The solubilities, which are presented in Figure 4 at temperatures from 10 °C to 80 °C with increments of 10 °C, were determined gravimetrically, and the measurements were duplicated twice in order to achieve sufficient accuracy. Precisely weighed samples, which were taken from the saturated homogeneous solutions at different temperatures through a 0.2 μm membrane filter, were evaporated to dryness at 125 °C and reweighed. Figure 4 shows the results from three parallel measurements carried out for each solvent and temperature. As can be noticed, the variation between the results obtained from similar measurements is fairly small. Some scattering can be observed at the highest temperature (80 °C) and it is assumed that this is mostly due to the evaporation of the solvent during the processing of the samples.

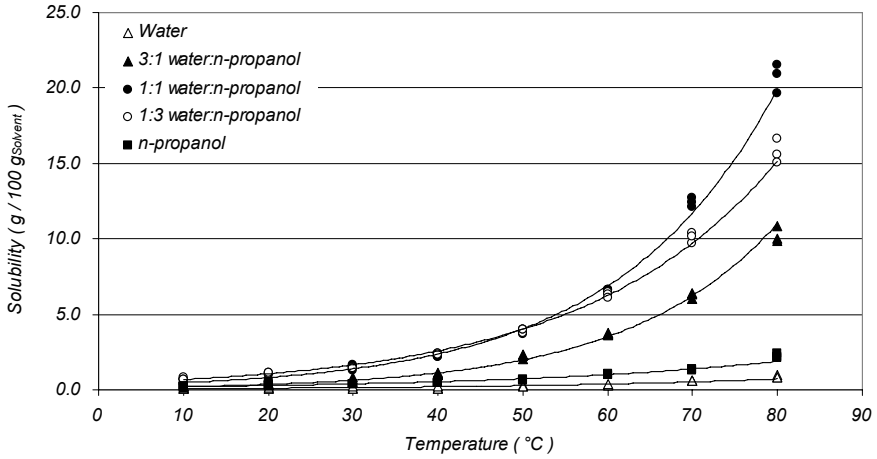

Figure 4 Solubilities of sulphathiazole in five different water:*n*-propanol solutions at temperature range from 10 °C to 80 °C. The results from three parallel measurements are presented for each solvent and temperature.

The solid concentrations of the product suspensions obtained from the crystallizer depend on the difference in solubilities between the initial and final temperatures of the cooling crystallization process. As it can be seen in the results presented in Figure 4, the solubility of sulphathiazole in pure water and in pure *n*-propanol was very low, which would have resulted in unacceptably low solid concentrations when considering the following pressure filtration experiments. Therefore the only solvents that were chosen to be used in the filtration experiments were the three different mixtures of water and *n*-propanol. The solubilities in these mixtures were clearly higher than in the pure solvents, and therefore also the solid concentrations of the final crystal suspensions were high enough for the filtration experiments.

6.3 Crystallization experiments

Unseeded laboratory scale batch cooling crystallization experiments were carried out using various cooling rates, cooling profiles and mixing conditions. All crystallization experiments were performed in a jacketed 4.0 dm^3 glass crystallizer (height = 250 mm, diameter = 160 mm), which was equipped with a programmable LAUDA RK 8 KP-thermostat unit and a condenser. Schematic illustration of the crystallization equipment is presented in Figure 5 and the exact dimensions of the crystallizer are presented later in Figure 8. Draft tube was not used in any of the experiments performed during this study.

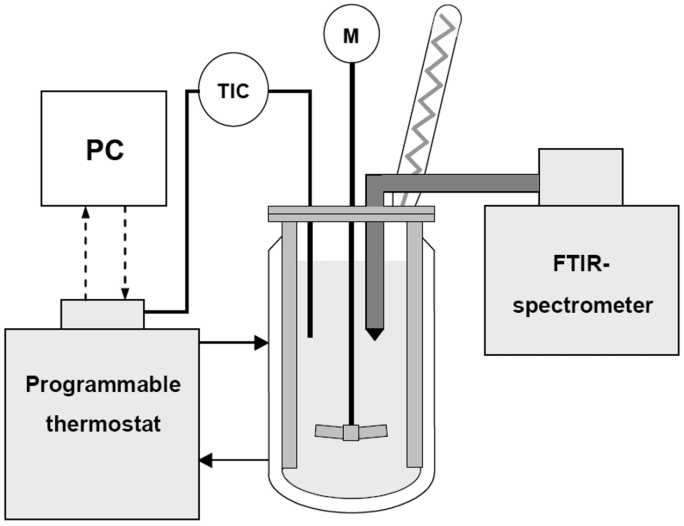

Figure 5 Crystallization equipment

The temperature in the crystallizer was measured with a Pt-100 sensor and registered on a computer. The crystallizer was also equipped with a BOMEM MB 155 spectrometer and Dipper 210 ATR-probe, which could be used for measuring the concentration of dissolved sulphathiazole in the solution during the crystallization process. The ATR-measurements and the resulting concentration profiles are not, however, considered in this thesis, because they were performed by other members of the research group. The main results obtained from the ATR-measurements and related analyses have been published elsewhere (Pöllänen *et al.* 2005a, 2005b, 2005c, 2006a and 2006b).

The batches for the crystallization experiments were prepared by introducing approximately 4.0 dm^3 of solvent mixture into the crystallizer and adding such an amount of sulphathiazole that it corresponded with the solubility in the chosen solvent at 80 °C. The solubility curves for different solvents were presented in Figure 4, and the exact numerical values can be found in Figure 3. Next, the solution was heated from 25 °C to 85 °C in two hours and kept at the constant temperature of 85 °C for one hour. The purpose of this procedure was to make certain that all the added sulphathiazole was dissolved before the beginning of the cooling stage. The cooling of the crystallizer was performed by using different cooling profiles and cooling times for the temperature interval from 80 °C to 25 °C.

6.3.1 Crystallization experiments for defining the influence of solvent composition

The first part of the experiments was carried out to compare the influence of solvent composition on the crystal properties and on the filtration characteristics of the sulphathiazole suspensions. These experiments were made by using pure water, pure *n*-propanol and three different binary mixtures as solvents. The weight fractions of water and *n*-propanol in the binary mixtures were 1:3, 1:1 and 3:1. The cooling in all of these experiments was carried out using a linear cooling policy with a constant cooling rate of either 27.5 °C/h or 3.9 °C/h, which resulted in total cooling times of 2.0 h or 14.0 h, respectively, for the temperature interval from 80 °C to 25 °C. The mixing was done with a three-blade curved blade impeller and four baffles, which were all made of PTFE. The rotation speed of the impeller in all tests was 400 rpm.

6.3.2 Crystallization experiments for defining the influence of cooling rate

Batch crystallization experiments for defining the influence of cooling rate were made with four different cooling rates, which were maintained constant throughout the whole crystallization process. The mixing was performed with a three-blade curved blade impeller at an agitation rate of 400 rpm. Experiments were made with four different constant cooling rates, which were 3.9, 5.5, 9.2 and 27.5 °C/h, which resulted in cooling times of 14.0, 10.0, 6.0 and 2.0 h for the temperature interval from 80 °C to 25 °C. The three different solvent mixtures were used with each cooling rate. A typical experimental procedure is clarified in Figure 6, which shows the measured temperatures inside the crystallizer during the different batches.

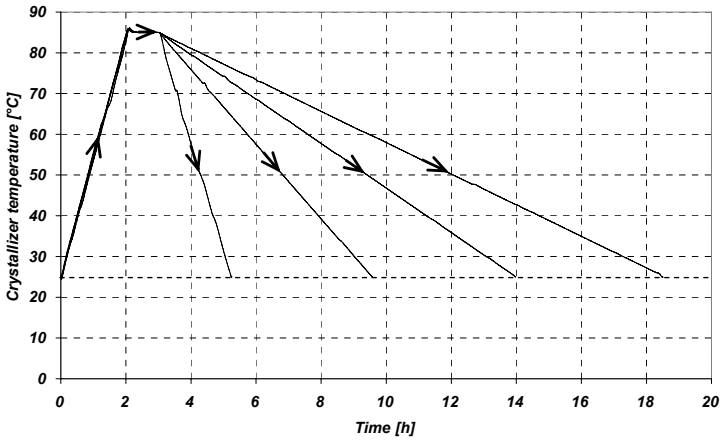

Figure 6 Measured temperature profiles inside the crystallizer during crystallization experiments at four different constant cooling rates.

6.3.3 Crystallization experiments for defining the influence of cooling profile

In this part of the study, unseeded batch cooling crystallization experiments were performed using three different cooling profiles. Typical experimental procedures are illustrated in Figure 7, which shows the measured temperature profiles inside the crystallizer during the different batches. The mixing was once again done with a three-blade curved blade impeller and four baffles, which were all made of PTFE. The rotation speed of the impeller in all experiments was 400 rpm.

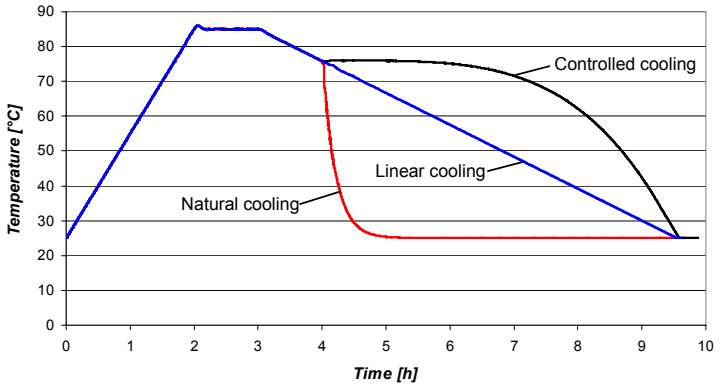

Figure 7 Examples of measured temperature profiles during the crystallization experiments with different cooling policies.

As in the earlier test series, the crystallization experiments were started by introducing approximately 4.0 dm^3 of the solvent mixture in the crystallizer and adding such a quantity of sulphathiazole that it corresponded to the measured solubility at 80 °C. After the raw materials had been introduced, the temperature of the solution was raised from 25 °C to 85 °C in two hours and maintained at that temperature for one hour so that all the added sulphathiazole was dissolved before the cooling stage.

The first crystallization experiments in this test series were carried out using a linear cooling profile, which means that the solution was cooled down from 85 °C to 25 °C with a constant cooling rate of 9.17 °C/h, which resulted in a cooling time of 6.0 h for the temperature interval from 80 °C to 25 °C. By using the temperature data collected during these experiments, it was possible to detect the point where the first crystals appeared spontaneously into the solutions when the limit of the metastable zone was exceeded. It was necessary to determine this so-called nucleation temperature before the experiments with the other cooling profiles could be performed, as the starting point (T_s) of the other profiles was decided to be 1.0 °C above the spontaneous nucleation temperature. At this temperature, the solution was clearly supersaturated but no crystals were present in the solution yet.

After the nucleation points for all the different solvent systems had been determined, crystallization experiments with natural and controlled cooling profiles were carried out. In these experiments, the solution was first cooled down from 85 °C to T_s with the cooling rate of 9.17 °C/h, after which the chosen cooling profile was started. The experiments with the natural cooling profile were performed by rapidly changing the temperature of the cooling medium to a constant temperature of 25 °C, which resulted in very high initial cooling rates and considerably lower cooling rates at the end of the batch. The experiments with the controlled cooling profile were performed using a PC that controlled the thermostat unit in such a way that the temperature in the crystallizer accurately followed the predefined profile that was calculated from equation (11) presented by Mullin and Nyvlt (1971).

Cooling profiles that would have taken into account the nonlinearity in the solubility curves of sulphathiazole, for example the profile derived by Alatalo *et al.* (1999), could not be utilized in the performed crystallization experiments because the required cooling rates at the final parts of the batch were so high that they could not be fully

followed in an accurately controlled manner with the available thermostat units. Typically, the most significant disadvantages of batch crystallization processes are their uncertainty and poor reproducibility (Lang *et al.* 1999), and therefore all crystallization experiments were repeated at least once. As considerable batch-to-batch variations were not observed between the properties of the product crystals obtained from parallel batches, the reproducibility of the crystallization experiments was considered to be sufficiently good.

6.3.4 Crystallization experiments for defining the influence of mixing conditions

The target of the last part of the experiments in this study was to explore the impact of mixing conditions in an unseeded batch cooling crystallizer on the crystal characteristics, and further, on the filterability of the final crystal suspension. The mixing of the solutions during the crystallization experiments was carried out with four different types of impellers, the designs of which are presented in Figure 8, and three different agitation rates with each impeller (shown in Table II). The purpose was to choose the impeller geometries in such a way that significant differences would exist between the different mixing regimes. The anchor impeller is a typical laminar flow impeller, which generates small shear stresses and is operated at relatively low rotation speeds. The bar turbine, on the other hand, generates a strongly turbulent flow with high shear stresses, and therefore needs to be operated at high rotation speeds. The curved blade and pitched blade turbines are both typical turbulent flow impellers, which are operated at medium rotation speeds. The main difference between these two types of turbines is that the flow generated by the curved blade turbine is mainly radial, whereas the pitched blade turbine also generates an axial flow towards the bottom of the crystallizer. The crystallizer could also be equipped with four baffles to prevent vortexing behavior of the suspension. The agitation rates used during the experiments, as well as the relevant dimensions for the different impellers are presented in Table II. The lowest agitation rates correspond to the minimum rotation speeds that were necessary to avoid the settling of the crystals. The highest agitation rates, on the other hand, are the maximum rotational speeds that could be used before the suspension began to splash too fiercely in the crystallizer.

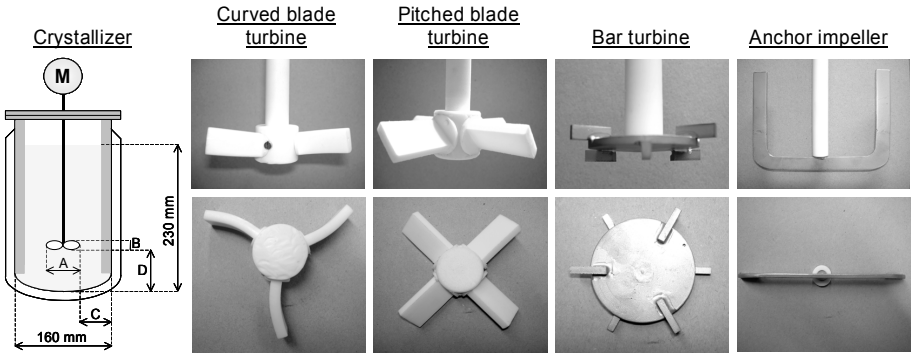

Figure 8 Schematic illustration of the crystallizer and the geometries of the four different impellers used in the batch cooling crystallization experiments.

Table II Dimensions of different impellers and the agitation rates used in the batch cooling crystallization experiments.

	Curved blade turbine	Pitched blade turbine	Bar turbine	Anchor impeller
Impeller diameter (A), mm	100	100	58	140
Impeller height (B), mm	20	17	13	100
Wall clearance (C), mm	30	30	51	10
Off-bottom clearance (D), mm	60	60	75	10
Number of blades	3	4	6	2
Number of baffles	4	4	4	0
Agitation rate 1, rpm	250	250	900	100
Agitation rate 2, rpm	400	400	1200	175
Agitation rate 3, rpm	550	550	1500	250

As can be noticed from the values presented in Table II, there were fairly large differences between the rotation speeds used with the different kinds of impellers. This is obviously due to the different diameters and operation principles of the compared impellers. The comparison between these impellers should most likely be done by using the effective mixing power as the basis of comparison. Some attempts were made to measure the mixing powers during the crystallization experiments but the results were found to be unreliable and that is the reason why the different impellers are compared in this thesis according to the applied rotation speeds. Exact determination of the effective mixing power is one of the topics that will be investigated in the future studies.

6.4 Characterization of the crystal suspensions

The characterization of the suspensions obtained from the crystallizer included the adjustment of solid concentration to 10 vol-% prior to filtration, experimental determination of filtrate density and viscosity, and analysis of crystal size and shape.

6.4.1 Solid concentration

As the final solid concentration of the suspension was determined by the solubility of sulphathiazole, the differences between the batches crystallized from different solvents were rather remarkable. As has been shown for example by Svarovsky (2000b), differences in the solid concentration can have a major influence on the filterability of a suspension. As the main aim of this study was to examine the differences caused by the crystallized material only, the solid concentrations were adjusted before the suspensions were filtered. This was done by first allowing the crystals to sediment and then removing such a volume of clear solvent from the crystallizer that the calculated solid concentrations were about 10.0 vol-%.

6.4.2 Solvent properties

The dynamic viscosity and density of the filtrate are important liquid properties when different filtration parameters are determined. As most of the solvents used in the experiments of this study were binary mixtures of water and *n*-propanol, and all the solvents were saturated with sulphathiazole, accurate values for density and viscosity could not be found in the existing literature. Therefore they were determined experimentally for all five solvent systems at 25 °C. Dynamic viscosities were measured by Schott-Geräte capillary viscometers, and densities were determined gravimetrically. All measurements were carried out three times in order to achieve sufficient accuracy, and the differences between the values obtained with parallel samples were found to be less than 2 % in all cases. The average results obtained from these measurements are presented in Table III.

Table III Measured densities and dynamic viscosities of the different solvents saturated with sulphathiazole at 25 ºC.

Solvent	Density	Dynamic viscosity
[-]	*[kg/m3]*	*[mPa s]*
water	996	0,92
3: 1 - water: *n* -propanol	910	2,00
1: 1 - water: *n* -propanol	962	2,70
1: 3 - water: *n* -propanol	862	2,58
n -propanol	802	1,98

6.4.3 Analysis of crystal size and shape

The samples for crystal characterization were collected immediately after the crystallization experiments at four different locations in the crystallizer by using a vacuum pipe. The four samples, which were combined to form a composite sample, were always taken from a mixed suspension in order to reduce undesired classification due to sedimentation of the largest crystals. The volume of each composite sample was approximately 500 ml, which corresponded to roughly 1/8 of the total volume of the crystal suspensions. The crystals of these composite samples were gently separated from the solvent with a Büchner funnel and dried in a vacuum oven. The dry crystals were then used for size and shape analyses that were performed using an automated image analyser (PharmaVision 830, Malvern Instruments, Ltd.).

The samples for the analyses were prepared by dispersing the crystals evenly onto a 100×100 mm sample plate placed underneath a video camera. The camera was then moved across the sample tray in a pre-programmed way by linear actuators, and a large set of digitized video images was automatically acquired. The obtained raw video images were processed using the PharmaVision 830 software (version 4.2.1.15) that separated all the crystals from the images and determined a set of various morphological parameters separately for each individual crystal in the sample. The completely automated operation of the analyzer meant that it was possible to analyze enough particles routinely in a reasonable period of time (approximately 20 000 particles in 10 minutes) in order to obtain results with sufficient statistical significance. The number of crystals analyzed from each sample in this study was approximately 100 000 – 200 000, depending on the properties of the crystals. Each crystal was described by 7 different size and shape parameters:

Mean Diameter: A value obtained by measuring the radius from the center of mass to the edge of the particle in steps of 3° and by calculating the mean value of these measurements.

Diameter: The diameter that is equal to the diameter of a circle with the same projected area as the particle.

Max Distance: The absolute maximum distance found within the particle.

Width: All possible lines from one point on the perimeter to another point on the perimeter are projected on the minor axis. The maximum length of these projections is the width of the object.

Length: All possible points from one point on the perimeter to another point on the perimeter are projected on the major axis. The maximum length of these projections is the length of the object.

Area: The visual projected surface area of the particle.

Roundness: The length-width relationship. A circle has the value 1.0; a rod approaches 0.

Convexity: The convexity is the object area divided by the area enclosed by an imaginary "rubber band" wrapped around the object. A circle has the value 1.0, a porous particle has a lower value, approaching 0.

The data obtained in the image analyses were used to create differential distributions for each size and shape parameter and for each crystal sample separately. These distributions were calculated in such a way that the number of classes in all distributions was 52.

Optimal conditions for the image analysis can only be achieved when the crystals are dispersed onto the sample plate in a mono-layer, as otherwise the obtained results may be significantly distorted as a result of overlapping of the analysed crystals. The formation of a perfect mono-layer is never possible in practice, and therefore the influence of the overlapping crystals needs to be eliminated somehow. By comparing the crystal images provided by the PharmaVision and the morphological parameters of the individual crystals, it was possible to detect the objects that contained overlapping crystals and automatically discharge them from the original data. This

technique was used here to ascertain that the results truly described the dimensions of individual crystals. Two or three sub-samples (approximately 0.3 – 0.4 g each) were taken from the dried composite samples and analyzed separately, and the crystal data obtained from these analyses were combined to give an average result.

An example of the different distributions for one of the crystal samples is given in Figure 9. In addition to the crystal data, Figure 9 also contains some properties of the solvent. As mentioned above, the crystallization experiments were performed with three different solvent mixtures. The viscosities and densities of these mixtures varied slightly, as can be seen in the experimentally determined values given in Table III. These values were included in the suspension data by simply forming distributions with a constant value for all classes.

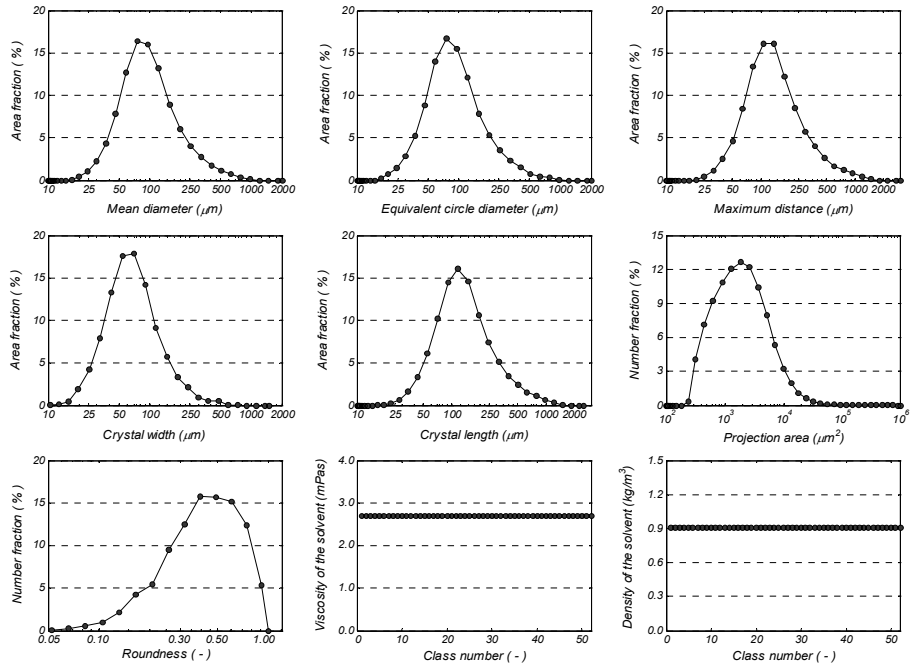

Figure 9 An example of the crystal and solvent data for one of the considered crystal suspensions

6.5 Filtration experiments

After the solid concentration of the suspension was adjusted to about 10 vol-%, the crystals were separated from the solvent through pressure filtration. As the solubilities of sulphathiazole in pure water and in pure *n*-propanol were low, the amount of product crystals obtained from one batch was too small for filtration experiments. Hence filtration experiments were made only with those three suspensions that were crystallized from the mixtures of water and *n*-propanol. The filtration experiments were carried out with a laboratory-scale pressure Nutsche filter (Seitz EDF 6-03, SeitzSchenk Filtersystems GmbH, Bad Kreuznach, Germany) that was equipped with a data collection program. A photo of the filter is shown in Figure 10.

The filtration pressure was produced with pressurized nitrogen and was measured and collected on a computer with a pressure transmitter of an accuracy of 0.01 bar. The filtration chamber volume was 350 ml and the area of the horizontal filtration surface was 19.6 cm^2. Seitz T-1000 cellulose discs, which were wetted with the filtrate before the experiments, were used as the filter media. The filtration pressure, as well as the cumulative mass of the filtrate, which was collected onto a scale with a resolution of 0.1 g, were registered by the data collection program using a 0.4 second sampling time. Immediately after the flow of filtrate had ceased, the thickness of the formed filter cake was measured and the cake was then removed from the filter chamber and weighed. The residual solvent contents of the crystal cakes were determined through thermal drying. The constant pressure filtration experiments were conducted in a pressure interval from 0.5 to 4.0 bar with increments of 0.5 bar in a completely random order and were all repeated at least once.

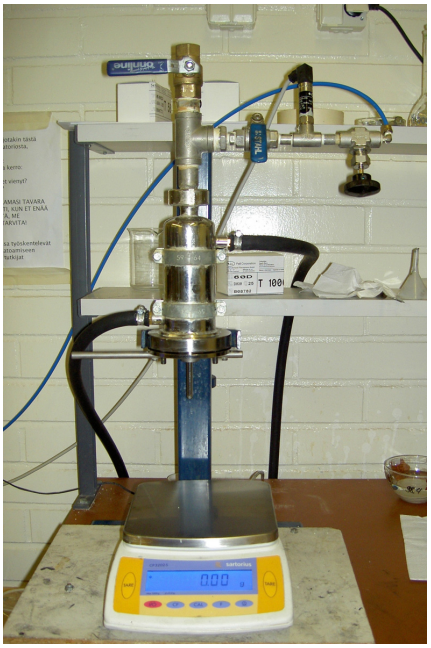

Figure 10 Laboratory-scale pressure Nutsche filter.

The parameters that were used to describe the filterability of the crystal suspensions were the average cake porosity and the average specific cake resistance, which were determined from the data collected during the experiments. Examples of the collected filtration data for one of the sample suspensions are presented in Figure 11 that shows the cumulative filtrate curves with four different filtration pressures. The average cake porosities were calculated using the measured values of cake height and dry cake mass, and the average cake resistances were determined from the plots of t/V vs. V using the classical constant pressure filtration equation derived from Darcy's law.

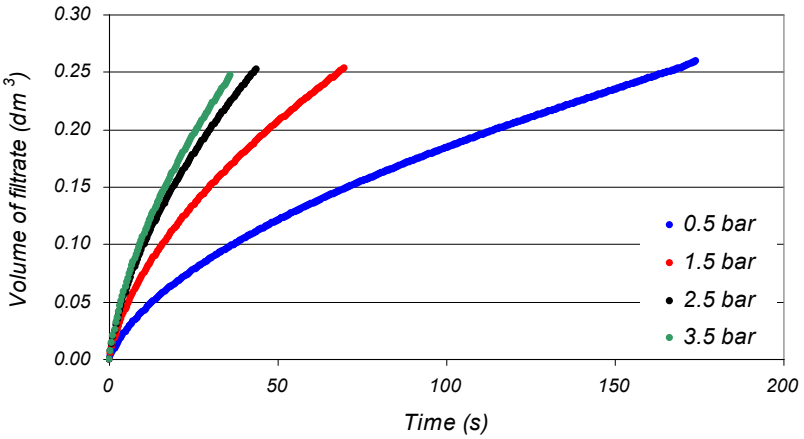

Figure 11 Examples of the data collected during the experiments for one of the tests suspensions.

Also the compressibility coefficients of the cakes were evaluated by using equations (20) and (21), where α_0 and ε_0 are empirical constants that in this case correspond to the values of the average cake resistance and the average cake porosity at 1.0 bar. An example of the determined filtration data for one of the sulphathiazole suspensions studied is given in Figure 12, which shows the average specific cake resistances and cake porosities as a function of the applied filtration pressure. The form of the two trendline equations presented in Figure 12 is similar to the form of the equations (20) and (21), and therefore the necessary parameters α_0, n, ε_0 and λ could be readily obtained from them.

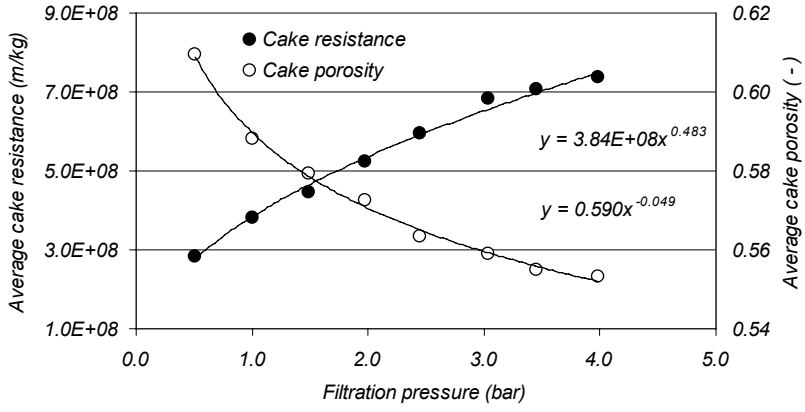

Figure 12 An example of experimental filtration data for one of the studied sulphathiazole suspensions.

7 RESULTS

This chapter contains the main results obtained from all the experiments. The structure of the experimental procedure was presented in Figure 3, and detailed experimental designs can be found in Appendix I.

Most of the crystallization experiments were repeated at least once. The crystal size and shape factor distributions that are presented in this chapter are therefore averages obtained from parallel experiments. The differences in statistical parameters between the parallel results were typically less than 5 %, which means that the average graphs presented here can be considered fairly reliable.

The image analysis software produced a very large amount of data, and presenting it all in this context is not possible. It was decided that the most descriptive parameter for illustrating the size of the produced crystals was the ‘Mean Diameter’, which was obtained by measuring the radius from the center of mass to the edge of the particle in steps of 3° and by calculating the mean value of these measurements. The shape of the crystals was presented in all cases by using the so-called ‘Aspect Ratio’, that was obtained by dividing the length of the crystal by its width. This chapter thus contains the ‘Mean Diameter’ and ‘Aspect Ratio’ distributions for the obtained crystal products. The mean diameters were presented in all cases as surface area distributions and the aspect ratios as number distributions. Comparison between the alternative methods to present the size and shape data revealed that these were the most illustrative graphs for investigating the differences between the crystal samples.

The graphs that present the results of the filtration experiments contain all the data points obtained also from the parallel tests. The reason for this is to show the variation between the experimentally determined filtration characteristics. As can be noticed, however, the variation is quite small in most cases. The actual equations (20) and (21) are not presented directly in the graphs, but the important filtration parameters existing in these equations are summarized in the tables in each sub-chapter.

7.1 Influence of the solvent composition

The first part of the experiments was carried out to determine the influence of the solvent composition on the crystal properties and on the filtration characteristics of the sulphathiazole suspensions. These experiments were made by using pure water, pure *n*-propanol and three different binary mixtures as solvents. The weight fractions of water and *n*-propanol in the binary mixtures were 1:3, 1:1 and 3:1. The cooling in all these experiments was carried out using a linear cooling policy with a constant cooling rate of either 27.5 °C/h or 3.9 °C/h, which resulted in total cooling times of 2.0 h or 14.0 h, respectively, for the temperature interval from 80 °C to 25 °C.

7.1.1 Crystal size and shape

7.1.1.1 Short cooling time

The size distributions of the crystals obtained in the crystallization experiments with five different solvents with the cooling time of 2 h are presented in Figure 13, and the shape factor distributions for the same samples are presented in Figure 14. The statistical parameters of the crystal size distributions, as well as the crystal shape distributions are summarized in Table IV. Some examples of the product crystals are also presented in the microscope images shown in Figure 15.

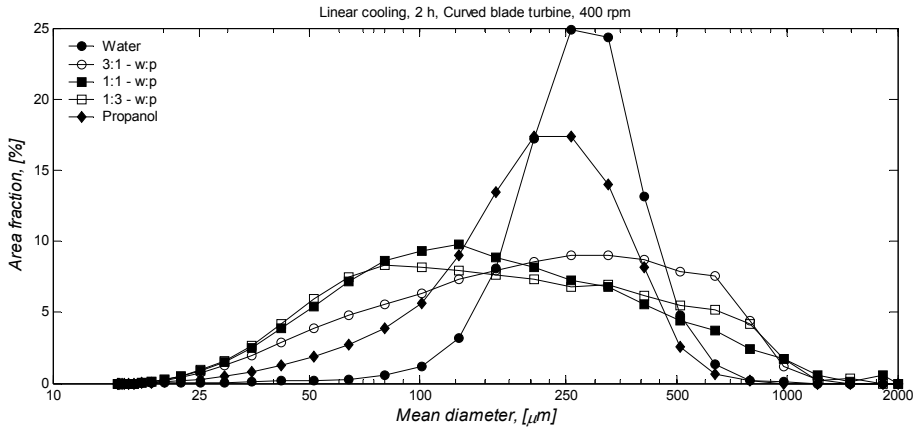

Figure 13 Crystal size distributions of sulphathiazole crystallized from five different mixtures of water and *n*-propanol with a cooling time of 2 h.

As can be seen in the crystal size distributions presented in Figure 13 and Table IV, the solvent composition has a great influence on the size of the crystals produced. The

size distributions of the crystals obtained from the three solvent mixtures are very wide, whereas the use of two pure solvents results in narrow distributions. The differences in the median sizes of the different samples are fairly small. The largest median size (272 μm) is observed with the crystals obtained from pure water, whereas the smallest crystals (143 μm) are obtained from 1:1 water:*n*-propanol mixture. The most significant difference between the crystal size distributions of these samples is thus seen in the widths of the distributions.

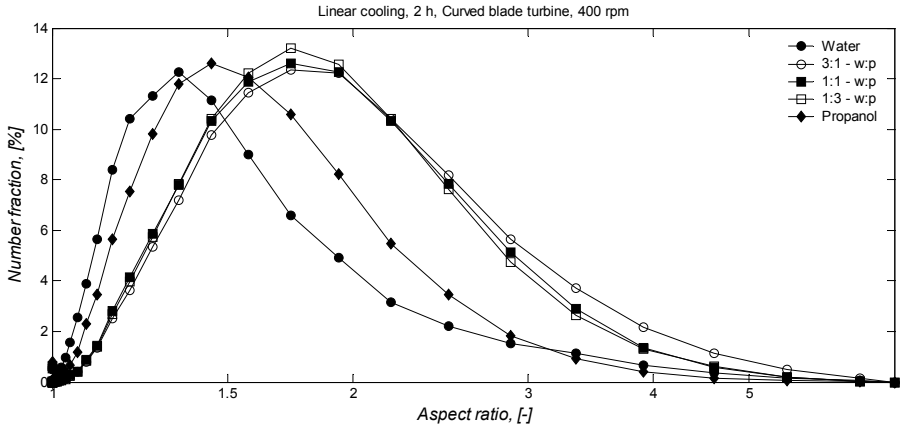

Figure 14 Crystal shape distributions of sulphathiazole crystallized from different mixtures of water and *n*-propanol with a cooling time of 2 h.

Figures 14 and 15 show that the composition of the solvent has a great influence on the shape of the crystals produced. The crystals obtained from the binary mixtures are more elongated than the crystals obtained from pure solvents, and significant differences do not seem to exist between the samples obtained from the three binary solvent mixtures.

Table IV Statistical parameters of the crystal size and shape distributions of sulphathiazole crystallized from different mixtures of water and *n*-propanol with the cooling time of 2 h.

	Cooling	Cooling		Mixing	Mean diameter *[2,2]*			Aspect Ratio *[1,0]*		
Solvent	method	time	Impeller	speed	MD_{10}	MD_{50}	MD_{90}	AR_{10}	AR_{50}	AR_{90}
(-)	(-)	(h)	(-)	(RPM)	(μm)	(μm)	(μm)	(-)	(-)	(-)
Water	Linear	2	CBT	400	165.0	272.0	417.0	1.09	1.32	2.00
3:1-w:p	Linear	2	CBT	400	52.8	217.0	623.0	1.23	1.74	2.89
1:1-w:p	Linear	2	CBT	400	47.0	143.0	542.0	1.21	1.69	2.68
1:3-w:p	Linear	2	CBT	400	45.8	151.0	606.0	1.22	1.69	2.65
n-propanol	Linear	2	CBT	400	81.9	208.0	372.0	1.13	1.44	2.15

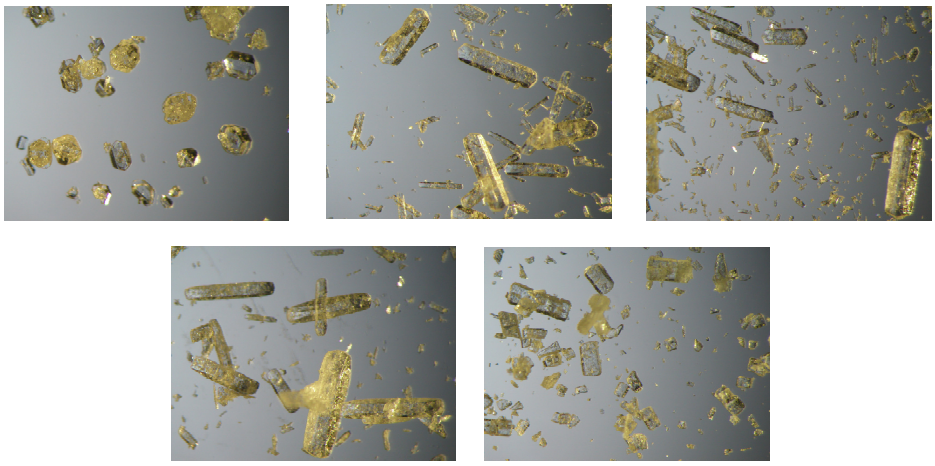

Figure 15 Examples of the sulphathiazole crystals obtained from different mixtures of water and *n*-propanol with a cooling time of 2 h

7.1.1.2 Long cooling time

The size distributions of the crystals obtained from the crystallization experiments with five different solvents with the cooling time of 14 h are presented in Figure 16, and the shape factor distributions for the same samples are presented in Figure 17. Some examples of the product crystals are also presented as SEM-images in Figure 18. The statistical parameters of the crystal size, as well as the crystal shape distributions are summarized in Table V.

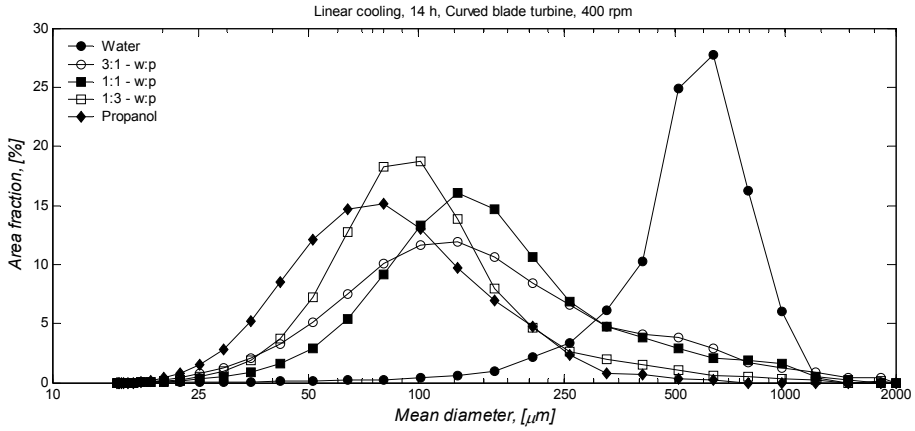

Figure 16 Crystal size distributions of sulphathiazole crystallized from different mixtures of water and *n*-propanol with the cooling time of 14 h.

The results presented in Figures 16 and 17 and in Table V clearly show that the composition of the solvent has a major influence on the shape and size of the obtained crystals also with the longer cooling time. The size distributions of the crystals obtained from the solvent mixtures are now narrower than those with the short cooling time. This is most probably a consequence of reduced primary nucleation due to the lower supersaturation during the crystallization. It can also be noticed that the size of the crystals obtained from pure propanol is now smaller than the size of the crystals obtained from the solvent mixtures. The crystals obtained from pure water are clearly larger than the crystals obtained from other solvents, and their size distribution is much narrower. The comparison of the shape factor distributions presented in Figure 17 shows that the differences in crystal shapes are now much smaller than with the shorter cooling time. Only the crystals obtained from water seem to deviate significantly from the other solvents. It can also be observed in the SEM-images presented in Figure 18 that the crystals grown from water are mainly shaped as hexagonal plates, whereas the crystals obtained from *n*-propanol seem to have a tendency to exist as stars consisting of small needle-like dendrites. The crystals obtained from the binary mixtures exist mostly as elongated rods, but a large amount of irregularly shaped small crystals can also be observed, especially in the image taken from the crystals obtained from 1:3 – water:*n*-propanol mixture.

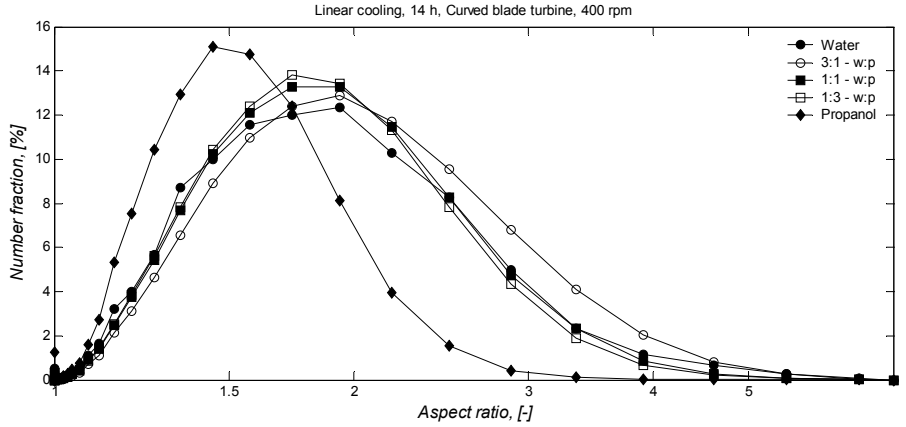

Figure 17 Crystal shape distributions of sulphathiazole crystallized from different mixtures of water and n-propanol with the cooling time of 14 h.

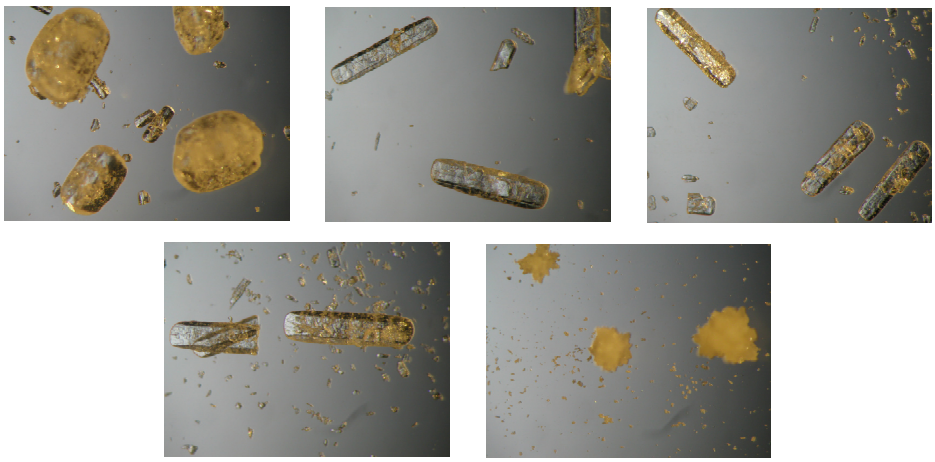

Figure 18 Examples of the sulphathiazole crystals obtained from different mixtures of water and *n*-propanol with a cooling time of 14 h

Table V Statistical parameters of the crystal size and shape distributions of sulphathiazole crystallized from different mixtures of water and *n*-propanol with the cooling time of 14 h

Solvent	Cooling method	Cooling time	Impeller	Mixing speed	Mean diameter [2,2]			Aspect Ratio [1,0]		
					MD_{10}	MD_{50}	MD_{90}	AR_{10}	AR_{50}	AR_{90}
(-)	(-)	(h)	(-)	(RPM)	(μm)	(μm)	(μm)	(-)	(-)	(-)
Water	Linear	14	CBT	400	310.0	570.0	823.0	1.20	1.68	2.65
3:1-w:p	Linear	14	CBT	400	50.6	131.0	491.0	1.25	1.80	2.90
1:1-w:p	Linear	14	CBT	400	67.0	142.0	431.0	1.22	1.70	2.58
1:3-w:p	Linear	14	CBT	400	50.2	93.8	215.0	1.22	1.69	2.52
n-propanol	Linear	14	CBT	400	36.9	75.3	174.0	1.15	1.43	1.92

The overall conclusion that can be drawn from the results presented in Figures 13 – 18 and Tables IV and V is that the solvent composition influences the crystal growth and nucleation rates considerably. When the observed crystal habits are compared with the ones reported for sulphathiazole crystals grown from water and from *n*-propanol in the literature (Bladgen *et al.* 1998a, Bladgen 2001, and Anderson *et al.* 2001), noticeable similarities can be detected. It should, however, also be pointed out in this context that the scale of the experiments made in this particular study was considerably larger, and also the mixing conditions in the crystallizer were different than in the studies reported earlier.

7.1.2 Filtration characteristics

7.1.2.1 Short cooling time

The average cake porosities and specific cake resistances of the suspensions crystallized by using the cooling time of 2 h are presented in Figures 19 and 20, and the filtration parameters for the different suspensions are summarized in Table VI. As can be seen in Figure 19, cake porosities depend both on the filtration pressure and on the composition of the solvent. Although the observed differences are rather small, they can be considered quite significant, as in the case of saturated cakes, the porosities correspond with the volume fractions of solvent retained in the cake. For example, reduction in the average cake porosity from 0.63 to 0.52, which are the extreme values in Figure 19, results in almost 20 % reduction in the final solvent volume of the sulfathiazole cakes.

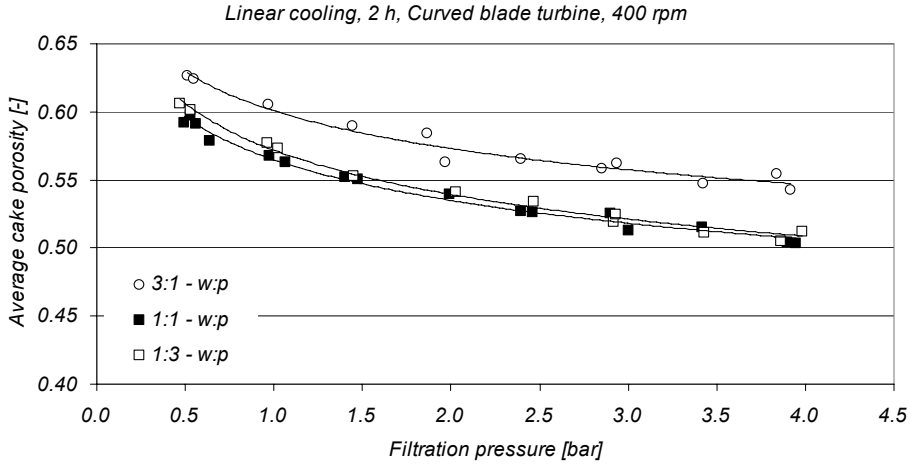

Figure 19 Average porosities of sulphathiazole cakes crystallized from different mixtures of water and *n*-propanol by using the cooling time of 2 h.

Figure 19 shows that the highest average cake porosities are observed with the suspension obtained from the 3:1 water:*n*-propanol mixture. The crystal size and shape data show that the median crystal size in this suspension is larger than in the other two suspensions, and although the widths of the size distributions are fairly similar, this suspension seems to contain a considerably higher amount of large crystals. Significant differences do not exist between the shapes of the crystals.

Comparison between the average specific cake resistances from the different suspensions reveals that there are fairly great differences between the obtained values. The resistances of cakes filtered from the 1:3 water:*n*-propanol mixture are the highest, and the smallest resistances are observed with the suspension crystallized from the 3:1 water:*n*-propanol mixture. This is most probably caused by the larger mean size of the crystals in the product from the 3:1 – mixture, and also due to the more porous filter cake structure.

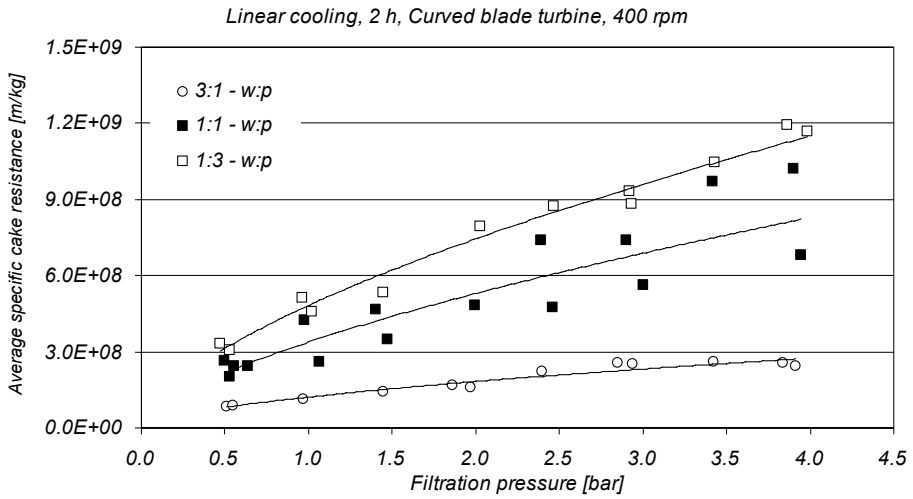

Figure 20 Average specific cake resistances of sulphathiazole cakes crystallized from different mixtures of water and *n*-propanol with the cooling time of 2 h.

Comparison of the filtration parameters summarized in Table VI shows that the cakes filtered from all three suspensions can be considered fairly compressible due to the relatively high values of compressibility coefficient *n*. Furthermore, when the determined cake porosities and resistances are compared with the values presented by Grace (1953) and Tiller (1953), it can be noticed that all the studied sulfathiazole suspensions are rather easy to filter. This conclusion is made on the basis of relatively low cake porosities, which are accompanied with very low cake resistances.

Table VI Summary of the filtration characteristics of the crystals suspensions obtained from different mixtures of water and *n*-propanol with the cooling time of 2 h.

	Cooling	Cooling		Mixing	Filtration parameters			
Solvent	method	time	Impeller	speed	α_0	n	ε_0	λ
(-)	(-)	(h)	(-)	(RPM)	($m\,kg^{-1}\,bar^{-n}$)	(-)	($bar^{-\lambda}$)	(-)
3:1 - w:p	Linear	2	CBT	400	1.22E+08	0.59	0.60	0.068
1:1 - w:p	Linear	2	CBT	400	3.38E+08	0.65	0.56	0.078
1:3 - w:p	Linear	2	CBT	400	4.83E+08	0.63	0.57	0.084

7.1.2.1 Long cooling time

The average cake porosities and average specific cake resistances of the suspension crystallized by using the cooling time of 14 h are presented in Figures 21 and 22, and the filtration parameters for the different suspensions are summarized in Table VII. Figure 21 shows that the differences in the average cake porosities are somewhat smaller than those with the cakes obtained from the suspensions crystallized with shorter cooling time. The relative order of the different suspensions has also changed, as now the highest porosities are observed with the cakes obtained from the 1:3 water:*n*-propanol mixture. Figure 16 shows that the crystals obtained from this suspension have the smallest size and the narrowest distribution.

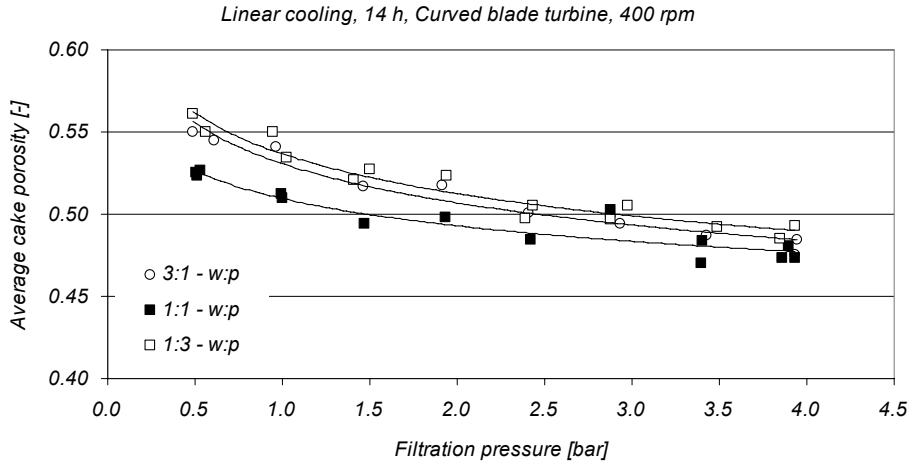

Figure 21 Average porosities of sulphathiazole cakes filtered from different mixtures of water and *n*-propanol by using the cooling time of 14 h.

Comparison between the determined average specific cake resistances from different suspensions reveals that the resistances of the cakes filtered from the 3:1 and 1:1 mixtures of water:*n*-propanol are almost equal, whereas the resistances of the cakes filtered from the 1:3 water:*n*-propanol mixture are almost 10 times higher. It is assumed that this is once again caused mainly by the large fraction of small crystals in the product from the 1:3-mixture. It should, however, be pointed out that this suspension has also the highest cake porosities, which means that these cakes are most difficult to filter and contain the highest amount of residual solvent.

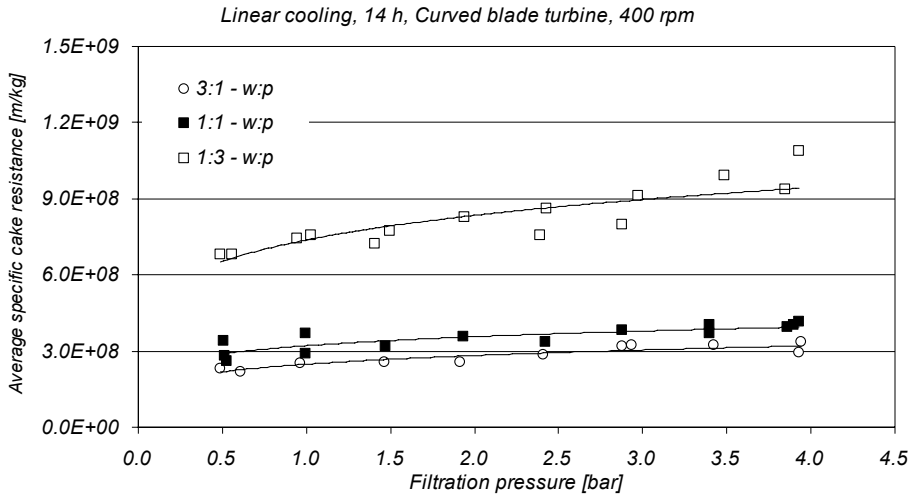

Figure 22 Average specific cake resistances of sulphathiazole cakes filtered from different mixtures of water and *n*-propanol with the cooling time of 14 h.

The filtration parameters presented in Table VII show that the compressibilities of the cakes are now much smaller that those with the short cooling time. This is an interesting result, and the explanation for this is not very clear. One possible reason could be that the higher cooling rate has caused the crystals to grow faster due to the higher supersaturation. This has probably caused more imperfections within the crystals thus weakening the mechanical strength of the crystals. The crystals produced with the shorter cooling time are therefore assumed to be more prone to breakage during the filtration tests.

Table VII Summary of the filtration characteristics of the crystals suspensions obtained from different mixtures of water and *n*-propanol with the cooling time of 14 h.

Solvent	Cooling method	Cooling time	Impeller	Mixing speed	Filtration parameters			
					α_0	n	ε_0	λ
(-)	(-)	(h)	(-)	(RPM)	($m\,kg^{-1}\,bar^{-n}$)	(-)	($bar^{-\lambda}$)	(-)
3:1 - w:p	Linear	14	CBT	400	2.48E+08	0.19	0.53	0.066
1:1 - w:p	Linear	14	CBT	400	3.21E+08	0.15	0.51	0.048
1:3 - w:p	Linear	14	CBT	400	7.38E+08	0.18	0.54	0.066

7.2 Influence of the cooling rate

Batch crystallization experiments for defining the influence of the cooling rate were done with four different cooling rates, which were maintained constant throughout the whole crystallization process. The applied cooling rates were 3.9, 5.5, 9.2 and 27.5 °C/h, which resulted in cooling times of 14.0, 10.0, 6.0 and 2.0 h for the temperature interval from 80 °C to 25 °C. The three different solvent mixtures were used with each cooling rate.

7.2.1 Crystal size and shape

7.2.1.1 3:1 water:n-propanol mixture

The size distributions of the crystals obtained from the crystallization experiments with the 3:1 water:*n*-propanol mixture with different constant cooling rates are presented in Figure 23, and the shape factor distributions for the same samples are presented in Figure 24. The statistical parameters of the crystal size, as well as the crystal shape distributions for these samples are summarized in Table VIII.

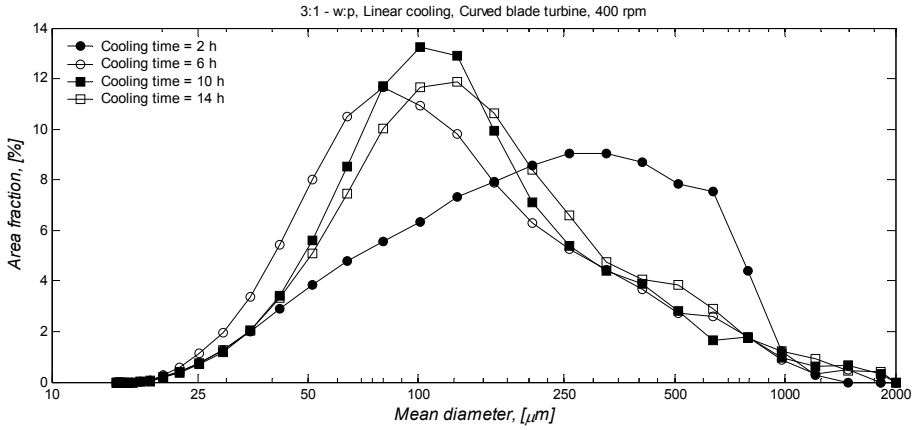

Figure 23 Crystal size distributions of sulphathiazole crystallized from 3:1 water:*n*-propanol mixture by using different cooling times.

The crystal size distributions presented in Figure 23 show that the largest crystals are obtained with the highest cooling rate, and when the cooling rate is lowered, the differences between the distributions practically disappear. These results suggest that the growth rate of sulphathiazole crystals in the 3:1 water:*n*-propanol mixture is very high, and that the maximum crystal size that can be achieved is probably strongly influenced by secondary nucleation. The role of secondary nucleation due to agitation, for example, is naturally more important when the batch time increases.

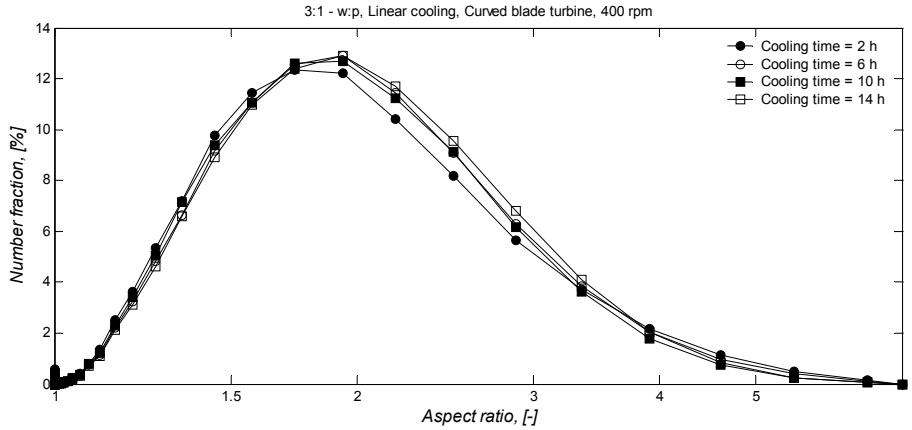

Figure 24 Crystal shape distributions of sulphathiazole crystallized from 3:1 water:*n*-propanol mixture by using different cooling times.

The results presented in Figure 24 show that although the cooling rate has a great influence on the crystal size distributions, the shape of the crystals is not influenced by the cooling rate.

Table VIII Statistical parameters of the crystal size and shape distributions of sulphathiazole crystallized from 3:1 water:*n*-propanol mixture by using different cooling times.

	Cooling	Cooling		Mixing	Mean diameter *[2,2]*			Aspect Ratio *[1,0]*		
Solvent	method	time	Impeller	speed	MD_{10}	MD_{50}	MD_{90}	AR_{10}	AR_{50}	AR_{90}
(-)	*(-)*	*(h)*	*(-)*	*(RPM)*	*(μm)*	*(μm)*	*(μm)*	*(-)*	*(-)*	*(-)*
3:1-w:p	Linear	2	CBT	400	52.8	217.0	623.0	1.23	1.74	2.89
3:1-w:p	Linear	6	CBT	400	42.1	103.0	421.0	1.25	1.78	2.89
3:1-w:p	Linear	10	CBT	400	50.3	119.0	439.0	1.24	1.76	2.82
3:1-w:p	Linear	14	CBT	400	50.6	131.0	491.0	1.25	1.80	2.90

7.2.1.2 1:1 water:n-propanol mixture

The size distributions of the crystals obtained from the crystallization experiments with the 1:1 water:n-propanol mixture with different constant cooling rates are presented in Figure 25, and the shape factor distributions for the same samples are presented in Figure 26. The statistical parameters of the crystal size, as well as the crystal shape distributions for these samples are summarized in Table IX.

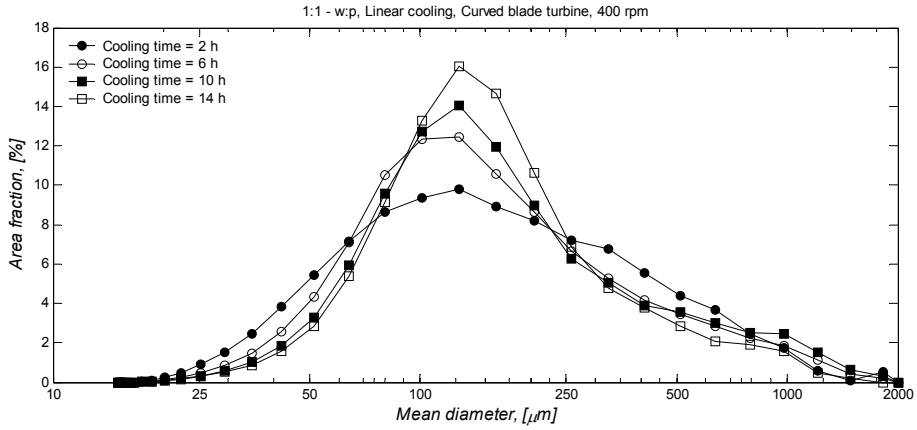

Figure 25 Crystal size distributions of sulphathiazole crystallized from 1:1 water:*n*-propanol mixture by using different cooling times.

Comparison of the results presented in figures 25 and 26 shows that the cooling rate does not have as great an influence on the crystal size distributions obtained from the 1:1 water:*n*-propanol mixture as with the 3:1 water:*n*-propanol mixture. The mean sizes of all samples are approximately equal, although some differences can be observed in the width of the distributions. The widest size distribution results from the use of the highest cooling rate, and the narrowest size distribution is observed with the slowest cooling. This suggests that the size of the crystals obtained by using the highest cooling rate is influenced by spontaneous nucleation, but also that attrition nucleation sets some limits on the maximum achievable crystal size. The differences in the crystal shapes are negligible also in this case.

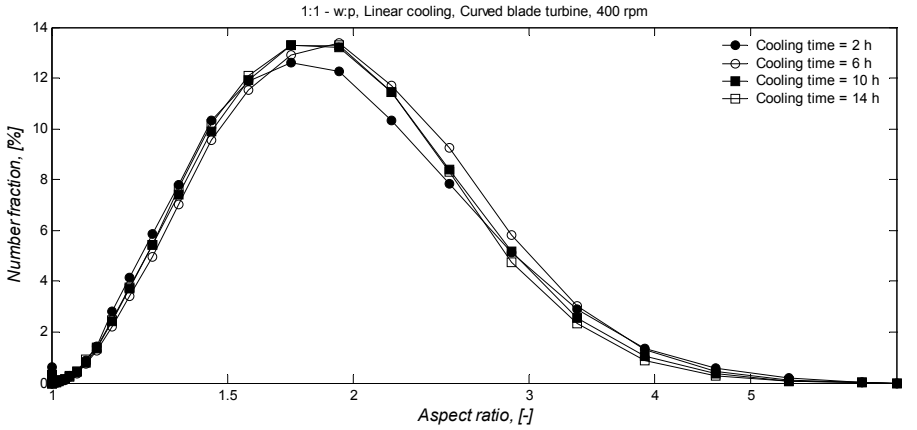

Figure 26 Crystal shape distributions of sulphathiazole crystallized from 1:1 water:*n*-propanol mixture by using different cooling times.

Table IX Statistical parameters of the crystal size and shape distributions of sulphathiazole crystallized from 1:1 water:*n*-propanol mixture by using different cooling times

Solvent	Cooling method	Cooling time	Impeller	Mixing speed	Mean diameter *[2,2]*			Aspect Ratio *[1,0]*		
					MD_{10}	MD_{50}	MD_{90}	AR_{10}	AR_{50}	AR_{90}
(-)	*(-)*	*(h)*	*(-)*	*(RPM)*	*(μm)*	*(μm)*	*(μm)*	*(-)*	*(-)*	*(-)*
1:1-w:p	Linear	2	CBT	400	47.0	143.0	542.0	1.21	1.69	2.68
1:1-w:p	Linear	6	CBT	400	56.8	136.0	520.0	1.24	1.75	2.71
1:1-w:p	Linear	10	CBT	400	63.7	143.0	594.0	1.23	1.72	2.63
1:1-w:p	Linear	14	CBT	400	67.0	142.0	431.0	1.22	1.70	2.58

7.2.1.3 1:3 water:n-propanol mixture

The size distributions of the crystals obtained from the crystallization experiments with the 1:3 water:*n*-propanol mixture with different constant cooling rates are presented in Figure 27, and the shape factor distributions for the same samples are presented in Figure 28. The statistical parameters of the crystal size and shape distributions for these samples are summarized in Table X.

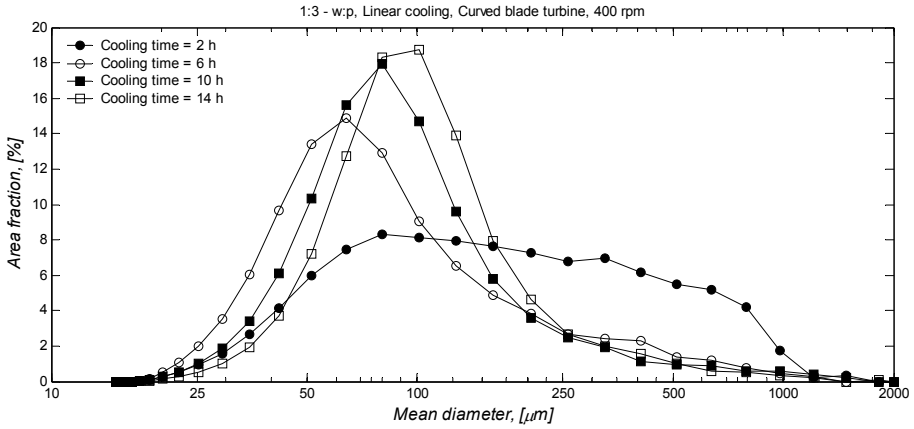

Figure 27 Crystal size distributions of sulphathiazole crystallized from 1:3 water:*n*-propanol mixture by using different cooling times.

Figures 27 and 28 show that the behaviour of the 1:3 water:*n*-propanol mixture is quite similar to the results presented for the 3:1 water:*n*-propanol mixture. The cooling rate influences the crystal size distributions considerably, but the differences observed in the shape factor distributions are once again fairly small. The largest crystals are obtained with the highest cooling rate, which also results in the widest size distribution.

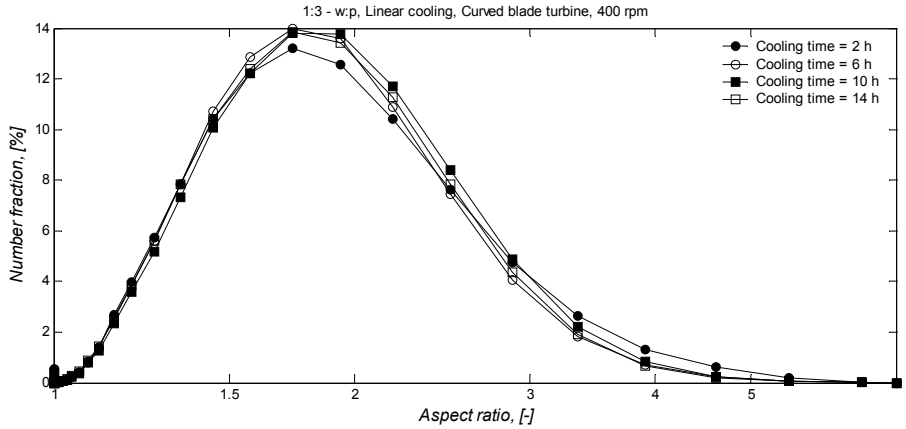

Figure 28 Crystal shape distributions of sulphathiazole crystallized from 1:3 water:*n*-propanol mixture by using different cooling times.

Table X Statistical parameters of the crystal size and shape distributions of sulphathiazole crystallized from 1:3 water:*n*-propanol mixture by using different cooling times

	Cooling	Cooling		Mixing	Mean diameter *[2,2]*			Aspect Ratio *[1,0]*		
Solvent	method	time	Impeller	speed	MD_{10}	MD_{50}	MD_{90}	AR_{10}	AR_{50}	AR_{90}
(-)	*(-)*	*(h)*	*(-)*	*(RPM)*	*(μm)*	*(μm)*	*(μm)*	*(-)*	*(-)*	*(-)*
1:3-w:p	Linear	2	CBT	400	45.8	151.0	606.0	1.22	1.69	2.65
1:3-w:p	Linear	6	CBT	400	34.6	69.6	254.0	1.22	1.68	2.50
1:3-w:p	Linear	10	CBT	400	42.1	81.4	215.0	1.24	1.72	2.58
1:3-w:p	Linear	14	CBT	400	50.2	93.8	215.0	1.22	1.69	2.52

7.2.2 Filtration characteristics

7.2.2.1 3:1 water:n-propanol mixture

The average cake porosities and average specific cake resistances of the suspensions crystallized from the 3:1 water:*n*-propanol mixture by using different constant cooling rates are presented in Figures 29 and 30, and the filtration parameters for the different suspensions are summarized in Table XI. Figure 29 shows that the differences in the average cake porosities are negligible for the suspension obtained by using the cooling rates of 6, 10 or 14 h, but the suspension obtained with the highest cooling rate results in much larger porosities. The reason for this is probably caused by the differences observed in the width of the size distributions (Figure 23 and Table VIII).

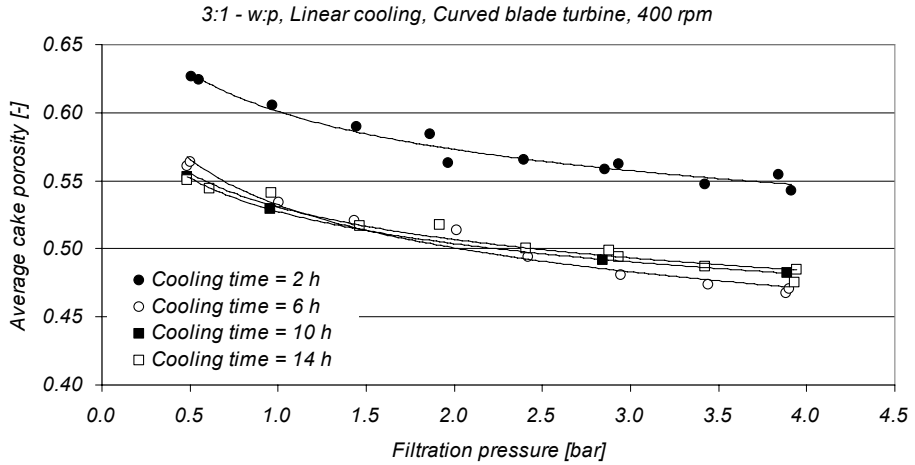

Figure 29 Average porosities of sulphathiazole cakes filtered from suspensions crystallized from 3:1 water:*n*-propanol mixture by using different constant cooling rates

Figure 30 shows that quite great differences can be observed also in the average specific cake resistances. The highest resistances are observed with the suspension obtained by using the cooling time of 6 h, whereas the lowest resistances are obtained with the fastest cooling rate. The fastest cooling also results in the largest crystal size, which is the most probable reason for the observed differences. Although the fast cooling seems to result in a suspension that is the easiest to filter, it should be noticed that this same suspension results in filter cakes that contain the largest amount of residual solvent. It therefore depends on the primary target of the filtration process and the required product characteristics whether it is advantageous to increase the capacity of the filter and at the same time increase the solvent content in the product.

The filtration parameters summarized in Table XI show that the cooling rate has a fairly great influence also on the value of the compressibility coefficient *n*. It can be noted that the cakes obtained from the suspensions crystallized by using the fastest cooling are the most compressible, and the compressibility decreases with the decreasing cooling rate. One explanation for this could be that the crystals produced with the fast cooling are mechanically weaker and break more easily at high filtration pressures.

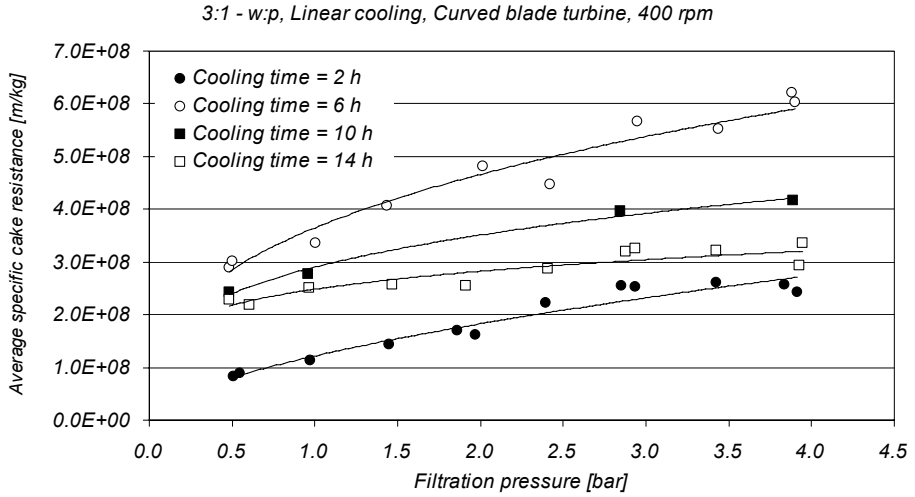

Figure 30 Average specific cake resistances of sulphathiazole cakes filtered from suspensions crystallized from 3:1 water:*n*-propanol mixture by using different constant cooling rates

Table XI Summary of the filtration characteristics of the crystal suspensions obtained from 3:1 water:*n*-propanol mixture by using different constant cooling rates.

	Cooling	Cooling		Mixing	Filtration parameters			
Solvent	method	time	Impeller	speed	α_0	n	ε_0	λ
(-)	(-)	(h)	(-)	(RPM)	(m kg^{-1} bar^{-n})	(-)	(bar$^{-\lambda}$)	(-)
3:1 - w:p	Linear	2	CBT	400	1.22E+08	0.59	0.60	0.068
3:1 - w:p	Linear	6	CBT	400	3.65E+08	0.35	0.53	0.088
3:1 - w:p	Linear	10	CBT	400	2.91E+08	0.27	0.53	0.066
3:1 - w:p	Linear	14	CBT	400	2.48E+08	0.19	0.53	0.066

7.2.2.2 1:1 water:n-propanol mixture

The average cake porosities and specific cake resistances of the suspensions crystallized from the 1:1 water:*n*-propanol mixture by using different constant cooling rates are presented in Figures 31 and 32, and the filtration parameters for these suspensions are shown in Table XII. Figure 31 shows that there are now greater differences in the average cake porosities than with the suspensions crystallized from the 3:1 water:n-propanol mixture. These differences are most likely caused by the differences observed in the widths of the crystal size distributions (Figure 25 and Table IX). The highest porosities are observed with the suspensions crystallized by using the highest cooling rate (the widest crystal size distribution), and the porosities decrease when the cooling rate decreases and the size distribution becomes narrower.

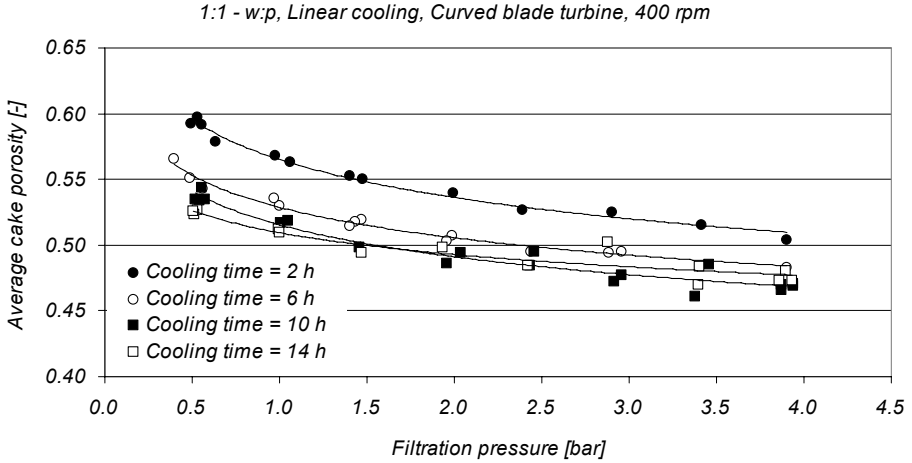

Figure 31 Average porosities of sulphathiazole cakes filtered from suspensions crystallized from 1:1 water:*n*-propanol mixture by using different constant cooling rates.

Figure 32 shows that significant differences are also observed in the average specific cake resistances. The highest resistances are observed with the suspension obtained by using the fastest cooling rate, and the lowest resistances with the longest cooling time. Comparison with the results in Figure 31 shows that the highest cake resistances are in this cake observed with the highest porosities and vice versa. It seems obvious according to the crystal size distributions presented in Figure 25 that these differences are caused by variations in the widths of the distributions. It can also be noticed that there are great variations in the cake compressibilities. The values of the compressibility coefficient *n* again seem to decrease with decreasing cooling rate.

Table XII Summary of the filtration characteristics of the crystal suspensions obtained from 1:1 water:*n*-propanol mixture by using different constant cooling rates.

	Cooling	Cooling		Mixing	Filtration parameters			
Solvent	method	time	Impeller	speed	α_0	n	ε_0	λ
(-)	(-)	(h)	(-)	(RPM)	(m kg^{-1} bar^{-n})	(-)	(bar$^{-\lambda}$)	(-)
1:1 - w:p	Linear	2	CBT	400	3.38E+08	0.65	0.56	0.078
1:1 - w:p	Linear	6	CBT	400	3.92E+08	0.30	0.53	0.072
1:1 - w:p	Linear	10	CBT	400	3.93E+08	0.19	0.52	0.070
1:1 - w:p	Linear	14	CBT	400	3.21E+08	0.15	0.51	0.048

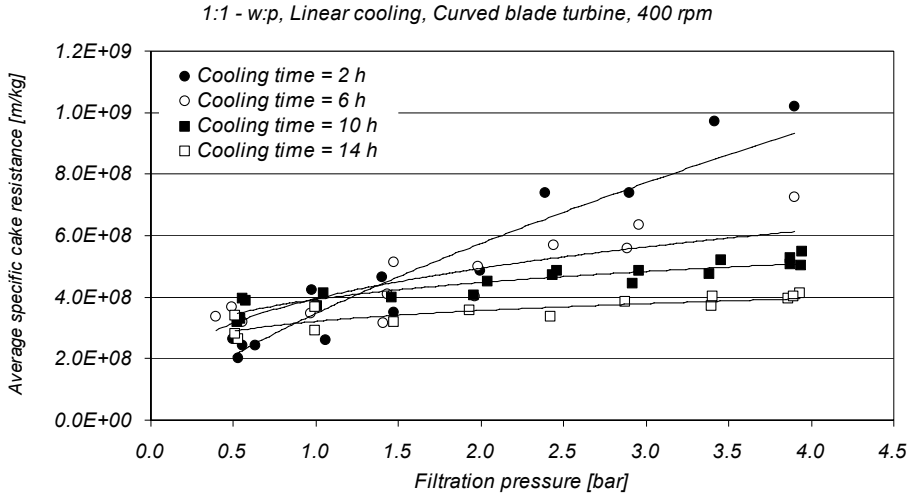

Figure 32 Average specific cake resistances of sulphathiazole cakes filtered from suspensions crystallized from 1:1 water:*n*-propanol mixture by using different constant cooling rates

7.2.2.3 1:3 water:n-propanol mixture

The average cake porosities and specific filter cake resistances of the suspensions crystallized from the 1:3 water:*n*-propanol mixture by using different constant cooling rates are presented in Figures 33 and 34, and the filtration parameters for the different suspensions are summarized in Table XIII. Figure 33 shows that the differences in the average cake porosities are smaller than with the suspensions crystallized from the other two mixtures. The highest porosities are again observed with the suspension crystallized by using the fastest cooling rate, which also results in the widest crystal size distribution. The differences between the porosities of the cakes filtered from the other three solvents are negligible, and also the cake compressibilities with respect to porosity seem to be similar.

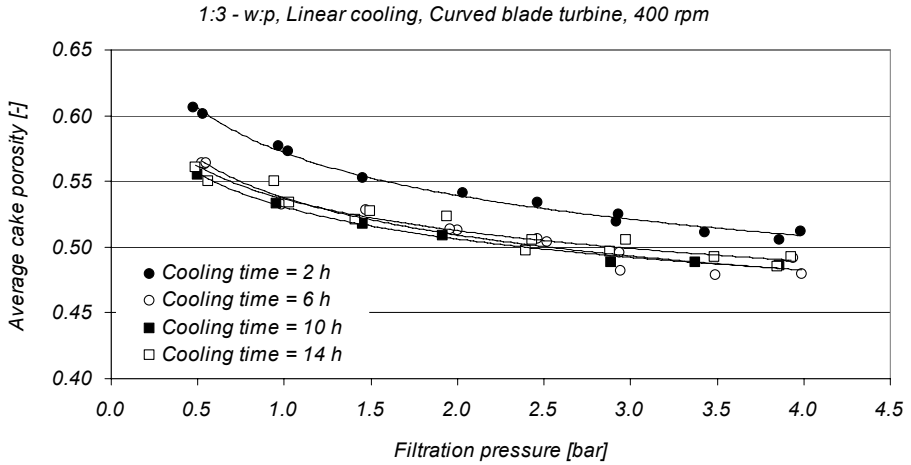

Figure 33 Average specific cake resistances of sulphathiazole cakes filtered from suspensions crystallized from 1:1 water:*n*-propanol mixture by using different constant cooling rates

Figure 34 shows that although the differences in the cake porosities are small, the resistance of one of the suspensions deviates clearly from the other. The resistances of the suspensions crystallized by using the cooling time of 6 hours are much higher than the resistances of the cakes obtained from the other three suspensions. This sample also has the smallest crystal size, as can be seen in Figure 25 and Table X, and this is most probably the main reason for the observed results. The resistances of the other cakes are of the same magnitude.

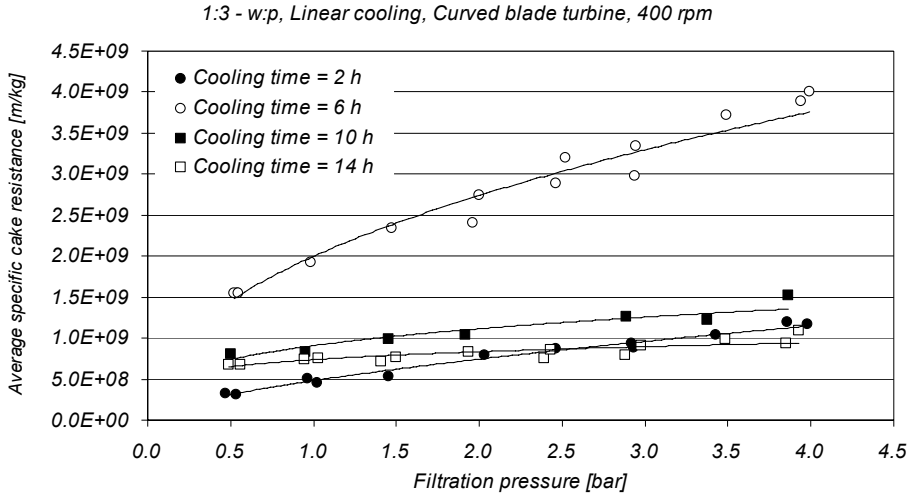

Figure 34 Average specific cake resistances of sulphathiazole cakes filtered from suspensions crystallized from 1:3 water:*n*-propanol mixture by using different constant cooling rates

The filtration parameters of the suspensions crystallized from the 1:3 water:*n*-propanol mixture, which are summarized in Table XIII, show that the cake compressibilities with respect to cake resistances (coefficient *n*) increase once again with the increasing cooling rate.

Table XIII Summary of the filtration characteristics of the crystal suspensions obtained from 1:3 water:*n*-propanol mixture by using different constant cooling rates.

	Cooling	Cooling		Mixing	Filtration parameters			
Solvent	method	time	Impeller	speed	α_0	n	ε_0	λ
(-)	(-)	(h)	(-)	(RPM)	($m\,kg^{-1}\,bar^{-n}$)	(-)	($bar^{-\lambda}$)	(-)
1:3 - w:p	Linear	2	CBT	400	4.83E+08	0.63	0.57	0.084
1:3 - w:p	Linear	6	CBT	400	2.00E+09	0.46	0.54	0.078
1:3 - w:p	Linear	10	CBT	400	9.09E+08	0.29	0.53	0.068
1:3 - w:p	Linear	14	CBT	400	7.38E+08	0.18	0.54	0.066

7.3 Influence of the cooling profile

In this part of the study, unseeded batch cooling crystallization experiments were performed using three different cooling profiles, as explained in Chapter 6.3.3 and illustrated in Figure 7.

7.3.1 Crystal size and shape

7.3.1.1 3:1 water:n-propanol mixture

The crystal size and shape distributions of the suspensions crystallized from the 3:1 water:n-propanol mixture by using different cooling profiles are presented in Figures 35 and 36, and the statistical parameters of the crystal size and shape distributions for these samples are summarized in Table XIV.

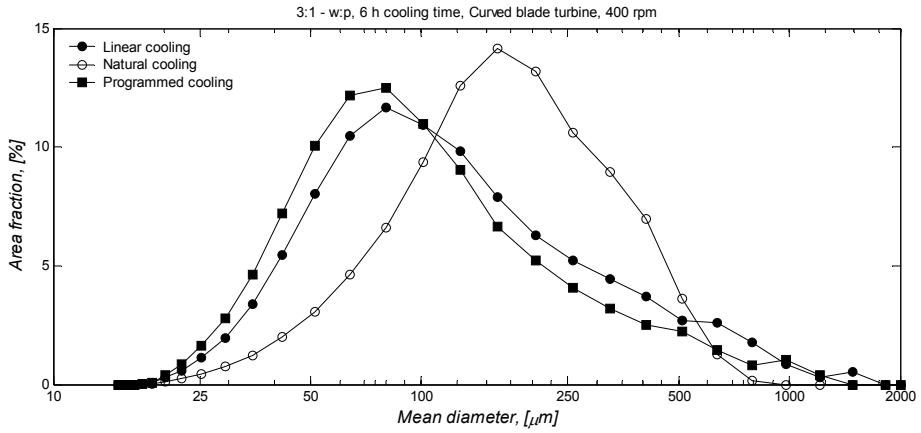

Figure 35 Crystal size distributions of sulphathiazole crystallized from 3:1 water:*n*-propanol mixture by using different cooling profiles.

The size distributions presented in Figure 35 show that the natural cooling profile results in the largest crystal size and programmed cooling in the smallest crystals. These are fairly surprising results, but they can be considered reliable, as similar trends were observed also in the repeated parallel batches. The crystal shape distributions presented in Figure 36 show that the crystals obtained by using natural cooling deviate from the other two samples so that the crystals are more elongated in this case.

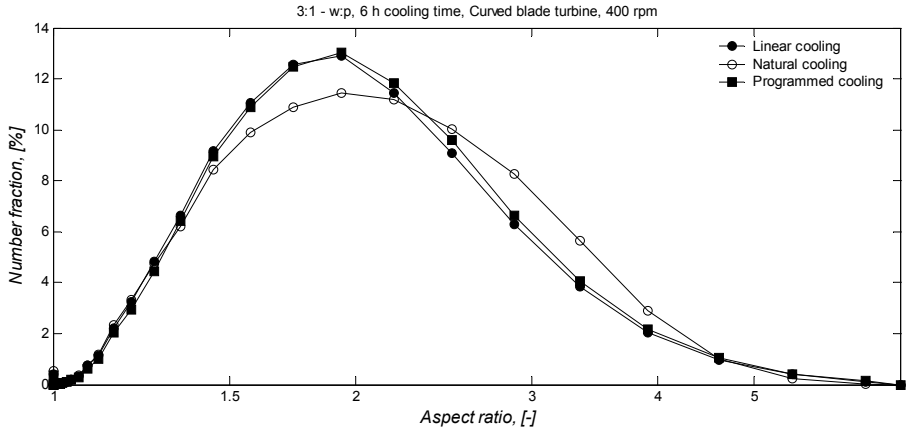

Figure 36 Crystal shape distributions of sulphathiazole crystallized from 3:1 water:*n*-propanol mixture by using different cooling profiles

Table XIV Statistical parameters of the crystal size and shape distributions of sulphathiazole crystallized from 3:1 water:*n*-propanol mixture by using different cooling profiles.

	Cooling	Cooling		Mixing	Mean diameter *[2,2]*			Aspect Ratio *[1,0]*		
Solvent	method	time	Impeller	speed	MD_{10}	MD_{50}	MD_{90}	AR_{10}	AR_{50}	AR_{90}
(-)	*(-)*	*(h)*	*(-)*	*(RPM)*	*(μm)*	*(μm)*	*(μm)*	*(-)*	*(-)*	*(-)*
3:1-w:p	Linear	6	Curved	400	42.1	103.0	421.0	1.25	1.78	2.89
3:1-w:p	Programmed	6	Curved	400	37.3	85.3	326.0	1.26	1.81	2.93
3:1-w:p	Natural	6	Curved	400	63.4	166.0	385.0	1.24	1.84	3.08

7.3.1.2 1:1 water:n-propanol mixture

The crystal size and shape distributions of the suspensions crystallized from the 1:1 water:*n*-propanol mixture by using different cooling profiles are presented in Figures 37 and 38, and the statistical parameters of the crystal size and shape distributions for these samples are summarized in Table XV.

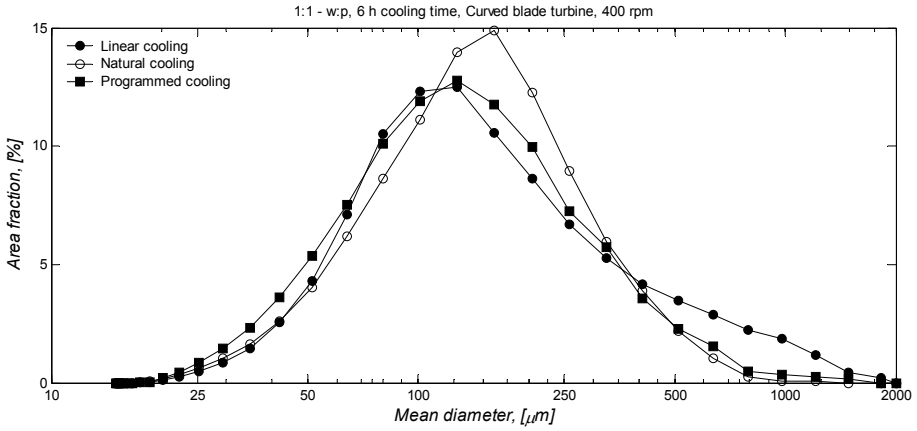

Figure 37 Crystal size distributions of sulphathiazole crystallized from 1:1 water:*n*-propanol mixture by using different cooling profiles.

Figure 37 shows that significant differences do not exist in the crystal size distribution between the different cooling profiles with the 1:1 water:*n*-propanol mixture as the solvent. The shape factor distributions in Figure 38, however, show that the differences in the shapes of the crystals are quite great. In this case, the programmed cooling results in the most needle-like crystals, whereas the aspect ratios are the smallest for the linear cooling profile.

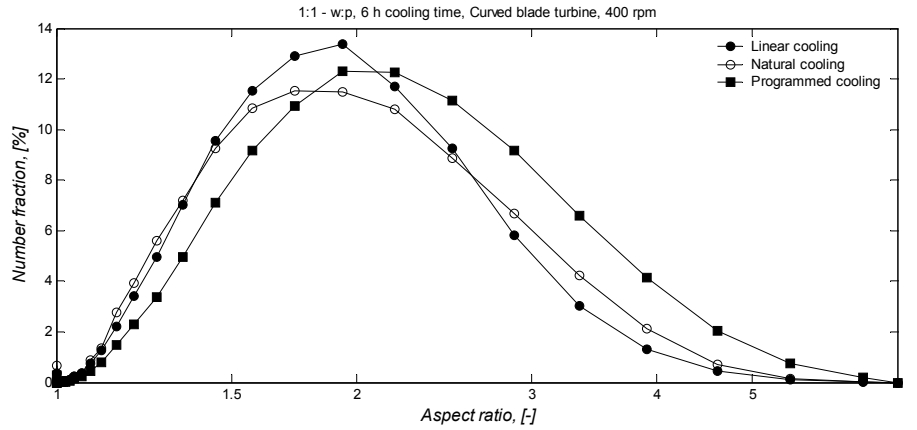

Figure 38 Crystal shape distributions of sulphathiazole crystallized from 1:1 water:*n*-propanol mixture by using different cooling profiles.

Table XV Statistical parameters of the crystal size and shape distributions of sulphathiazole crystallized from 1:1 water:*n*-propanol mixture by using different cooling profiles.

	Cooling	Cooling		Mixing	Mean diameter *[2,2]*			Aspect Ratio *[1,0]*		
Solvent	method	time	Impeller	speed	MD_{10}	MD_{50}	MD_{90}	AR_{10}	AR_{50}	AR_{90}
(-)	*(-)*	*(h)*	*(-)*	*(RPM)*	*(μm)*	*(μm)*	*(μm)*	*(-)*	*(-)*	*(-)*
1:1-w:p	Linear	6	Curved	400	56.8	136.0	520.0	1.24	1.75	2.71
1:1-w:p	Programmed	6	Curved	400	48.3	126.0	342.0	1.31	1.98	3.34
1:1-w:p	Natural	6	Curved	400	55.6	141.0	326.0	1.22	1.74	2.89

7.3.1.3 1:3 water:n-propanol mixture

The crystal size and shape distributions of the suspensions crystallized from the 1:3 water:*n*-propanol mixture by using different cooling profiles are presented in Figures 39 and 40, and the statistical parameters of the crystal size and shape distributions for these samples are summarized in Table XVI.

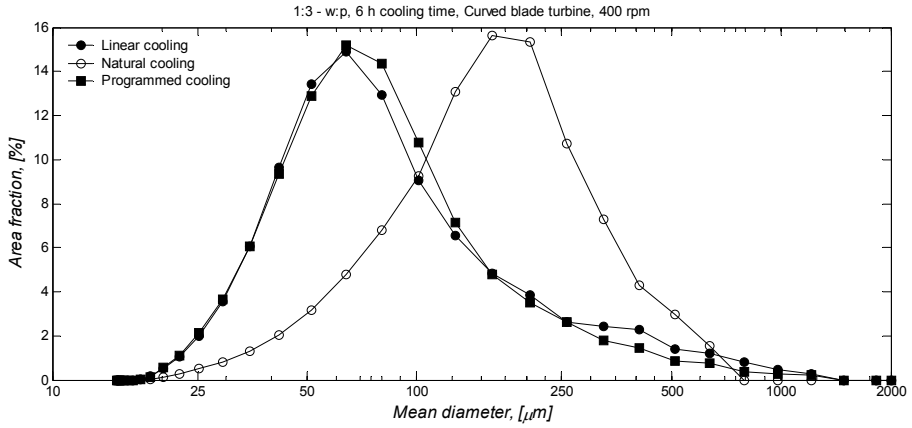

Figure 39 Crystal size distributions of sulphathiazole crystallized from 1:3 water:*n*-propanol mixture by using different cooling profiles.

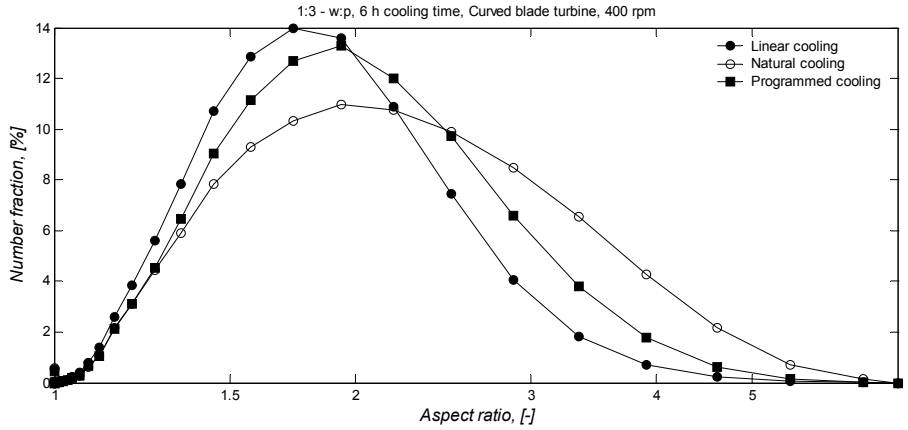

Figure 40 Crystal shape distributions of sulphathiazole crystallized from 1:3 water:*n*-propanol mixture by using different cooling profiles.

Figures 39 and 40 show that the behavior of the 1:3 water:*n*-propanol mixture is once again similar with the 3:1 water:*n*-propanol mixture. The largest crystals are obtained from the batch cooled by using the natural cooling profile, whereas linear and programmed cooling result in similar distributions. Large variations are also seen in the crystal shapes, that the aspect ratios are the highest for the crystals produced by natural cooling and lowest for those produced by the linear cooling profile.

Table XVI Statistical parameters of the crystal size and shape distributions of sulphathiazole crystallized from 1:3 water:*n*-propanol mixture by using different cooling profiles

	Cooling	Cooling		Mixing	Mean diameter *[2,2]*			Aspect Ratio *[1,0]*		
Solvent	method	time	Impeller	speed	MD_{10}	MD_{50}	MD_{90}	AR_{10}	AR_{50}	AR_{90}
(-)	(-)	(h)	(-)	(RPM)	(μm)	(μm)	(μm)	(-)	(-)	(-)
1:3-w:p	Linear	6	Curved	400	34.6	69.6	254.0	1.22	1.68	2.50
1:3-w:p	Programmed	6	Curved	400	34.2	69.9	203.0	1.26	1.80	2.83
1:3-w:p	Natural	6	Curved	400	62.2	161.0	345.0	1.26	1.90	3.36

7.3.2 Filtration characteristics

7.3.2.1 3:1 water:n-propanol mixture

Average cake porosities and specific cake resistances of the suspensions crystallized from the 3:1 water:*n*-propanol mixture by using three different cooling rates are presented in Figures 41 and 42, and the filtration parameters for the different suspensions are summarized in Table XVII. Figure 41 shows that the differences

observed between the average cake porosities of the cakes obtained from different suspensions are fairly great. The suspension crystallized by using the natural cooling profile results in the highest porosities, and the lowest cake porosities are obtained from the suspension crystallized by using the linear cooling profile.

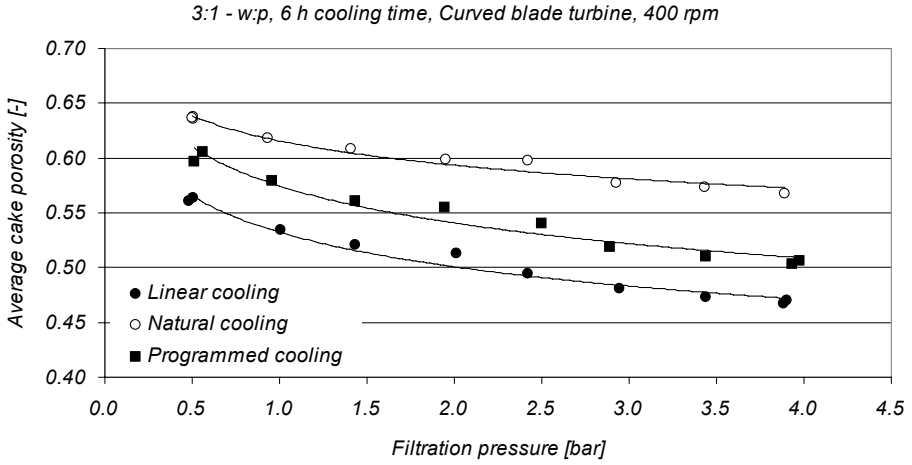

Figure 41 Average porosities of sulphathiazole cakes filtered from suspensions crystallized from 3:1 water:*n*-propanol mixture by using three different cooling profiles.

The results obtained from the filtration experiments carried out with the suspensions crystallized from the 3:1 – water: *n*-propanol solution with different cooling policies show that the differences between the average specific cake resistances in the different suspensions are fairly small. The lowest cake resistances are found with the suspension crystallized with natural cooling, whereas the cake resistances with the suspensions crystallized with the other two profiles are approximately equal.

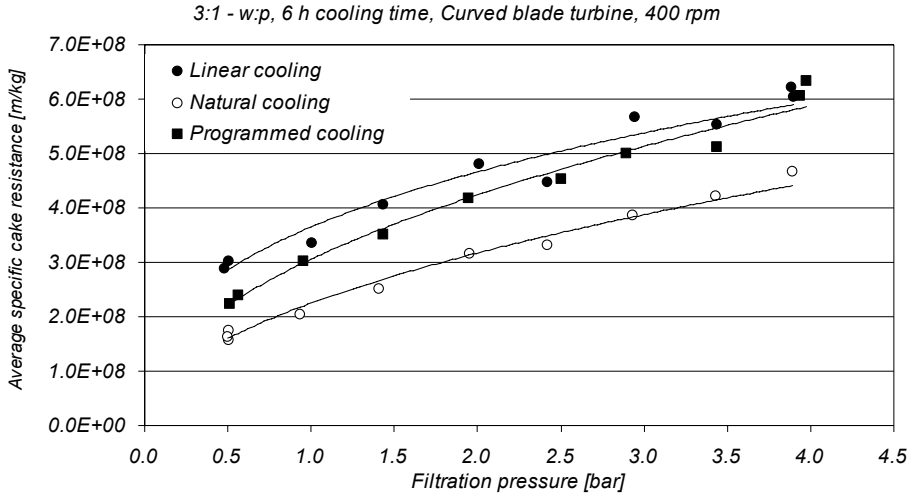

Figure 42 Average specific cake resistances of sulphathiazole cakes filtered from suspensions crystallized from 3:1 water:*n*-propanol mixture by using three different cooling profiles

Table XVII Summary of the filtration characteristics of the crystals suspensions obtained from 3:1 water:*n*-propanol mixture by using three different cooling profiles.

	Cooling	Cooling		Mixing	Filtration parameters			
Solvent	method	time	Impeller	speed	α_0	n	ε_0	λ
(-)	(-)	(h)	(-)	(RPM)	($m\,kg^{-1}\,bar^{-n}$)	(-)	($bar^{-\lambda}$)	(-)
3:1 - w:p	Linear	6	CBT	400	3.65E+08	0.35	0.53	0.088
3:1 - w:p	Programmed	6	CBT	400	3.06E+08	0.47	0.57	0.087
3:1 - w:p	Natural	6	CBT	400	2.25E+08	0.49	0.62	0.053

7.3.2.2 1:1 water:n-propanol mixture

The average cake porosities and specific cake resistances of the suspensions crystallized from the 1:1 water:*n*-propanol mixture by using three different cooling rates are presented in Figures 43 and 44, and the filtration parameters for the different suspensions are summarized in Table XVIII. Figure 43 shows that the differences between the average cake porosities of the cakes obtained from different suspensions are quite great. The suspension that has been crystallized by using the natural cooling profile results in the highest porosities, and the lowest cake porosities are obtained from the suspension crystallized by using the linear cooling profile.

The cake porosities seem to depend strongly on the cooling policy used in

crystallization. The lowest porosities can be found with linear cooling, which produces crystals with the widest distributions both in size and shape. Controlled cooling, which leads to crystals with a wide size range but a more uniform shape, results in cake porosities that are approximately 10 % higher than the porosities with the linear cooling profile in the studied pressure range. Natural cooling, on the other hand, results in cake porosities that are of about the same magnitude as the porosities with controlled cooling at low filtration pressures. However, when the filtration pressure is increased, the porosities with the natural cooling profile do not decrease as drastically as the porosities with the controlled cooling. This implies that the crystal cakes obtained from the suspensions crystallized with natural cooling are not as compressible as the cakes obtained from suspensions crystallized with the other two cooling policies. This is most likely a result of the narrower crystal size distribution and more rounded crystal shape.

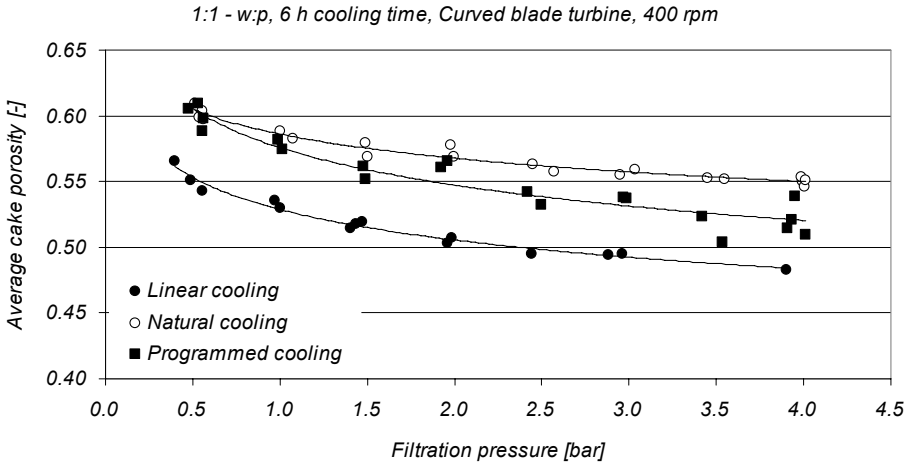

Figure 43 Average porosities of sulphathiazole cakes filtered from suspensions crystallized from 1:1 water:*n*-propanol mixture by using three different cooling profiles.

Comparison of the average specific filter cake resistances of the suspensions crystallized from the 1:1 water:*n*-propanol mixture shows that even if the properties of the product crystals differ clearly from each other between the different cooling policies, significant differences can not be observed in the determined crystal cake resistances. The programmed cooling profile seems to result in slightly lower cake resistances than the linear or natural cooling, which leads to the highest resistances.

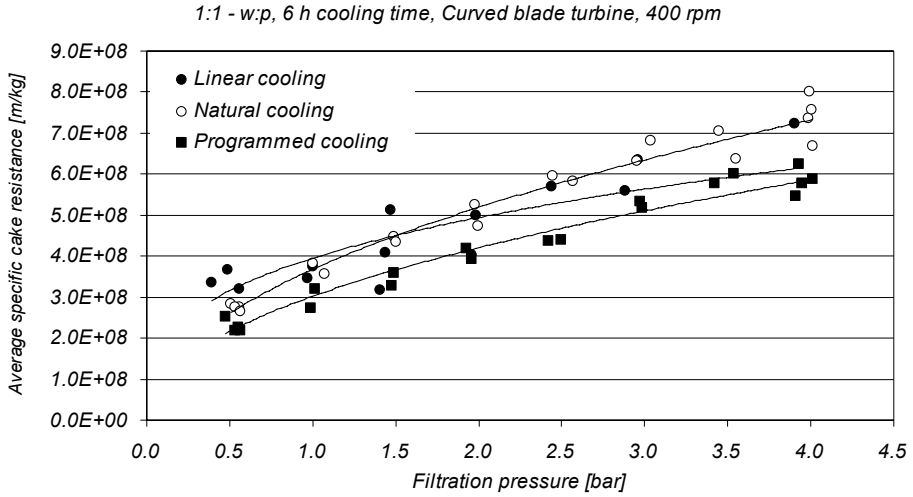

Figure 42 Average specific cake resistances of sulphathiazole cakes filtered from suspensions crystallized from 1:1 water:*n*-propanol mixture by using three different cooling profiles.

Table XVIII Summary of the filtration characteristics of the crystals suspensions obtained from 1:1 water:*n*-propanol mixture by using three different cooling profiles.

	Cooling	Cooling		Mixing	Filtration parameters			
Solvent	method	time	Impeller	speed	α_0	n	ε_0	λ
(-)	(-)	(h)	(-)	(RPM)	(m kg^{-1} bar^{-n})	(-)	(bar$^{-\lambda}$)	(-)
1:1 - w:p	Linear	6	CBT	400	3.92E+08	0.30	0.53	0.072
1:1 - w:p	Programmed	6	CBT	400	3.02E+08	0.48	0.58	0.073
1:1 - w:p	Natural	6	CBT	400	3.68E+08	0.50	0.59	0.046

7.3.2.3 1:3 water:n-propanol mixture

The average cake porosities and specific cake resistances of the suspensions crystallized from the 1:3 water:*n*-propanol mixture by using three different cooling rates are presented in Figures 45 and 46, and the filtration parameters for the different suspensions are summarized in Table XIX. Figure 45 shows that the differences between the average cake porosities of the cakes obtained from different suspensions are fairly great. The suspension that has been crystallized by using the natural cooling profile results in the highest porosities, and the lowest cake porosities are obtained from the suspension crystallized by using the linear cooling profile.

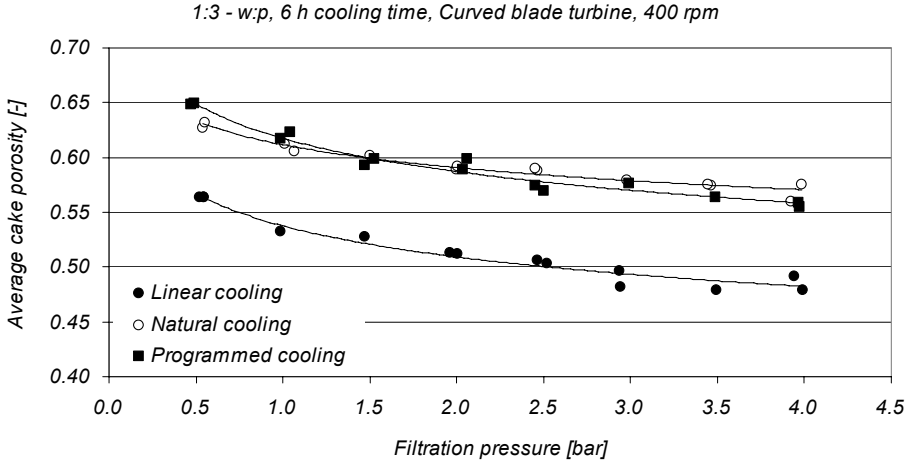

Figure 45 Average porosities of sulphathiazole cakes filtered from suspensions crystallized from 1:3 water:*n*-propanol mixture by using three different cooling profiles.

The differences between the presented average specific cake resistances with different cooling policies appear to be much greater with these suspensions than with the suspensions crystallized from the other two water:*n*-propanol solutions. In this case the natural cooling profile results in cake resistances that are clearly lower than the resistances observed with the other two cooling profiles. The largest cake resistances are found with the suspensions crystallized using the linear cooling profile, which can be considered rather unexpected. Programmed cooling, however, appears to lead in the highest cake porosities, which again implies that the structure of the crystal cakes is fairly open, and this might explain the relatively low cake resistances. The suspensions produced with the linear cooling profile have the highest cake resistances and the lowest porosities throughout the considered pressure range. It is, however, difficult to speculate whether this effect is primarily caused by the differences in the crystal shapes or by the differences in the crystal size distributions.

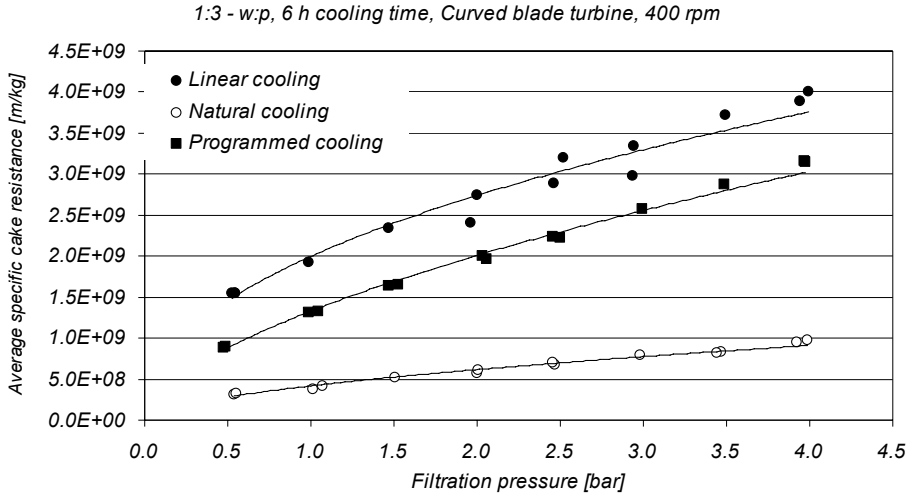

Figure 46 Average specific cake resistances of sulphathiazole cakes filtered from suspensions crystallized from 1:3 water:*n*-propanol mixture by using three different cooling profiles.

Table XIX Summary of the filtration characteristics of the crystal suspensions obtained from 1:3 water:*n*-propanol mixture by using three different cooling profiles.

	Cooling	Cooling		Mixing	Filtration parameters			
Solvent	method	time	Impeller	speed	α_0	n	ε_0	λ
(-)	(-)	(h)	(-)	(RPM)	(m kg^{-1} bar^{-n})	(-)	(bar$^{-\lambda}$)	(-)
1:3 - w:p	Linear	6	CBT	400	2.00E+09	0.46	0.54	0.078
1:3 - w:p	Programmed	6	CBT	400	1.33E+09	0.59	0.62	0.072
1:3 - w:p	Natural	6	CBT	400	4.19E+08	0.56	0.61	0.050

7.4 Influence of the mixing conditions

The objective of the last part of the experiments in this study was to explore the impact of mixing conditions in an unseeded batch cooling crystallizer on the crystal characteristics, and further, on the filterability of the final crystal suspension. Mixing of the solutions during the crystallization experiments was carried out using four different types of impellers, the designs of which were presented in Figure 8, and three different agitation rates with each impeller (shown in Table II). All these crystallization experiments were performed by using linear cooling profiles with the cooling time of 6 hours and the 1:1 water:*n*-propanol mixture as the solvent.

7.4.1 Crystal size and shape

7.4.1.1 Curved Blade Turbine

The crystal size and shape distributions of the suspensions crystallized from the 1:1 water:*n*-propanol mixture by using the constant cooling rate of 9.2 °C/h and a curved blade turbine with three different rotation speeds are presented in Figures 47 and 48. The statistical parameters of the distributions are summarized in Table XX.

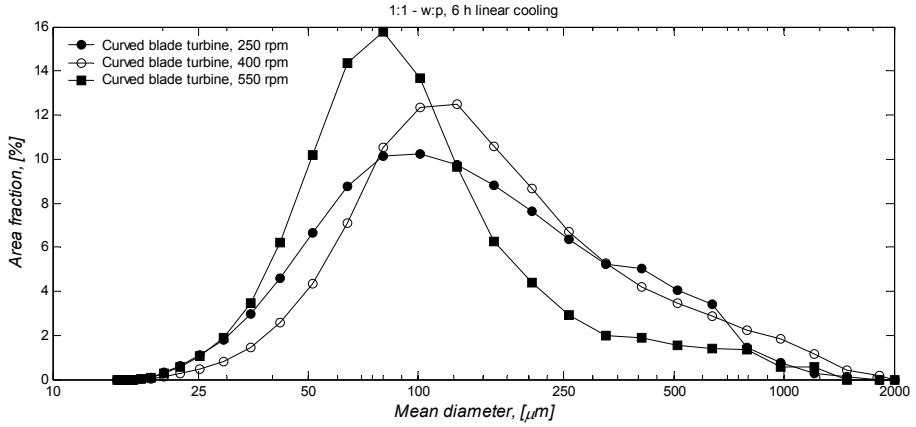

Figure 47 Crystal size distributions of sulphathiazole crystallized from 1:1 water:*n*-propanol mixture by using the constant cooling rate of 9.2 °C/h and a curved blade turbine with three different rotation speeds.

Figures 47 and 48 show that the mixing intensity has a significant influence on the crystal size and shape distributions. The smallest crystal size and lowest aspect ratio is observed with the highest mixing intensity, and when the mixing intensity is lowered, the crystals become larger in size and more elongated in shape. It is noticed that the difference in the crystal size distributions between the lowest and the second lowest mixing intensities is fairly small, but the highest mixing intensity results in a clear decrease in the crystal size.

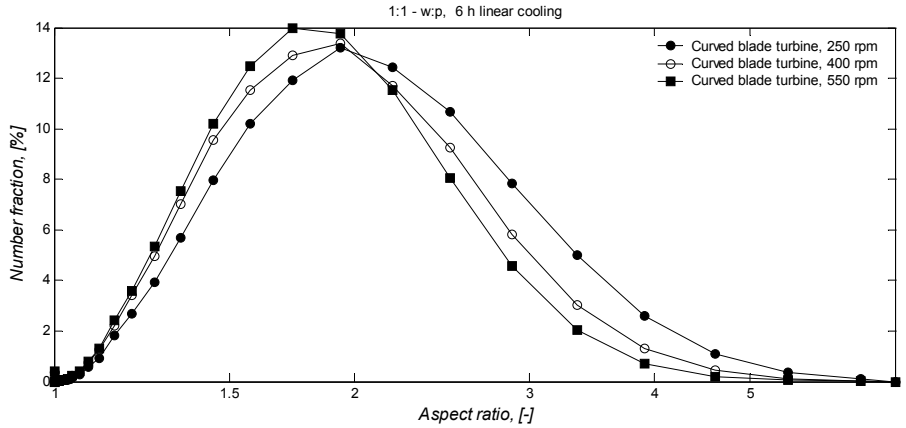

Figure 48 Crystal shape distributions of sulphathiazole crystallized from 1:1 water:*n*-propanol mixture by using the constant cooling rate of 9.2 °C/h and a curved blade turbine with three different rotation speeds.

Table XX Statistical parameters of the crystal size and shape distributions of sulphathiazole crystallized from 1:1 water:*n*-propanol mixture by using the constant cooling rate of 9.2 °C/h and a curved blade turbine with three different rotation speeds.

	Cooling	Cooling		Mixing	Mean diameter *[2,2]*			Aspect Ratio *[1,0]*		
Solvent	method	time	Impeller	speed	MD_{10}	MD_{50}	MD_{90}	AR_{10}	AR_{50}	AR_{90}
(-)	(-)	(h)	(-)	(RPM)	(μm)	(μm)	(μm)	(-)	(-)	(-)
1:1-w:p	Linear	6	CBT	250	43.7	120.0	454.0	1.28	1.88	3.04
1:1-w:p	Linear	6	CBT	400	56.8	136.0	520.0	1.24	1.75	2.71
1:1-w:p	Linear	6	CBT	550	41.8	84.4	267.0	1.23	1.71	2.54

7.4.1.2 Pitched Blade Turbine

The crystal size and shape distributions of the suspensions crystallized by using a pitched blade turbine with three different rotation speeds are presented in Figures 49 and 50. The statistical parameters of the crystal size and shape distributions for these samples are summarized in Table XXI.

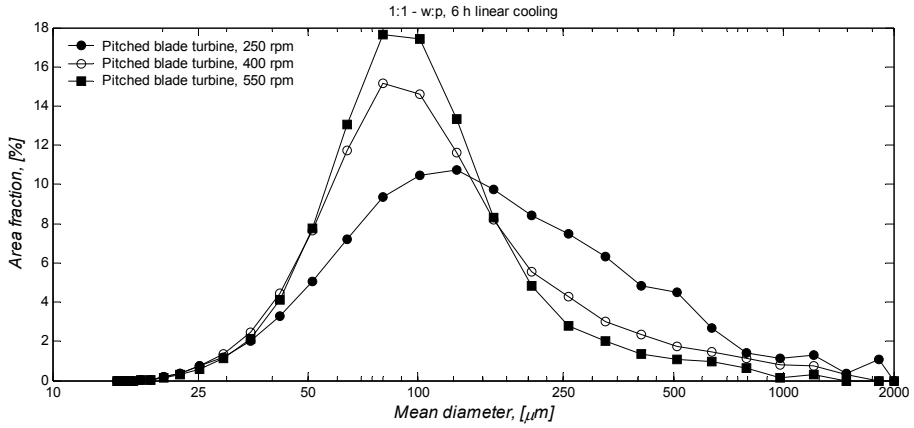

Figure 49 Crystal size distributions of sulphathiazole crystallized from 1:1 water:*n*-propanol mixture by the using constant cooling rate of 9.2 °C/h and a pitched blade turbine with three different rotation speeds.

Figures 49 and 50 show similar trends to those observed with the curved blade impeller. It can be observed that especially the shape of the crystals is strongly influenced by the mixing conditions. In this case, the crystal size distributions obtained with the highest and the second highest mixing intensities are almost identical, but the lowest mixing intensity results in a larger crystal size.

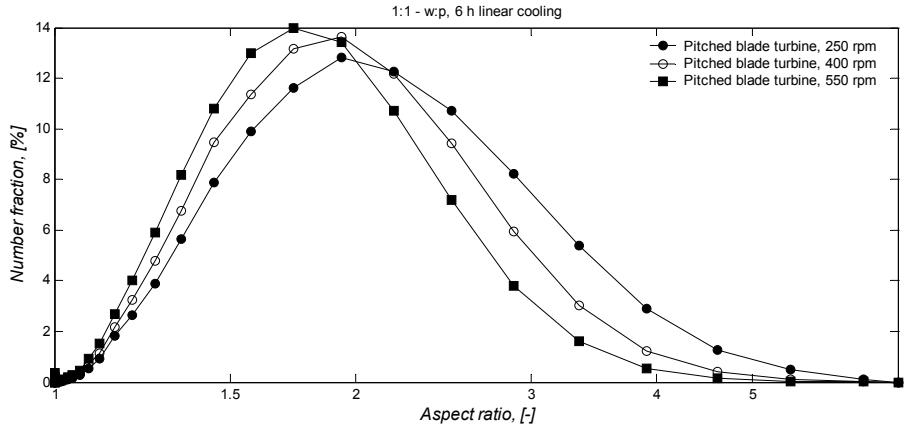

Figure 50 Crystal shape distributions of sulphathiazole crystallized from 1:1 water:*n*-propanol mixture by using the constant cooling rate of 9.2 °C/h and a pitched blade turbine with three different rotation speeds.

Table XXI Statistical parameters of the crystal size and shape distributions of sulphathiazole crystallized from 1:1 water:*n*-propanol mixture by using the constant cooling rate of 9.2 °C/h and a pitched blade turbine with three different rotation speeds.

	Cooling	Cooling		Mixing	Mean diameter *[2,2]*			Aspect Ratio *[1,0]*		
Solvent	method	time	Impeller	speed	MD_{10}	MD_{50}	MD_{90}	AR_{10}	AR_{50}	AR_{90}
(-)	*(-)*	*(h)*	*(-)*	*(RPM)*	*(μm)*	*(μm)*	*(μm)*	*(-)*	*(-)*	*(-)*
1:1-w:p	Linear	6	PBT	250	50.8	140.0	512.0	1.28	1.89	3.11
1:1-w:p	Linear	6	PBT	400	46.8	97.5	321.0	1.25	1.77	2.71
1:1-w:p	Linear	6	PBT	550	48.7	93.0	220.0	1.22	1.66	2.45

7.4.1.3 Bar Turbine

The crystal size and shape distributions of the suspensions crystallized by using a bar turbine with three different rotation speeds are presented in Figures 51 and 52. The statistical parameters of the crystal size and shape distributions for these samples are summarized in Table XXII.

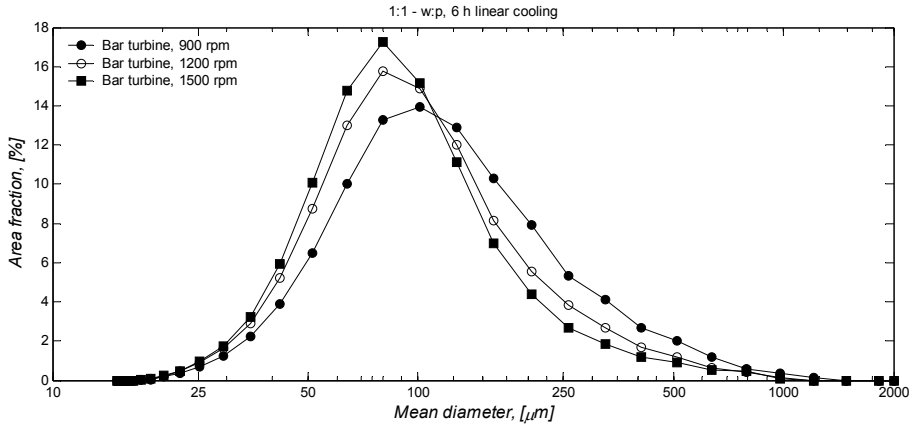

Figure 51 Crystal size distributions of sulphathiazole crystallized from 1:1 water:*n*-propanol mixture by using the constant cooling rate of 9.2 °C/h and a bar turbine with three different rotation speeds.

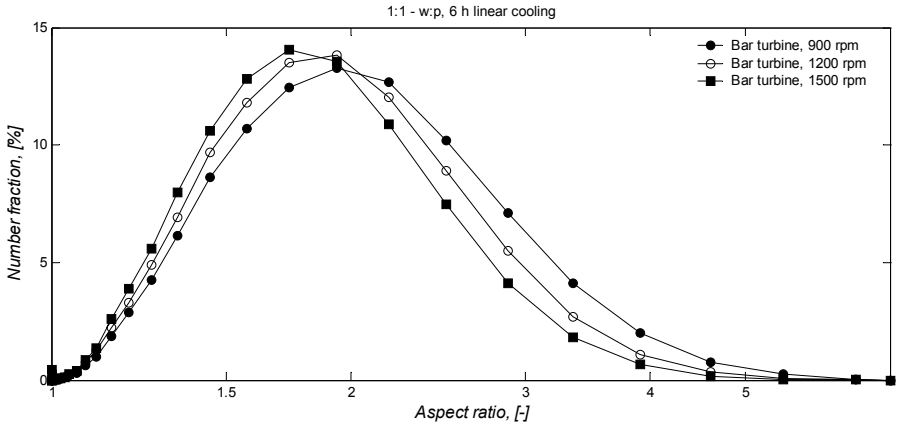

Figure 52 Crystal shape distributions of sulphathiazole crystallized from 1:1 water:*n*-propanol mixture by using the constant cooling rate of 9.2 °C/h and a bar turbine with three different rotation speeds.

The data presented in Figures 51 and 52 shows a similar behavior as with the other two impellers. A significant reduction can be observed in the crystal size when the mixing intensity is increased. The aspect ratios also decrease rationally when the agitation intensity is increased.

Table XXII Statistical parameters of the crystal size and shape distributions of sulphathiazole crystallized from 1:1 water:*n*-propanol mixture by using the constant cooling rate of 9.2 °C/h and a bar turbine with three different rotation speeds.

	Cooling	Cooling		Mixing	Mean diameter *[2,2]*			Aspect Ratio *[1,0]*		
Solvent	method	time	Impeller	speed	MD_{10}	MD_{50}	MD_{90}	AR_{10}	AR_{50}	AR_{90}
(-)	*(-)*	*(h)*	*(-)*	*(RPM)*	*(μm)*	*(μm)*	*(μm)*	*(-)*	*(-)*	*(-)*
1:1-w:p	Linear	6	BT	900	48.5	108.0	304.0	1.27	1.83	2.89
1:1-w:p	Linear	6	BT	1200	44.2	90.8	234.0	1.25	1.75	2.66
1:1-w:p	Linear	6	BT	1500	42.8	83.8	199.0	1.22	1.68	2.50

7.4.1.4 Anchor Impeller

The crystal size and shape distributions of the suspensions crystallized from the 1:1 water:*n*-propanol mixture by using the constant cooling rate of 9.2 °C/h and an anchor impeller with three different rotation speeds are presented in Figures 53 and 54. The statistical parameters of the crystal size and shape distributions for these samples are summarized in Table XXIII.

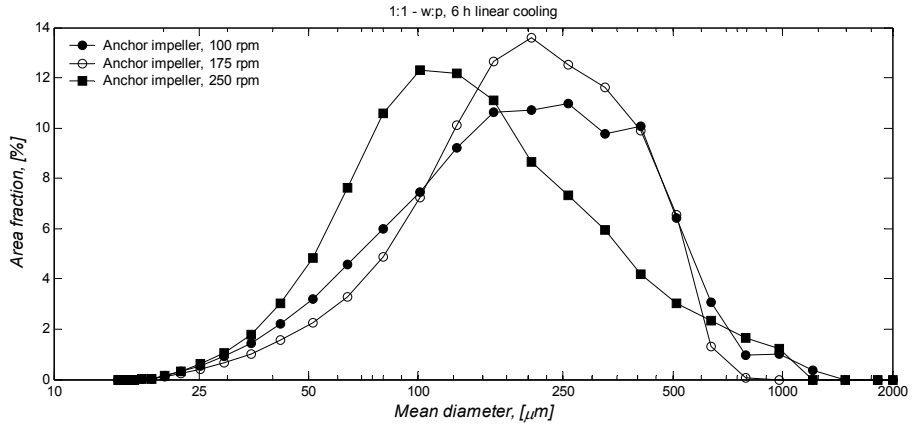

Figure 53 Crystal size distributions of sulphathiazole crystallized from 1:1 water:*n*-propanol mixture by using the constant cooling rate of 9.2 °C/h and an anchor impeller with three different rotation speeds.

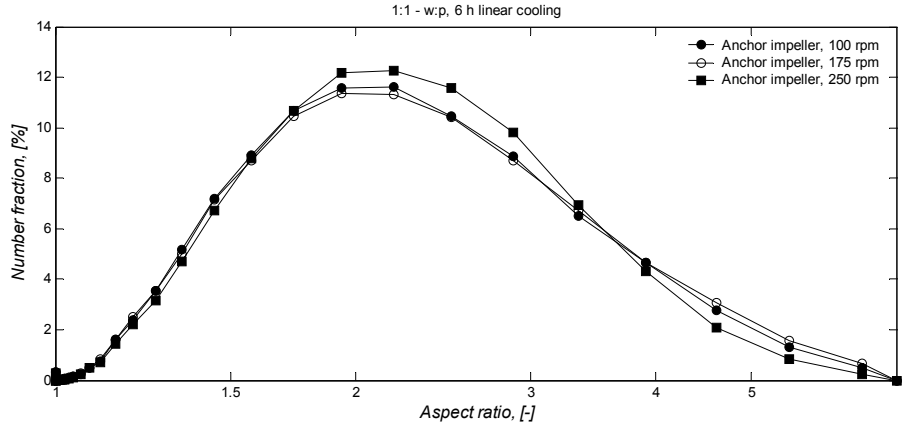

Figure 54 Crystal shape distributions of sulphathiazole crystallized from 1:1 water:*n*-propanol mixture by using the constant cooling rate of 9.2 °C/h and an anchor impeller with three different rotation speeds.

The size distributions presented in Figure 53 show that the smallest crystals are obtained with the highest agitation rate. The influence of the mixing intensity on the size distributions in this case resembles the behavior observed when the mixing was accomplished by using a curved blade turbine, i.e. the difference in the crystal size distributions between the lowest and the second lowest mixing intensities is fairly small, but the highest mixing intensity results in a clear decrease in the crystal size. The shape factor distributions presented in Figure 54 show that although some changes can be observed, the effect of agitation rate is not as large in this case as with the other three impellers.

Table XXIII Statistical parameters of the crystal size and shape distributions of sulphathiazole crystallized from 1:1 water:*n*-propanol mixture by using the constant cooling rate of 9.2 °C/h and an anchor impeller with three different rotation speeds.

	Cooling	Cooling		Mixing	Mean diameter *[2,2]*			Aspect Ratio *[1,0]*		
Solvent	method	time	Impeller	speed	MD_{10}	MD_{50}	MD_{90}	AR_{10}	AR_{50}	AR_{90}
(-)	*(-)*	*(h)*	*(-)*	*(RPM)*	*(μm)*	*(μm)*	*(μm)*	*(-)*	*(-)*	*(-)*
1:1-w:p	Linear	6	AI	100	60.8	194.0	483.0	1.30	1.98	3.55
1:1-w:p	Linear	6	AI	175	72.5	198.0	434.0	1.30	1.99	3.63
1:1-w:p	Linear	6	AI	250	53.0	130.0	408.0	1.32	2.00	3.39

7.4.2 Filtration characteristics

7.4.2.1 Curved Blade Turbine

The average cake porosities and specific cake resistances of the suspensions crystallized from the 1:1 water:*n*-propanol mixture by using the constant cooling rate of 9.2 °C/h and a curved blade turbine with three different rotation speeds are presented in Figures 55 and 56, and the filtration parameters for the different suspensions are summarized in Table XXIV.

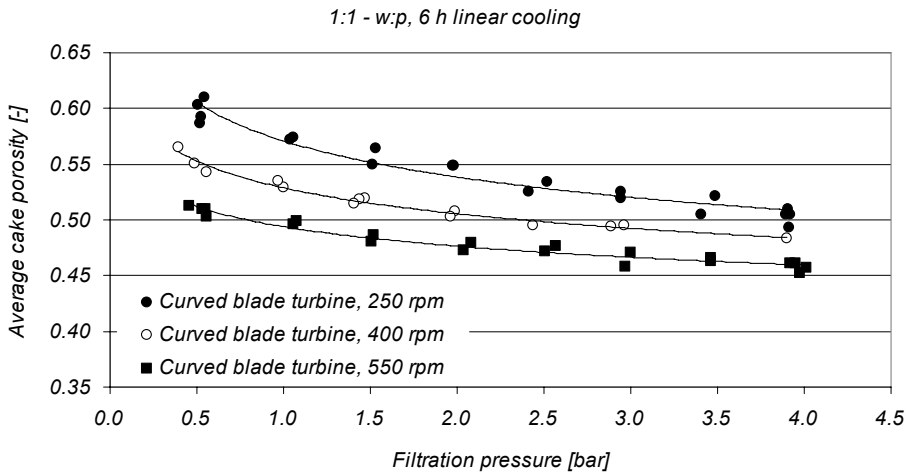

Figure 55 Average porosities of sulphathiazole cakes obtained from suspensions crystallized from 1:1 water:*n*-propanol mixture by using constant cooling rate of 9.2 °C/h and a curved blade turbine with three different rotation speeds.

Comparison of the average cake porosities presented in Figure 55 shows that the values decrease regularly with the increasing mixing intensity. Although the crystal size distributions presented for these samples in Figure 47, imply that the difference between the lowest and the second lowest agitation rates is almost negligible, a significant difference can be noticed in the porosities. This result suggests that the difference in the cake porosities is therefore mostly caused by the differences in the shape of the crystals.

The average specific cake resistances presented in Figure 56 show that the lowest resistances are obtained with the lowest agitation rate. The crystals obtained with the lowest agitation rate are fairly large, have the highest aspect ratio and result in filter cakes with the highest porosity. It is quite difficult to estimate which one of these parameters has the greatest effect on the cake resistances.

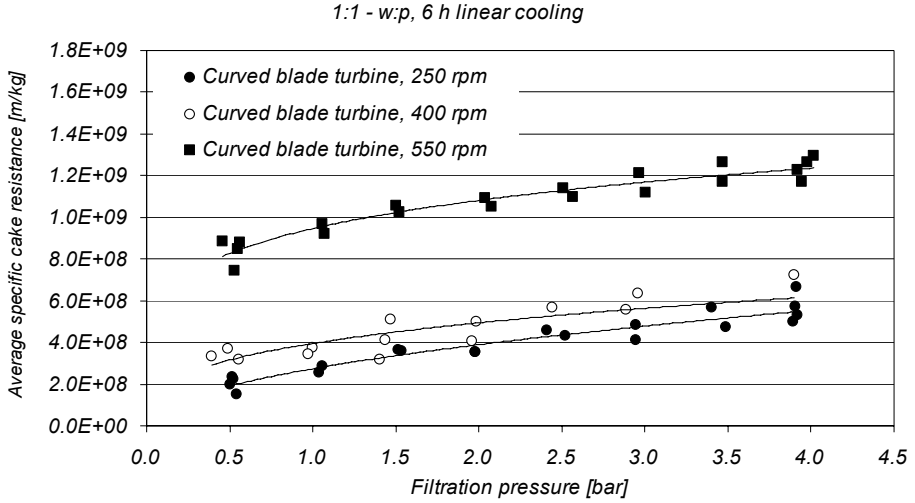

Figure 56 Average specific resistances of sulphathiazole cakes obtained from suspensions crystallized from 1:1 water:*n*-propanol mixture by using the constant cooling rate of 9.2 °C/h and a curved blade turbine with three different rotation speeds.

Comparison of the filtration characteristics summarized in Table XXIV reveals that the compressibilities of the cakes are influenced strongly by the agitation rate. Cakes with the highest compressibilities are obtained with the lowest cooling rate. It is assumed that this is due to changes in the crystal shape, i.e. crystals with a higher aspect ratio break more easily during the filtration stage.

Table XXIV Summary of the filtration characteristics of the crystal suspensions obtained from suspensions crystallized from 1:1 water:*n*-propanol mixture by using the constant cooling rate of 9.2 °C/h and a curved blade turbine with three different rotation speeds.

	Cooling	Cooling		Mixing	Filtration parameters			
Solvent	method	time	Impeller	speed	α_0	n	ε_0	λ
(-)	(-)	(h)	(-)	(RPM)	(m kg^{-1} bar^{-n})	(-)	(bar$^{-\lambda}$)	(-)
1:1 - w:p	Linear	6	CBT	250	2.74E+08	0.50	0.57	0.084
1:1 - w:p	Linear	6	CBT	400	3.92E+08	0.30	0.53	0.072
1:1 - w:p	Linear	6	CBT	550	9.46E+08	0.19	0.49	0.052

7.4.2.2 Pitched Blade Turbine

The average cake porosities and specific cake resistances of the suspensions crystallized from the 1:1 water:n-propanol mixture by using the constant cooling rate of 9.2 °C/h and a pitched blade turbine with three different rotation speeds are presented in Figures 57 and 58, and the filtration parameters for the different suspensions are summarized in Table XXV.

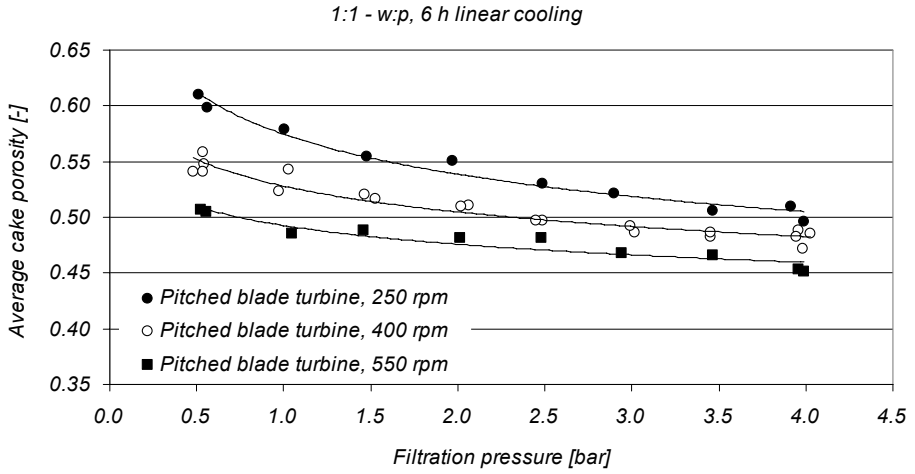

Figure 57 Average porosities of sulphathiazole cakes obtained from suspensions crystallized from 1:1 water:*n*-propanol mixture by using the constant cooling rate of 9.2 °C/h and a pitched blade turbine with three different rotation speeds.

The average cake porosities presented in Figure 57 show a similar trend as observed with the curved blade impeller, i.e. the values decrease regularly with increasing mixing intensity. When compared with the crystal size distributions presented in

Figure 48, it is noticed that the highest porosities are obtained with the sample that has the largest crystal size. The difference in the crystal size distributions between the highest and the second highest agitation rates is almost negligible, but there is, however, a significant difference in the porosities. This again suggests that the difference in the cake porosities is caused mainly by differences in the shape of the crystals.

The average specific cake resistances are presented in Figure 58 and show that the lowest resistances are again obtained with the lowest agitation rate (<=> largest crystal size, highest aspect ratio, highest cake porosities). This trend is similar to the one observed already with the curved blade impeller, and it is difficult to detect the main reason for the differences in the cake resistances also in this case.

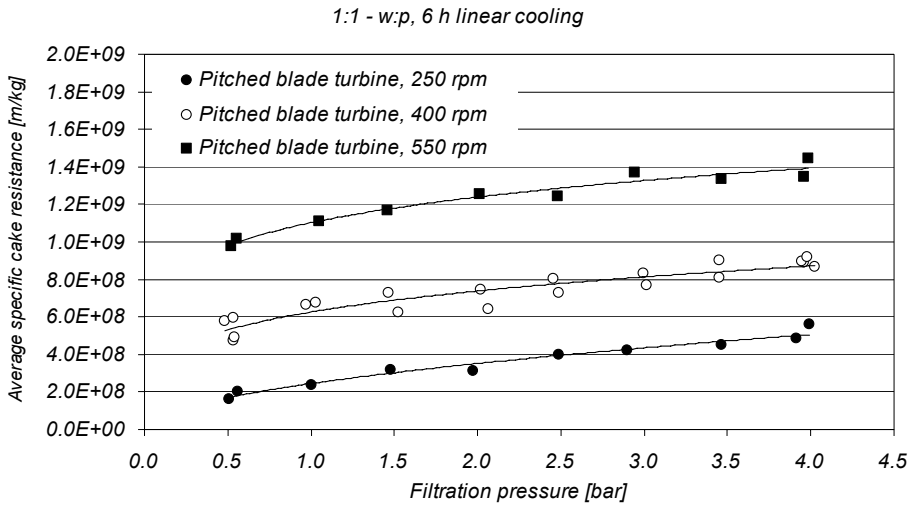

Figure 56 Average specific resistances of sulphathiazole cakes obtained from suspensions crystallized from 1:1 water:*n*-propanol mixture by using constant cooling rate of 9.2 °C/h and a pitched blade turbine with three different rotation speeds.

The filtration characteristics for the samples obtained by using the pitched blade impeller are summarized in Table XXV, and they again show that the compressibilities of the cakes are strongly influenced by the agitation rate. Cakes with the highest compressibilities are obtained with the lowest cooling rate. As already mentioned, this is probably due to changes in the crystal shape, i.e. crystals with a higher aspect ratio break more easily during the filtration stage.

Table XXV Summary of the filtration characteristics of the crystal suspensions obtained from suspensions crystallized from 1:1 water:*n*-propanol mixture by using the constant cooling rate of 9.2 °C/h and a pitched blade turbine with three different rotation speeds.

	Cooling	Cooling		Mixing	Filtration parameters			
Solvent	method	time	Impeller	speed	α_0	n	ε_0	λ
(-)	(-)	(h)	(-)	(RPM)	(m kg^{-1} bar^{-n})	(-)	(bar$^{-\lambda}$)	(-)
1:1 - w:p	Linear	6	PBT	250	2.45E+08	0.52	0.57	0.093
1:1 - w:p	Linear	6	PBT	400	6.26E+08	0.24	0.53	0.065
1:1 - w:p	Linear	6	PBT	550	1.10E+09	0.17	0.49	0.050

7.4.2.3 Bar Turbine

The average cake porosities and specific cake resistances of the suspensions crystallized from the 1:1 water:*n*-propanol mixture by using the constant cooling rate of 9.2 °C/h and a bar turbine with three different rotation speeds are presented in Figures 59 and 60, and the filtration parameters for the different suspensions are summarized in Table XXVI.

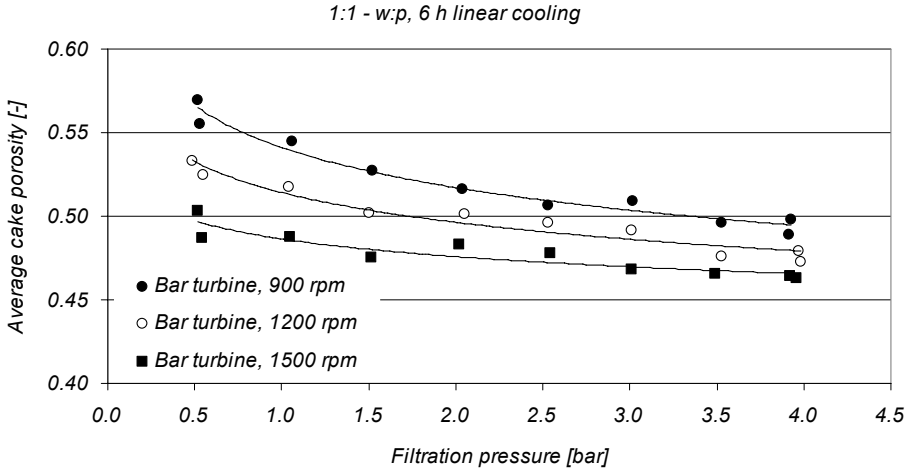

Figure 59 Average porosities of sulphathiazole cakes obtained from suspensions crystallized from 1:1 water:*n*-propanol mixture by using the constant cooling rate of 9.2 °C/h and a bar turbine with three different rotation speeds.

The average cake porosities presented in Figure 59 one again show a similar trend as observed with the other impellers. The porosities decrease regularly with increasing mixing intensity. The average specific cake resistances for these samples are presented in Figure 60 and it can be noted that the lowest resistances are obtained with

the lowest agitation rate (<=> largest crystal size, highest aspect ratio, highest cake porosities).

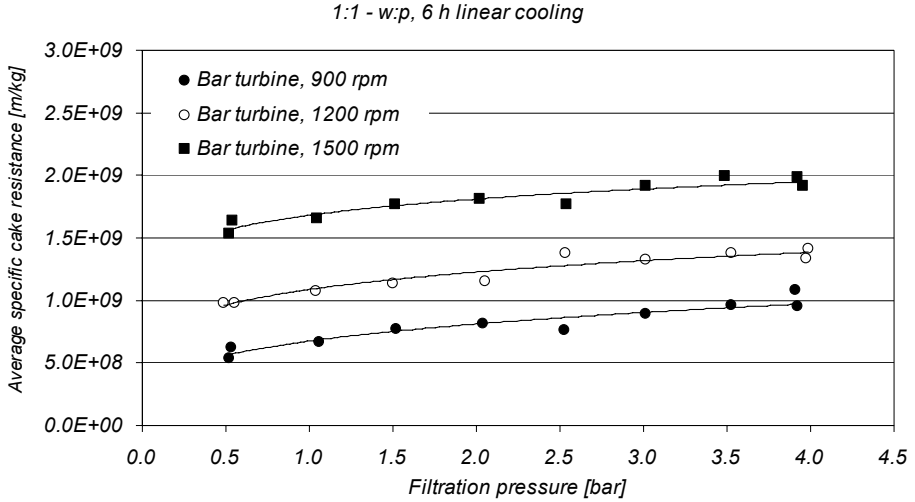

Figure 60 Average specific resistances of sulphathiazole cakes obtained from suspensions crystallized from 1:1 water:*n*-propanol mixture by using the constant cooling rate of 9.2 °C/h and a bar turbine with three different rotation speeds.

Table XXVI Summary of the filtration characteristics of the crystals suspensions obtained from suspensions crystallized from 1:1 water:*n*-propanol mixture by using constant cooling rate of 9.2 °C/h and a bar turbine with three different rotation speeds.

	Cooling	Cooling		Mixing	Filtration parameters			
Solvent	method	time	Impeller	speed	α_0	n	ε_0	λ
(-)	(-)	(h)	(-)	(RPM)	(m kg^{-1} bar^{-n})	(-)	(bar$^{-\lambda}$)	(-)
1:1 - w:p	Linear	6	BT	900	6.75E+08	0.27	0.54	0.065
1:1 - w:p	Linear	6	BT	1200	1.09E+09	0.17	0.51	0.051
1:1 - w:p	Linear	6	BT	1500	1.68E+09	0.11	0.49	0.032

7.4.1.4 Anchor Impeller

The average cake porosities and average specific cake resistances of the suspensions crystallized from 1:1 water:n-propanol mixture by using constant cooling rate of 9.2 °C/h and an anchor impeller with three different rotation speeds are presented in Figures 61 and 62 and the filtration parameters for the different suspensions are summarized in Table XXVII.

Comparison of the average cake porosities presented in Figure 61 shows that the values decrease regularly with the increasing mixing intensity. The crystal size distributions presented for these samples in Figure 53, show that the difference between the lowest and the second lowest agitation rates is almost negligible. Despite this, a significant difference can anyway be noticed in the porosities. The average specific cake resistances presented in Figure 62 show that the lowest resistances are obtained with the lowest agitation rate as was the case also with the other three impellers.

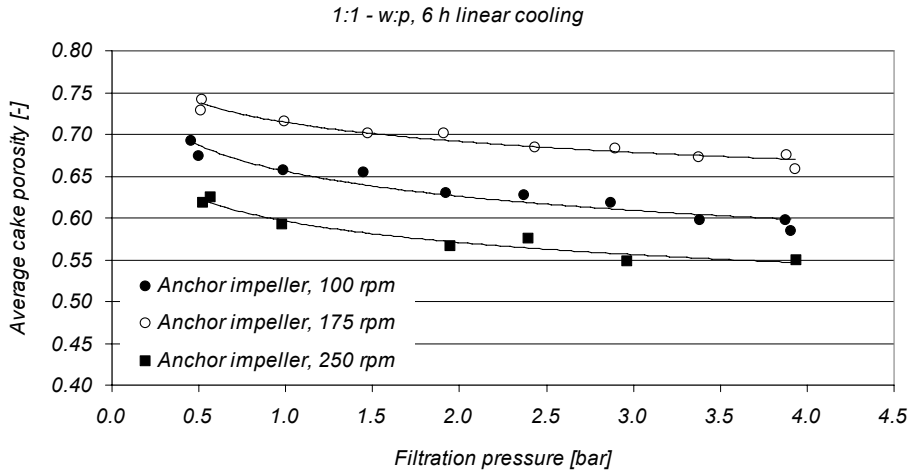

Figure 61 Average porosities of sulphathiazole cakes obtained from suspensions crystallized from 1:1 water:*n*-propanol mixture by using the constant cooling rate of 9.2 °C/h and an anchor impeller with three different rotation speeds.

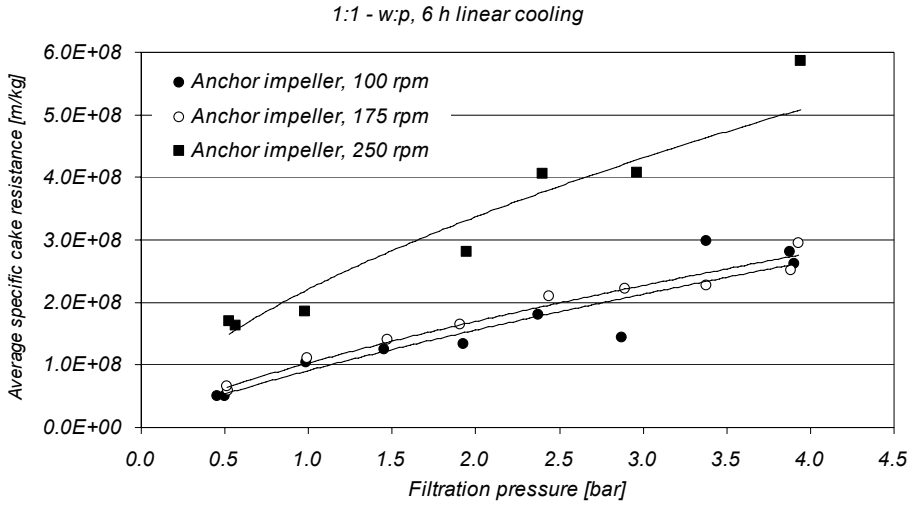

Figure 62 Average specific resistances of sulphathiazole cakes obtained from suspensions crystallized from 1:1 water:*n*-propanol mixture by using the constant cooling rate of 9.2 °C/h and an anchor impeller with three different rotation speeds.

Table XXVII Summary of the filtration characteristics of the crystals suspensions obtained from suspensions crystallized from 1:1 water:*n*-propanol mixture by using the constant cooling rate of 9.2 °C/h and an anchor impeller with three different rotation speeds.

	Cooling	Cooling		Mixing	Filtration parameters			
Solvent	method	time	Impeller	speed	α_0	n	ε_0	λ
(-)	(-)	(h)	(-)	(RPM)	(m kg^{-1} bar^{-n})	(-)	(bar$^{-\lambda}$)	(-)
1:1 - w:p	Linear	6	AI	100	9.14E+07	0.77	0.66	0.067
1:1 - w:p	Linear	6	AI	175	1.03E+08	0.72	0.71	0.047
1:1 - w:p	Linear	6	AI	250	2.07E+08	0.56	0.59	0.070

8 MULTIVARIATE MODELLING

This chapter introduces a method that can be used for predicting the filtration characteristics of solid-liquid suspensions according to the measured particle size and shape data. The main principle is to use multilinear partial least squares regression (*N-PLS*) for creating empirical models between experimentally determined filtration parameters and particle size and shape data obtained by image analysis. Separate models are derived for each filtration parameter and they are all validated with an external test set. The presented results show that the filtration characteristics of the considered test suspensions could be correlated relatively well with the obtained models.

The data set used to demonstrate the calculation procedure was obtained from a broad set of crystallization and filtration experiments introduced in the previous chapters. The aim of these experiments was to study the influence of crystallization conditions on the properties of the crystal product and on the pressure filtration characteristics of the crystal suspensions produced by laboratory scale crystallization experiments. The product obtained from the crystallization experiments was characterized, after which the crystals were separated from the crystallizing solvents by a pressure filter. The main parts of the performed experimental work are shown schematically in Figure 63, and a more detailed description of these experiments has been presented in the previous chapters.

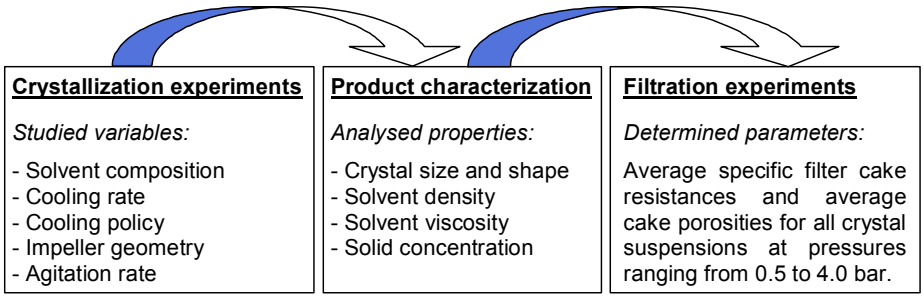

Figure 63 Different parts of the experimental work.

Based on the information collected during the filtration experiments, it was possible to determine some of the commonly applied filtration parameters for each of the investigated suspensions.

The experimentally determined values of the four parameters in equations (20) and (21) for the 48 different sulphathiazole suspensions considered in this study are presented in Figures 64 – 67. The purpose of these figures is to show the average order of magnitude of the experimental results, and also to illustrate the variation between the different samples. When observing the figures, it can be noticed that the differences in the values of the four parameters are fairly great in all cases. These figures show that the experimental data is presented in a relatively random manner, as obvious trends cannot be discovered in the figures. Figure 64 shows that the average specific cake resistances at 1.0 bar (α_0) vary from approximately $1 \cdot 10^8$ to $2 \cdot 10^9$ m/kg. These values can be considered as relatively low, which is apparently a consequence of a fairly large average crystal size.

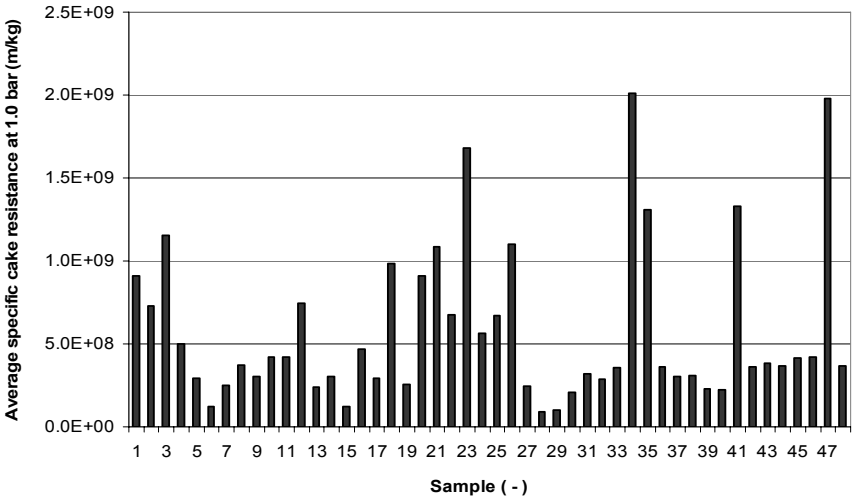

Figure 64 Experimentally determined α_0 -values for the crystal suspensions.

The values of the compressibility coefficients (n) given in Figure 65 imply that the compression characteristics of the sulphathiazole cakes differ considerably from practically incompressible (0.09) to highly compressible (0.78). As the filtered material in all these experiments was the same, the large variation is caused solely by differences in the crystal size and shape. Although it cannot be seen directly in Figure 65, it has been shown earlier that for example the cooling and mixing conditions can have a great influence on the compressibility of crystal cakes.

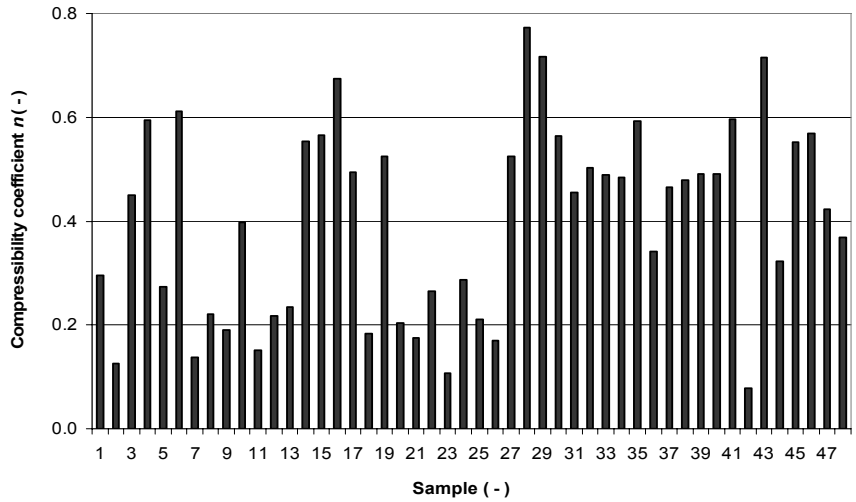

Figure 65 Experimentally determined *n*-values for the crystal suspensions.

Figure 66 shows the average porosities of the sulphathiazole cakes at 1.0 bar (ε_0) for the examined suspensions. It can be clearly seen that there are significant differences between the packing densities of different kinds of crystals, as the porosities range from about 0.48 to 0.71.

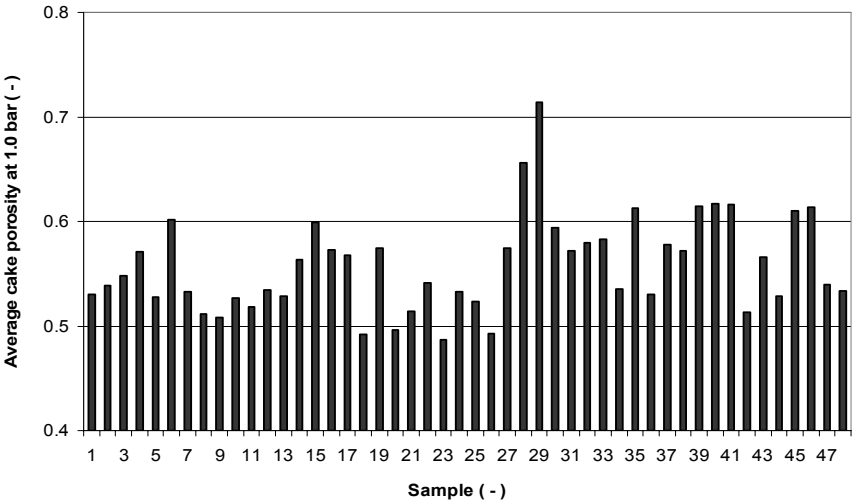

Figure 66 Experimentally determined ε_0 -values for the crystal suspensions

The λ - values presented in Figure 67 also show that the influence of the applied filtration pressure on the average crystal cake porosity differs considerably between the suspensions. The values of these compressibility coefficients (λ) vary between 0.03 and 0.09. The values presented in Figures 66 and 67 clearly show that it would be misleading to assume a constant average cake porosity for different samples or for a single sample at different filtration pressures. For this reason, it is clear that the application of theoretical models for predicting the average specific cake resistances from measured particle properties would require an accurate method for first predicting the cake porosities at given conditions.

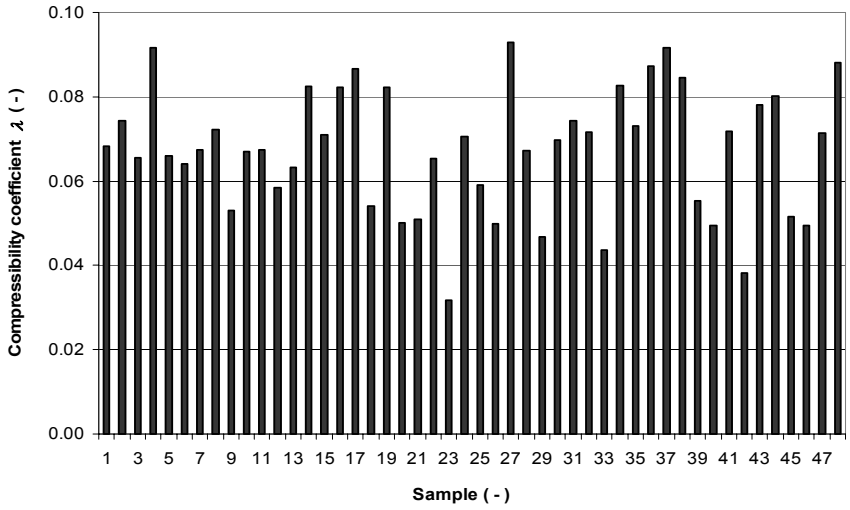

Figure 67 Experimentally determined λ - values for the crystal suspensions.

Some attempts were made during this study to predict the crystal cake properties from the image analysis results by applying some of the theoretical models presented in the literature. However, the obtained results showed quite clearly that the existing models could not be used to obtain reasonable predictions. It was therefore concluded that alternative modelling methods are required in order to be able to predict the filtration behaviour of the examined suspensions from the size and shape data provided by the image analyzer.

8.1 Multilinear partial least squares regression

The modelling technique that was chosen to be applied in this study was multilinear partial least squares regression (*N-PLS*). In *N-PLS*, a regression model is created between a multidimensional set of independent variables (**X**) and dependent variables (**y**). Figure 68 illustrates the principle of this method for a three-dimensional data set. The three-way array of original variables is decomposed into a number of trilinear components that each consist of one score vector and two weight vectors. The remaining residual (**E**) contains the measurement and model errors. Simultaneously with the decomposition, a regression model is created between the trilinear components and the dependent variables. This means that the dependent variables are not regressed directly on the original variables but on the score vectors of the triads. Descriptions of the detailed theory and previous application areas of N-PLS are not be provided in this thesis, but can be found in the literature (Bro, 1996; Bro, 1998 and Gurden *et al.*, 2001).

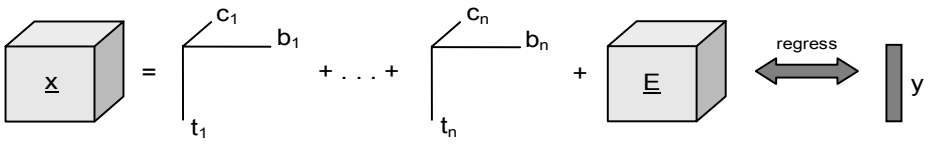

Figure 68 The principle of multilinear partial least squares regression.

The multilinear partial least squares regression technique was used here to create four different models, one for each of the considered filtration parameters. The original three-dimensional data array (**X**) consisted of the measured properties of the crystal suspensions. Each of the 48 crystal suspensions was described by 9 different distributions, which were shown in Figure 9 above. These distributions could be represented numerically as a table of 9 columns and 52 rows where each column corresponded to one of the crystal parameters or solvent properties and each row corresponded to one size or shape class. In other words, each crystal suspension was represented by 468 input variables. By combining the data tables of all the crystal samples, a three-dimensional data array (48×52×9) could be formed. The experimentally determined filtration parameters, shown in Figures 64 – 67, formed the four vectors (1×48) of the dependent variables (**y**).

Before creating the models, the initial data of 48 samples was divided randomly into two sets; a calibration set of 40 samples and an independent test set of 8 samples. The samples in the test set were not included in the data when the models were created, and they could therefore be used for reliable validation of the obtained models. By comparing the experimentally determined values of the test set samples to the values provided by the models, the ability of the models to predict the filtration properties of unknown samples could be estimated. All the calculations were done in Matlab 6.5 (MathWorks, Inc.) using the N-way Toolbox for MATLAB, provided by Andersson and Bro (1998). The selection of the number of PLS-components in the models was based on the *R*oot *M*ean *S*quared *E*rror of *P*rediction (*RMSEP*) of the calibration set and was chosen to be 9 in all models.

8.2 Modelling Results

The results of the multivariate modelling are summarized in Figures 69 - 72, which show the experimentally determined values of the four filtration parameters, together with the values predicted with the created models. Each figure also shows the percentage of variation explained by the models for the calibration set (R^2) and for the test set (Q^2). Figure 69 shows the results for parameter α_0, and as can be seen, the model seems to fit quite well. All the data points are distributed evenly on both sides of the diagonal line, and the values for R^2 and Q^2 are both around 90 %.

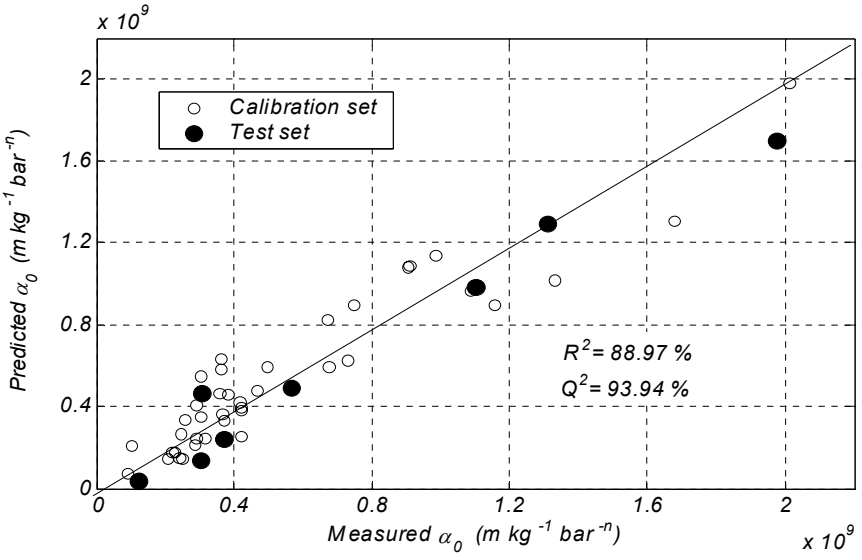

Figure 69 Experimentally determined α_0 - values vs. the α_0 - values predicted by applying the N-PLS – model.

Similar results are obtained by applying the model for the compressibility coefficient *n*. These are presented in Figure 70, and also here the percentage of variation explained by the model is about 90 %. These results imply that the created multivariate models can be applied for predicting the average specific resistances of the sulphathiazole cakes at different pressures in a fairly accurate manner.

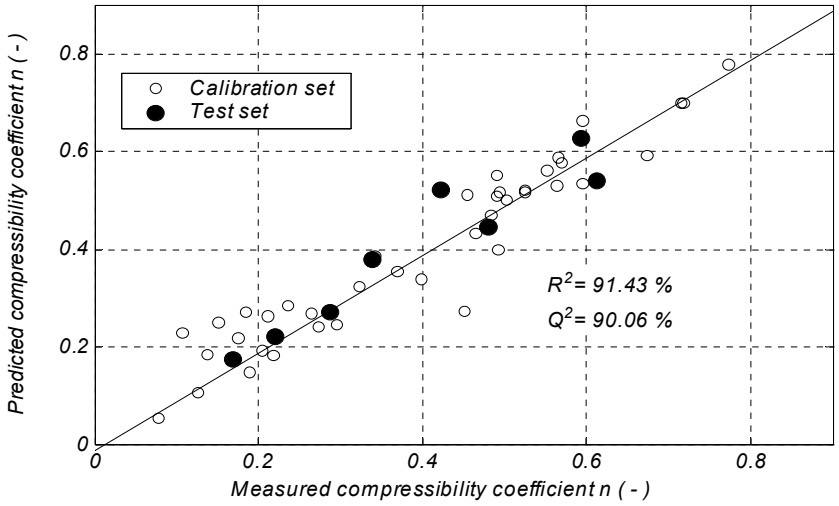

Figure 70 Experimentally determined *n* - values vs. the *n* - values predicted by applying the N-PLS – model.

Figure 71 shows that the model for the parameter ε_0 manages to explain the existing variation with an accuracy of over 91 %. The maximum prediction error in the values of ε_0 appears to be approximately 0.03 (6 %), which may be considered very low. The results obtained by the model for the compressibility coefficient λ are given in Figure 72. The values of R^2 and Q^2 in this case are clearly lower than those with the other three models. Figure 72 shows that none of the data points can be considered an obvious outlier which would somehow distort the model, and therefore it is probable that the poor values for the correlation coefficients are a result of the fact that the average deviation between the measured and predicted values is much larger than in Figures 69 – 72. The reason for this diverging result can probably be found in the original filtration data.

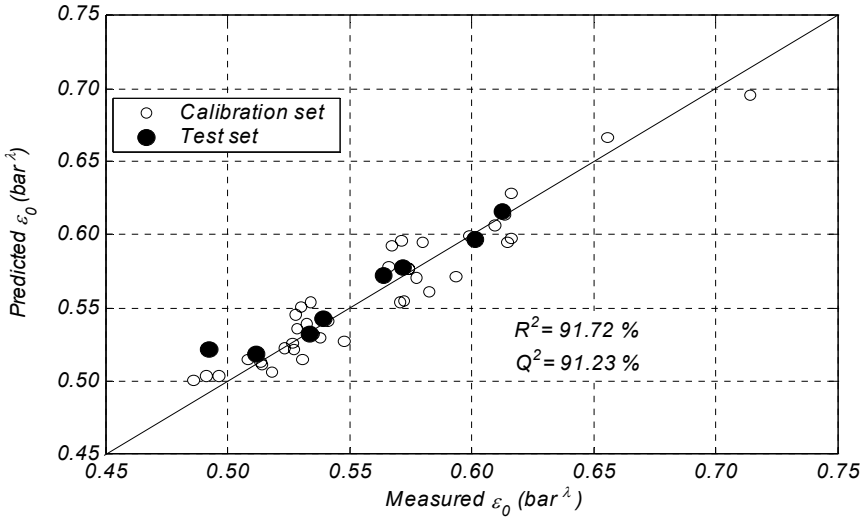

Figure 71 Experimentally determined ε_0 - values vs. the ε_0 - values predicted by applying the N-PLS – model.

Parameter λ describes the influence of the applied filtration pressure on the internal packing structure of the cake. It has been observed in earlier studies that sulphathiazole crystals are very sensitive to all kinds of mechanical stresses, and it can therefore be assumed that part of the crystals break apart during the filtration experiments, especially at higher filtration pressures. The influence of crystal breakage would be seen most notably on the values of λ as they describe the variations in the average cake porosities. Predicting the changes caused by crystal breakage from the measured crystal dimensions alone is, however, difficult, if not impossible. It can therefore be assumed that the lower percentages of variation explained by the λ - model are mainly caused by the breakage of the crystals during the cake formation. The accuracy of this model could be possibly improved by supplementing the original data with a variable that somehow describes the mechanical strength of the crystals.

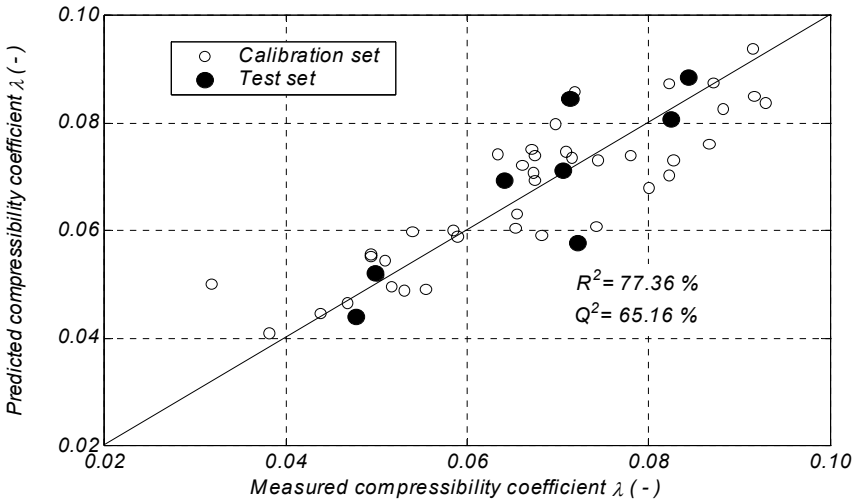

Figure 72 Experimentally determined λ - values vs. the λ - values predicted by applying the N-PLS – model.

The models introduced here were created by using raw data obtained directly from image analysis. It is therefore likely that the accuracy of the models could be further improved by utilizing some mathematical data preprocessing methods or by modifying the manner of representation of the variables in the original data array. N-PLS also allows the interpretation of the relative effects of different crystal and solvent properties on the individual filtration parameters by using so-called variable loadings. These diagnostics are not presented in this context but may be utilized in further studies for more thorough analysis of the relationships between the crystal properties and the filtration characteristics.

9 CONCLUSIONS

The aim of this work was to find out if the solid-liquid separation characteristics of crystallized sulfathiazole suspensions could be modified by changing the operating parameters of the crystallization process. The different parameters that were studied were the composition of the solvent, the cooling rate during the cooling crystallization processes carried out by using a constant cooling rate throughout the whole batch, the cooling profile, as well as the mixing intensity during the batch. The obtained results showed that fairly great differences were observed between the size and shape of the crystals produced, and it was also shown experimentally that the changes in the crystal size and shape had a direct impact on the pressure filtration characteristics of the crystal suspensions. The most significant factor that influenced the quality of the product crystals, and therefore also their filterability, seemed to be secondary nucleation caused either by breakage of the formed crystals during the crystallization process or by surface nucleation under supersaturated conditions. It can be assumed that the long and thin shape of typical sulphathiazole crystals makes the crystals extremely fragile, and it is therefore likely that the final size and shape distributions are in this case strongly affected by the attrition nucleation.

The pressure filtration characteristics of the suspensions obtained in the crystallization experiments were evaluated on the basis of average filter cake porosities and average specific cake resistances that were determined on the basis of experimentally obtained filtration data. Observation of these filtration characteristics showed that considerable differences existed between the different suspensions, and it can therefore be concluded that the pressure filtration process was influenced by the operation conditions applied during the crystallization. In general, the filterability of all the studied sulphathiazole suspensions was found to be rather good, based on the relatively low cake porosities, accompanied with low cake resistances. Comparison between the crystal properties and the results obtained in the filtration experiments revealed that it was impossible to directly the filtration characteristics of different sulphathiazole suspensions directly on the basis of any single crystal parameter. It seems therefore obvious that the packing structure of the crystals in the filter cake is determined by several different crystal parameters, and the filterability of the suspensions should thus be estimated by taking all the different crystal properties into account simultaneously.

The last chapter of this thesis introduced a method that can be used for examining the relationship between crystal parameters and pressure filtration characteristics. The target of the data analysis was to find correlations between the properties of the product crystals and the experimentally determined filtration coefficients $\alpha 0$, n, $\varepsilon 0$ and λ. The results presented in this thesis showed that such correlations could be found, and it was therefore possible to develop an empirical model that could be used for predicting the filtration parameters based on the given crystal data. This kind of models could be easily used also for industrial filtration processes and with them, variations in the properties of the solids to be separated could be taken into account. If the filtration parameters could be approximated prior to filtration, it would be possible to adjust the operating conditions of the filter in such a way that either the batch time (i.e. cake resistance) or the solvent content of the filter cake (i.e. cake porosity) could be maintained constant despite changes in the properties of the filtered material. This kind of a model would, of course, be valid only for the particular system where the data was obtained from and it should not therefore be considered as a general solution for all filtration problems. The most problematic part of using this kind of predictive models in practice at the moment seems to be the lack of suitable particle size and shape analyzers. An ideal analyzer would be one that could measure the particle properties online just before the filtration process. Such analyzers do not exist at the moment, but several companies are developing online image analyzers, and it is therefore probably only a question of time when the first ones become available.

It would be of academic interest to broaden the models presented in this paper by extending the diversity of the samples. A great amount of experimental work would obviously be required in order to obtain valid and reliable models for a wide range of solid/liquid-suspensions, but the results presented in this paper clearly demonstrated that suitable tools for the modelling are already available. If the variations between the material properties of the considered suspensions were extensive enough, the information provided by these kinds of models could be applied to predicting the filtration parameters of new samples and also used for improving theoretical understanding of the influence of different particle properties on filtration. Thorough analysis of the internal variables of the multivariate models would then make it possible to estimate the relative effects of the considered particle and liquid properties on the filtration characteristics. Considerable efforts are, however, required before

sufficient experimental information will be available to permit the development of more extensive models.

10 REFERENCES

Aaltonen, J., Rantanen, J., Siiriä, S., Karjalainen, M., Jørgensen, A., Laitinen, N., Savolainen, M., Seitavuopio, P., Louhi-Kultanen, M., and Yliruusi, J., (2003). Polymorph screening using near-infrared spectroscopy, *Anal. Chem.*, 75(19): 5267-5273.

Abreu, C. R. A., Tavares, F. W., and Castier, M., (2003). Influence of particle shape on the packing and on the segregation of spherocylinders via Monte-Carlo simulations, *Powder Technol.*, 134(1-2): 167-180.

Alatalo, H., Louhi-Kultanen, M., and Palosaari, S., (1999). Operation of batch crystallization: non-linear solubility effects, *BIWIC 1999 - 7th International Workshop on Industrial Crystallization*, Halle, Germany.

Anderson, J. E., Moore, S., Tarczynski, F., and Walker, D., (2001). Determination of the onset of crystallization of N^1-2-(thiazolyl)sulfanilamide (sulphathiazole) by UV-Vis and calorimetry using an automated reaction platform; subsequent characterization of polymorphic forms using dispersive Raman spectroscopy, *Spectroc. Acta Pt. A: Molec. Biomolec. Spectr.*, 57(9): 1793-1808.

Andersson, C. A., and Bro, R., (2000). The N-way Toolbox for MATLAB, *Chemometrics Intell. Lab. Syst.*, 52(1):1-4.

Anwar, J., Tarling, S. E., and Barnes, P., (1989). Polymorphism of sulphathiazole, *J. Pharm. Sci.*, 78(4): 337-342.

Apperley, D. C., Fletton, R. A., Harris, R. K., Lancaster, R. W., Tavener, S., and Threlfall, T. L., (1999). Sulphathiazole polymorphism studied by magic-angle spinning NMR, *J. Pharm. Sci.*, 88(12): 1275-1280.

Bauer, M., de Leede, L., and Van Der Waart, M., (1998). Purity as an issue in pharmaceutical research and development, *Eur. J. Pharm. Sci.,* 6(4): 331-335.

Beckmann, W., (2000). Seeding the desired polymorph: background, possibilities, limitations, and case studies, *Org. Process Res. Dev.*, 4(5): 372-383.

Berglund, K. A., and Murphy, V. G., (1986). Modeling growth rate dispersion in a batch sucrose crystallizer, *Ind. Eng. Chem. Fundamen.*, 25*(*1): 174–176.

Bernard-Michel, B., Pons, M. N., and Vivier, H., (2002). Quantification, by image analysis, of effect of operational conditions on size and shape of precipitated barium sulphate, *Chem. Eng. J.*, 87(2): 135-147.

Besra, L., Sengupta, D. K., and Roy, S. K., (2000). Particle characteristics and their influence on dewatering of kaolin, calcite and quartz suspensions, *Int. J. Miner. Process.*, 59(2): 89-112.

Blagden, N., Davey, R. J., Lieberman, H. F., Williams, L., Payne, R., Roberts, R, Rowe, R., and Docherty, R., (1998a). Crystal chemistry and solvent effects in polymorphic systems: sulphathiazole, *J. Chem. Soc., Faraday Trans.,* 94(8): 1035-1044.

Blagden, N., Davey, R. J., Rowe, R., and Roberts, R., (1998b). Disappearing polymorphs and the role of reaction by-products: the case of sulphathiazole, *Int. J. Pharm.*, 172(1-2): 169-177.

Bladgen, N., (2001). Crystal engineering of polymorph appearance: the case of sulphathiazole, *Powder Technol.*, 121(1): 46-52.

Brittain, H. G., and Byrn, S. R., (1999). Structural aspects of polymorphism, In: *Polymorphism in Pharmaceutical Solids*, 1st ed., Brittain, H. G., ed., Marcel Dekker, Inc., New York, NY, United States: 73-124.

Brittain, H. G., and Grant, D. J. W., (1999). Effects of polymorphism and solid-state solvation on solubility and dissolution rate, In: *Polymorphism in Pharmaceutical Solids*, 1st ed., Brittain, H. G., ed., Marcel Dekker, Inc., New York, NY, United States: 279-331.

Bro, R., (1996). Multi-way calibration. Multi-linear PLS, *J. Chemom.*, 10(1): 47-62.

Bro, R. (1998). Multi-way analysis in the food industry: models, algorithms, and applications, Royal Veterinary and Agricultural University, Denmark.

Bugay, D. E., (2001). Characterization of the solid-state: spectroscopic techniques, *Adv. Drug Deliv. Rev.*, 48(1): 43-65.

Byrn, S. R., Pfeiffer, R. R., and Stowell, J. G., (1999). *Solid State Chemistry of Drugs*, 2nd ed., SSCI, Inc., West Lafayette, IN, United States.

Calderon De Anda, J., Wang, X. Z., and Roberts, K. J., (2005a). Multi-scale segmentation image analysis for the in-process monitoring of particle shape with batch crystallizers, *Chem. Eng. Sci.*, 60(4): 1053-1065.

Calderon De Anda, J., Wang, X. Z., Lai, X., and Roberts, K. J., (2005b). Classifying organic crystals via in-process image analysis and the use of monitoring charts to follow polymorphic and morphological changes, *J. Process Control*, 15(7): 785-797.

Calderon De Anda, J., Wang, X. Z., Lai, X., Roberts, K. J., Jennings, K. H., Wilkinson, M. J., Watson, D., and Roberts, D., (2005c). Real-time product morphology monitoring in crystallization using imaging technique, *AIChE Journal*, 51(5): 1406-1414.

Chan, F. C., Anwar, J., Cernik, R., Barnes, P., and Wilson, R**.**, (1999). Ab initio structure determination of sulphathiazole polymorph V from synchrotron X-ray powder diffraction data**,** *J. Appl. Crystallogr.*, 32(3): 436-441.

Coulson, J. M., Richardson, J. F., Backhurst, J. R., and Harker, J. H., (1978). *Chemical Engineering, Vol. 2*, 3rd ed., Pergamon Press plc, Oxford, UK.

Darcy, H. P. G., (1856). *Les Fontaines Publiques de la Villa de Dijon*, Dalamont, Paris.

Davey, R., and Garside, J., (2000). *From Molecules to Crystallizers*, 1st ed., Oxford University Press, Oxford, United Kingdom.

Faria, N., Pons, M. N., Feyo de Azevedo, S., Rocha, F. A., and Vivier, H., (2003). Quantification of the morphology of sucrose crystals by image analysis, *Powder Technol.*, 133(1-3): 54-67.

FDA, (2003). *Draft guidance for industry. PAT — a framework for innovative pharmaceutical manufacturing and quality assurance*, Office of Pharmaceutical Science, Center for Drug Evaluation and Research, Food and Drug Administration, U.S. Department of Health and Human Services, Rockville, MD, United States.

Ferreira, A., Faria, N., Rocha, F., Feyo de Azevedo, S., and Lopes, A., (2005). Using image analysis to look into the effect of impurity concentration in NaCl crystallization, *Chem. Eng. Res. Des.*, 83(A4): 331-338.

Grace, H. P., (1953a). Resistance and compressibility of filter cakes, *Chemical Engineering Progress*, 49(6): 303-318.

Grace, H. P., (1953b). Resistance and compressibility of filter cakes. Part II: Under conditions of pressure filtration, *Chem. Eng. Prog.*, 49(7): 367-377.

Grant, D. J. W., (1999). Theory and origin of polymorphism, *Polymorphism in Pharmaceutical Solids*, 1st ed., Brittain, H. G., ed., Marcel Dekker, Inc., New York, NY, United States: 1-34.

Guillory, J. K., (1999). Generation of polymorphs, hydrates, solvates and amorphous solids, In: *Polymorphism in Pharmaceutical Solids*, 1st ed., Brittain, H. G., ed., Marcel Dekker, Inc., New York, NY, United States: 183-226.

Gurden, S. P., Westerhuis, J. A., Bro, R., and Smilde, A. K., (2001). A comparison of multiway regression and scaling methods, *Chemometrics Intell. Lab. Syst.*, 59(1-2): 121-136.

Hentschel, M. L., and Page, N. W., (2003). Selection of descriptors for particle shape characterization, *Part. Part. Syst. Charact.*, 20(1): 25-38.

Hurley, L. A., Jones, A. G., and Hammond, R. B., (2004). Molecular packing, morphological modeling, and image analysis of cyanazine crystals precipitated from aqueous ethanol solutions, *Cryst. Growth Des.*, 4(4): 711-715.

Hwang, K. J., Wu, Y. S., and Lu, W. M., (1996). The surface structure of cake formed by uniform-sized rigid spheroids in cake filtration, *Powder Technol.*, 87(2): 161-168.

Hwang, K. J., Wu, Y. S, and Lu, W. M., (1997). Effect of the size distribution of spheroidal particles on the surface structure of a filter cake, *Powder Technol.*, 91(2): 105-113.

Iritani, E., Mukai, Y., and Toyoda, Y., (2002). Properties of a filter cake formed in dead-end microfiltration of binary particulate mixtures, *Journal of Chemical Engineering of Japan*, 35(3): 226-233.

Jagadesh, D., Kubota, N., Yokota, M., Sato, A., and Tavare, N. S., (1996). Large and mono-sized product crystals from natural cooling mode batch crystallizer, *J. Chem. Eng. Jpn.*, 29(5): 865-873.

Jones, A. G., and Mullin, J. W., (1974). Programmed cooling crystallization of potassium sulphate solutions, *Chem. Eng. Sci.*, 29(1): 105-118.

Jones, A. G., Budz, J., and Mullin, J. W., (1987). Batch crystallization and solid-liquid separation of potassium sulphate, *Chemical Engineering Science*, 42(4): 619-629.

Jones, A. G., (2002). *Crystallization process systems*, 1st ed., Butterworth-Heinemann, Great Britain.

Khoshkhoo, S., and Anwar, J., (1993). Crystallization of polymorphs: the effect of solvent, J. Phys. D: Appl. Phys., 26(8B): B90-B93.

Klein, J. P., and David, R., (1995). Reaction crystallization, In: *Crystallization technology handbook*, 1st ed., A. Mersmann, ed., Marcel Dekker, New York: 513 – 557.

Kolář, P., Shen, J. W., Tsuboi, A., and Ishikawa, T., (2002). Solvent selection for pharmaceuticals, *Fluid Phase Equilib.*, 194-197: 771-782.

Lahav, M., and Leiserowitz, L., (2001). The effect of solvent on crystal growth and morphology, *Chem. Eng. Sci.*, 56(7): 2245-2253.

Lang, Y., Cervantes A. M., and Biegler, L. T., (1999). Dynamic optimization of a batch cooling crystallization process, *Ind. Eng. Chem. Process Des. Dev.*, 38(4): 1469-1477.

Lee, S. A., Fane, A. G., Amal, R., and Waite, T. D., (2003). The effect of floc size and structure on specific cake resistance and compressibility in dead-end microfiltration, *Separation Science and Technology*, 38(4): 869-887.

Lewiner, F., Klein, J. P., Puel, F. and Fevotte, G., (2001a). On-line ATR FTIR measurement of supersaturation during solution crystallization processes. Calibration and applications on three solute solvent systems, *Chem. Eng. Sci.*, 56(6): 2069-2084.

Lewiner, F., Fevotte G., Klein, J. P. and Puel, F., (2001b). Improving batch cooling seeded crystallization of an organic weed-killer using on-line ATR FTIR measurement of supersaturation, *J. Cryst. Growth*, 226(2-3): 348-362.

Lewiner, F., Fevotte, G., Klein, J. P., and Puel, F., (2002). An online strategy to increase the average crystal size during organic batch cooling crystallization, *Ind. Eng. Chem. Res.*, 41(5): 1321-1328.

Matthews, H. B. and Rawlings, J. B., (1998). Batch crystallization of a photochemical: modeling, control, and filtration, *AIChE J.*, 44(5): 1119-1127.

Meeten, G. H. (2000). Septum and filtration properties of rigid and deformable particle suspensions, *Chem. Eng. Sci.*, 55(10): 1755-1767.

Mersmann, A., (1995). Fundamentals of Crystallization, In: *Crystallization technology handbook*, 1st ed., A. Mersmann, ed., Marcel Dekker, New York: 1 – 44.

Mersmann, A., (1996). Supersaturation and nucleation, *Trans. IChemE, Part A, Chem. Eng. Res. Des.*, 74(A7): 812-820.

Mersmann, A., (1999). Crystallization and precipitation, *Chem. Eng. Process.*, 38(4-6): 345-353.

Mersmann, A., and Löffelmann, M., (2000). Crystallization and precipitation: the optimal supersaturation, *Chem. Eng. Technol.*, 23(1): 11-15.

Mersmann, A., and Rennie, F. W., (2001). Operation of Crystallizers, In: *Crystallization technology handbook*, 2nd ed., A. Mersmann, ed., CRC Press: 393 - 474.

Mersmann, A., Eble, A., and Heyer, C., (Ed.), (2001). Crystal Growth, In: *Crystallization technology handbook*, 2nd ed., A. Mersmann, ed., CRC Press: 81 - 144.

Mersmann, A. (Ed.), (2001). *Crystallization Technology Handbook*, 2nd edition, Marcel Dekker, New York.

Mota, M., Teixeira, J. A., Bowen, W. R., and Yelshin, A., (2001). Binary spherical particle mixed beds: porosity and permeability relationship measurement, *Transactions of the Filtration Society*, 1(4): 101-106.

Mullin, J. W., and Nývlt, J., (1971). Programmed cooling of batch crystallizers, *Chem. Eng. Sci.*, 26(3): 369-377.

Mullin, J. W., (1997). *Crystallization*, 3rd ed., Butterworth-Heinemann, United Kingdom:

Myerson, A. S., Decker, S. E., and Weiping, F., (1986). Solvent selection and batch crystallization, *Ind. Eng. Chem. Process Des. Dev.*, 25(4): 925-929.

Ni, L. A., Yu, A. B., Lu, G. Q., and Howes, T., (2006). Simulation of cake formation and growth in cake filtration, *Minerals Engineering*, 19(10): 1084-1097.

Nienow, A. W., The mixer as a reactor: Liquid/solid systems, In: *Mixing in the process industries*, 2nd ed., Harnby, N., Edwards, M. F., and Nienow, A. W., eds., Butterworth-Heinemann, Oxford, United Kingdom

Oja, M., (1996). *Pressure filtration of mineral slurries: Modelling and particle shape characterization*, Doctoral Thesis, Lappeenranta University of Technology, Finland.

Pons, M. N., Vivier, H., Delcour, V., Authelin, J.-R., and Paillères-Hubert, L., (2002). Morphological analysis of pharmaceutical powders, *Powder Technol.*, 128(2-3): 276-286.

Pöllänen, K., Häkkinen, A., Reinikainen, S-P., Louhi-Kultanen, M., Nyström, L., (2005a). ATR-FTIR in monitoring of crystallization processes: comparison of indirect and direct OSC methods, *Chemometrics and Intelligent Laboratory Systems*, 76(1): 25-35.

Pöllänen, K., Häkkinen, A., Reinikainen, S-P., Rantanen, J., Karjalainen, M., Louhi-Kultanen, M., Nyström, L., (2005b). IR spectroscopy together with multivariate data analysis as a process analytical tool for in-line monitoring of crystallization process and solid state analysis of crystalline product, *Journal of Pharmaceutical and Biomedical Analysis*, 38(2): 275-284.

Pöllänen, K., Häkkinen, A., Huhtanen, M., Reinikainen, S-P., Karjalainen, M., Rantanen, J., Louhi-Kultanen, M., Nyström, L., (2005c). DRIFT-IR for quantitative characterization of polymorphic composition of sulphathiazole, *Analytica Chimica Acta*, 544(1-2): 108-117.

Pöllänen, K., Häkkinen, A., Reinikainen, S-P., Rantanen, J., Minkkinen, P., (2006a). Dynamic PCA-based MSPC charts for nucleation prediction in batch cooling crystallization processes, *Chemometrics and Intelligent Laboratory Systems*, 84(1-2): 126-133.

Pöllänen, K., Häkkinen, A., Reinikainen, S-P., Louhi-Kultanen, M., Nyström, L., (2006b). A study on batch cooling crystallization of sulphathiazole: process monitoring using ATR-FTIR and product characterization by automated image analysis, *Chemical Engineering Research and Design*, 84(A1): 47-59.

Rushton, A., Ward, A. S., and Holdich, R. G. (2000). *Solid-Liquid Filtration and Separation Technology*, 2nd ed., Wiley-VCH Verlag GmbH, Weinheim, Germany.

Shirato, M., Murase, T., Iritani, E., Tiller, F. M., and Alciatore, A. F. (1987). Filtration in the chemical process industry, In: *Filtration: principles and practices*, 2nd edition, Matteson, M. J. and Orr, C., eds., Marcel Dekker, Inc., New York, NY, United States: 299-423.

Sorrentino, J. A., and Anlauf, H., (2004). Prediction of filter-cake properties from particle collective characteristics, *Fluid/Particle Separation Journal*, 16(2): 135-145.

Srinivasakannan, C., Vasanthakumar, R., Iyappan, K., and Rao, P. G. (2002). A study on crystallization of oxalic acid in batch cooling crystallizer, *Chem. Biochem. Eng. Q.*, 16(3): 125-129.

Svarovsky, L. (1981a). Characterization of particles suspended in liquids, In: *Solid-Liquid Separation (Butterworth Monographs in Chemistry and Chemical Engineering)*, 2nd ed., Svarovsky, L. ed., Butterworth-Heinemann, London, United Kingdom: 8-32.

Svarovsky, L. (1981b). Filtration fundamentals, In: *Solid-Liquid Separation (Butterworth Monographs in Chemistry and Chemical Engineering)*, 2nd ed., Svarovsky, L. ed., Butterworth-Heinemann, London, United Kingdom: 242-264.

Svarovsky, L. (1993). Filtration, In: *Kirk-Othmer Encyclopedia of Chemical Technology*, 4th ed., Kroschwitz, J. I., Howe-Grant, M., eds., John Wiley & Sons, Inc., New York, NY, United States, vol. 10: 788-853.

Svarovsky, L. (2000a). Characterization of particles suspended in liquids, In: *Solid-Liquid Separation*, 4th ed., Svarovsky, L. ed., Butterworth-Heinemann, Oxford, United Kingdom: 30 - 65.

Svarovsky, L. (2000b). Filtration fundamentals, In: *Solid-Liquid Separation*, 4th ed., Svarovsky, L. ed., Butterworth-Heinemann, Oxford, United Kingdom: 302-334.

Threlfall, T., (2000). Crystallization of polymorphs: thermodynamic insight into the role of solvent, *Org. Process Res. Dev.*, 4(5): 384-390.

Tiller, F. M., (1953). The role of porosity in filtration. Numerical methods for constant rate and constant pressure filtration based on Kozeny's law, *Chem. Eng. Prog.*, 49(9): 467-479.

Togkalidou, T., Braatz, R. D., Johnson, B. K., Davidson, O., and Andrews, A., (2001). Experimental design and inferential modeling in pharmaceutical crystallization, *AIChE J.*, 47(1): 160-168.

Ulrich, J., and Strege, C., (2002). Some aspects of the importance of metastable zone width and nucleation in industrial crystallizers, *J. Cryst. Growth*, 237-239(3): 2130-2135.

Vippagunta, S. R., Brittain, H. G., and Grant, D. J. W., (2001). Crystalline solids, *Adv. Drug Deliv. Rev.*, 48(1): 3-26.

Wakemann, R. J., (1975). *Filtration post-treatment processes*, 1st ed., Elsevier Scientific Publishing Company, Amsterdam, Netherlands.

Wakeman, R. J., and Tarleton, E. S., (1999). Filtration: equipment selection, modelling and process simulation, 1st ed., Elsevier Science Ltd, Oxford, United Kingdom.

Wang, W. S., Aggarval, M. D., Choi, J., Gebre, T., Shields, A. D., Penn, B. G., Frazier, D. O., (1999). Solvent effects and polymorphic transformation of organic nonlinear optical crystal L-pyroglutamic acid in solution growth processes: I. Solvent effects and growth morphology, *J. Cryst. Growth*, 198/199(1): 578-582.

Wibowo, C., Chang, W. C., and Ng, K. M., (2001). Design of integrated crystallization systems, *AIChE J.*, 47(11): 2474-2492.

Wibowo, C., and Ng, K. M., (2002). Workflow for process synthesis and development: crystallization and solids processing, *Ind. Eng. Chem. Process Des. Dev.*, 41(16): 3839-3848.

Winn, D., and Doherty, M. F., (2002). Predicting the shape of organic crystals grown from polar solvents, *Chem. Eng. Sci.*, 57(10): 1805-1813.

Yu, A. B., and Standish, N., (1993). A study of the packing of particles with a mixture size distribution, *Powder Technol.*, 76(2): 113-124.

Yu, A. B., Bridgewater, J., and Burbidge, A., (1997). On the modelling of the packing of fine particles, *Powder Technology*, 92(3): 185-194.

Zou, R. P., and Yu, A. B., (1996). Evaluation of the packing characteristics of mono-sized non-spherical particles, *Powder Technol.*, 88(1): 71-79.

Zwietering, T. N., Suspension of solid particles in liquids by agitators, *Chemical Engineering Science*, 8(3-4): 244-253.

Ålander, E. M., Uusi-Penttilä, M. S., and Rasmuson, Å. C., (2003). Characterization of paracetamol agglomerates by image analysis and strength measurement, *Powder Technol.*, 130(1-3): 298-306.

Appendix I

EXPERIMENTAL DESIGNS SHOWING ALL OF THE LABORATORY TESTS AND ANALYSES CARRIED OUT DURING THIS STUDY

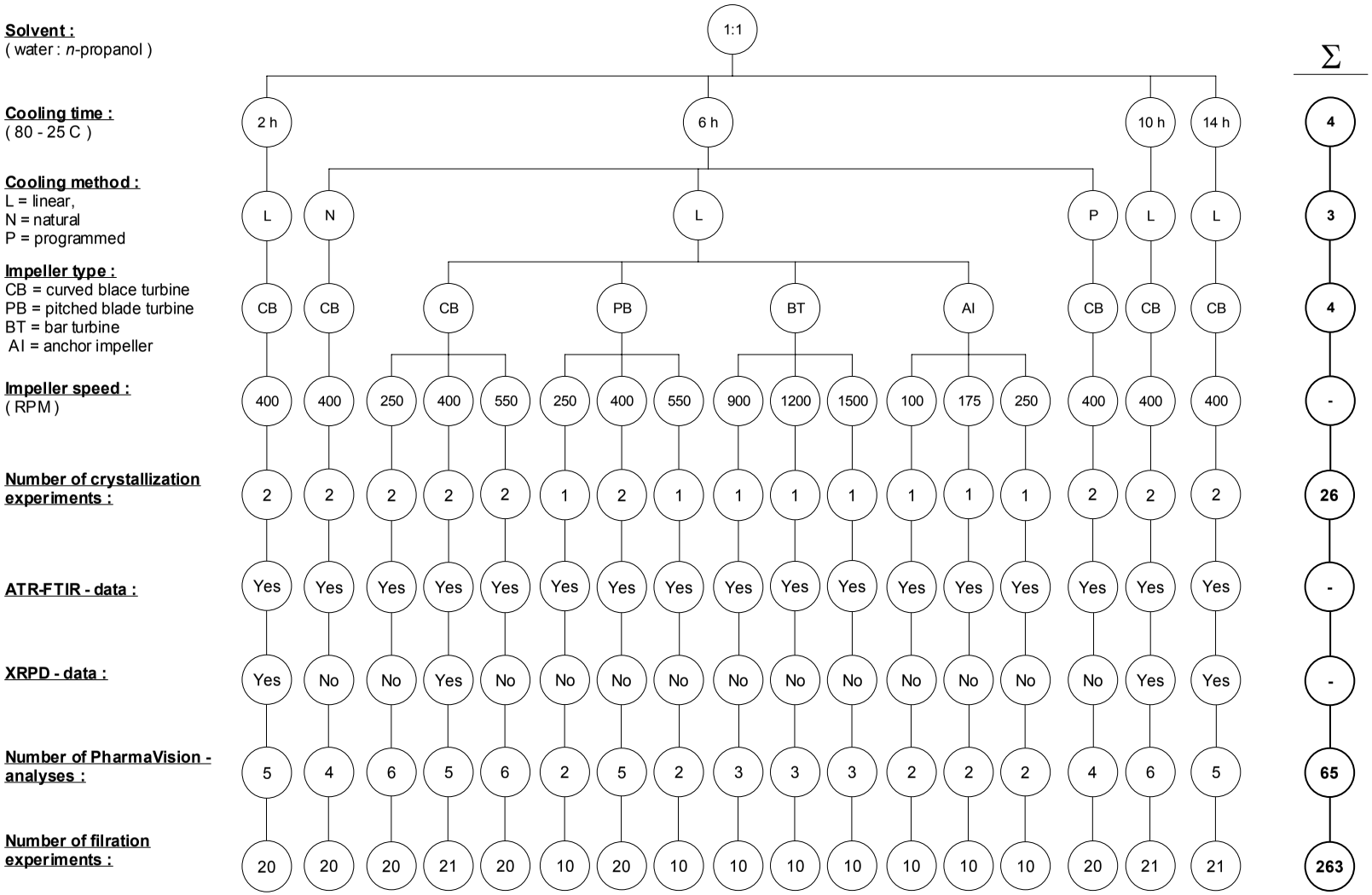
Solvent :
(water : n-propanol)
1:1
Σ
Cooling time :
(80 - 25 C)
2 h
6 h
10 h
14 h
4
Cooling method :
L = linear,
N = natural
P = programmed
L
N
L
P
L
L
3
Impeller type :
CB = curved blace turbine
PB = pitched blade turbine
BT = bar turbine
AI = anchor impeller
CB
CB
CB
PB
BT
AI
CB
CB
CB
4
Impeller speed :
(RPM)
400
400
250
400
550
250
400
550
900
1200
1500
100
175
250
400
400
400
-
Number of crystallization experiments :
2
2
2
2
2
1
2
1
1
1
1
1
1
1
2
2
2
26
ATR-FTIR - data :
Yes
Yes
Yes
Yes
Yes
Yes
Yes
Yes
Yes
Yes
Yes
Yes
Yes
Yes
Yes
Yes
Yes
-
XRPD - data :
Yes
No
No
Yes
No
No
No
No
No
No
No
No
No
No
No
Yes
Yes
-
Number of PharmaVision - analyses :
5
4
6
5
6
2
5
2
3
3
3
2
2
2
4
6
5
65
Number of filration experiments :
20
20
20
21
20
10
20
10
10
10
10
10
10
10
20
21
21
263

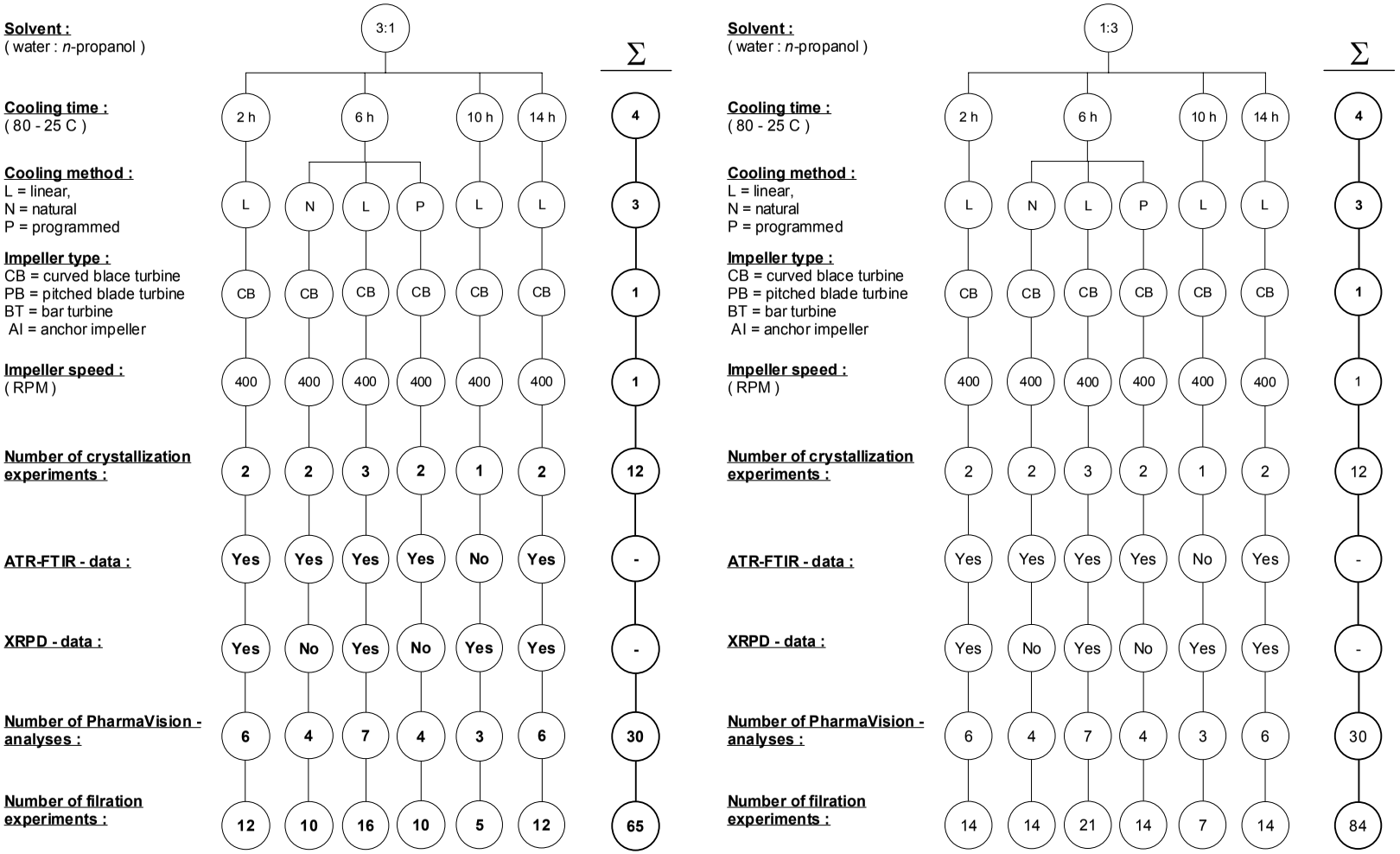
Solvent :
(water : n-propanol)
3:1
Σ
Cooling time :
(80 - 25 C)
2 h
6 h
10 h
14 h
4
Cooling method :
L = linear,
N = natural
P = programmed
L
N
L
P
L
L
3
Impeller type :
CB = curved blace turbine
PB = pitched blade turbine
BT = bar turbine
AI = anchor impeller
CB
1
Impeller speed :
(RPM)
400
1
Number of crystallization experiments :
2
2
3
2
1
2
12
ATR-FTIR - data :
Yes
No
-
XRPD - data :
Yes
No
-
Number of PharmaVision - analyses :
6
4
7
4
3
6
30
Number of filration experiments :
12
10
16
10
5
12
65
Solvent :
(water : n-propanol)
1:3
Σ
Cooling time :
(80 - 25 C)
2 h
6 h
10 h
14 h
4
Cooling method :
L = linear,
N = natural
P = programmed
L
N
L
P
L
L
3
Impeller type :
CB = curved blace turbine
PB = pitched blade turbine
BT = bar turbine
AI = anchor impeller
CB
1
Impeller speed :
(RPM)
400
1
Number of crystallization experiments :
2
2
3
2
1
2
12
ATR-FTIR - data :
Yes
No
-
XRPD - data :
Yes
No
-
Number of PharmaVision - analyses :
6
4
7
4
3
6
30
Number of filration experiments :
14
14
21
14
7
14
84

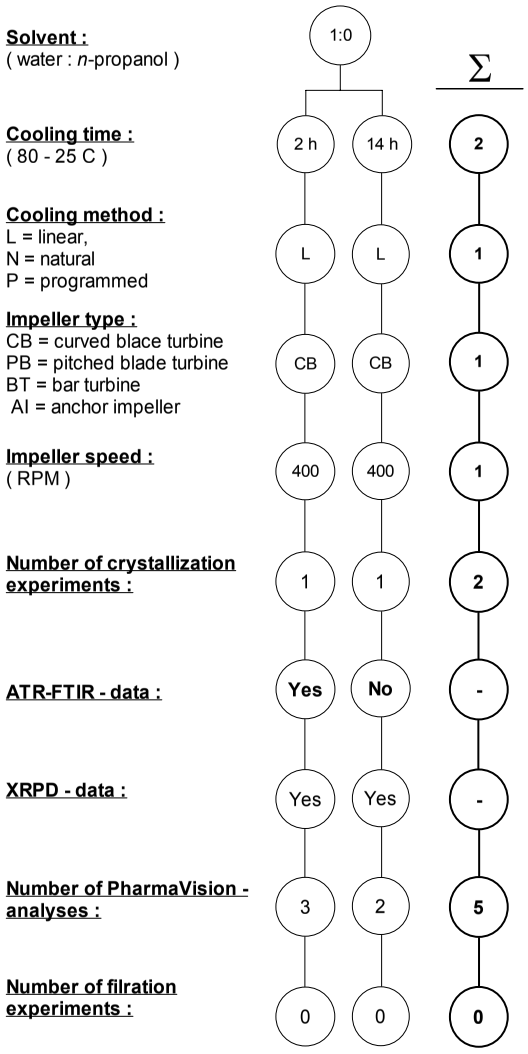
Solvent :
(water : n-propanol)
1:0
Σ
Cooling time :
(80 - 25 C)
2 h
14 h
2
Cooling method :
L = linear,
N = natural
P = programmed
L
L
1
Impeller type :
CB = curved blace turbine
PB = pitched blade turbine
BT = bar turbine
AI = anchor impeller
CB
CB
1
Impeller speed :
(RPM)
400
400
1
Number of crystallization experiments :
1
1
2
ATR-FTIR - data :
Yes
No
-
XRPD - data :
Yes
Yes
-
Number of PharmaVision - analyses :
3
2
5
Number of filration experiments :
0
0
0

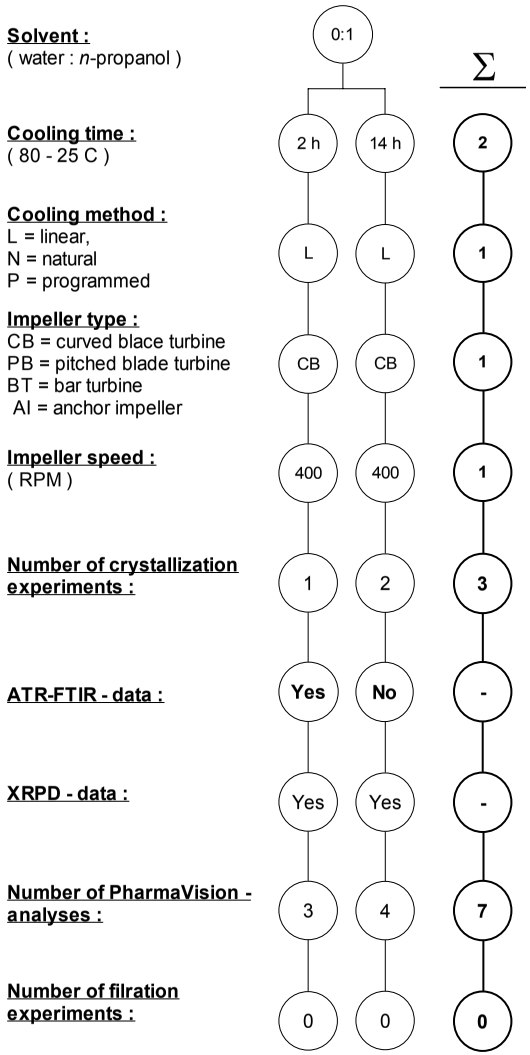
Solvent :
(water : n-propanol)
0:1
Σ
Cooling time :
(80 - 25 C)
2 h
14 h
2
Cooling method :
L = linear,
N = natural
P = programmed
L
L
1
Impeller type :
CB = curved blace turbine
PB = pitched blade turbine
BT = bar turbine
AI = anchor impeller
CB
CB
1
Impeller speed :
(RPM)
400
400
1
Number of crystallization experiments :
1
2
3
ATR-FTIR - data :
Yes
No
-
XRPD - data :
Yes
Yes
-
Number of PharmaVision - analyses :
3
4
7
Number of filration experiments :
0
0
0

ACTA UNIVERSITATIS LAPPEENRANTAENSIS

333. JAFARI, AREZOU. CFD simulation of complex phenomena containing suspensions and flow through porous media. 2008. Diss.

334. KOIVUNIEMI, JOUNI. Managing the front end of innovation in a networked company environment – Combining strategy, processes and systems of innovation. 2008. Diss.

335. KOSONEN, MIIA. Knowledge sharing in virtual communities. 2008. Diss.

336. NIEMI, PETRI. Improving the effectiveness of supply chain development work – an expert role perspective. 2008. Diss.

337. LEPISTÖ-JOHANSSON, PIIA. Making sense of women managers´ identities through the constructions of managerial career and gender. 2009. Diss.

338. HYRKÄS, ELINA. Osaamisen johtaminen Suomen kunnissa. 2009. Diss.

339. LAIHANEN, ANNA-LEENA. Ajopuusta asiantuntijaksi – luottamushenkilöarvioinnin merkitys kunnan johtamisessa ja päätöksenteossa. 2009. Diss.

340. KUKKURAINEN, PAAVO. Fuzzy subgroups, algebraic and topological points of view and complex analysis. 2009. Diss.

341. SÄRKIMÄKI, VILLE. Radio frequency measurement method for detecting bearing currents in induction motors. 2009. Diss.

342. SARANEN, JUHA. Enhancing the efficiency of freight transport by using simulation. 2009. Diss.

343. SALEEM, KASHIF. Essays on pricing of risk and international linkage of Russian stock market. 2009. Diss.

344. HUANG, JIEHUA. Managerial careers in the IT industry: Women in China and in Finland. 2009. Diss.

345. LAMPELA, HANNELE. Inter-organizational learning within and by innovation networks. 2009. Diss.

346. LUORANEN, MIKA. Methods for assessing the sustainability of integrated municipal waste management and energy supply systems. 2009. Diss.

347. KORKEALAAKSO, PASI. Real-time simulation of mobile and industrial machines using the multibody simulation approach. 2009. Diss.

348. UKKO, JUHANI. Managing through measurement: A framework for successful operative level performance measurement. 2009. Diss.

349. JUUTILAINEN, MATTI. Towards open access networks – prototyping with the Lappeenranta model. 2009. Diss.

350. LINTUKANGAS, KATRINA. Supplier relationship management capability in the firm´s global integration. 2009. Diss.

351. TAMPER, JUHA. Water circulations for effective bleaching of high-brightness mechanical pulps. 2009. Diss.

352. JAATINEN, AHTI. Performance improvement of centrifugal compressor stage with pinched geometry or vaned diffuser. 2009. Diss.

353. KOHONEN, JARNO. Advanced chemometric methods: applicability on industrial data. 2009. Diss.

354. DZHANKHOTOV, VALENTIN. Hybrid LC filter for power electronic drivers: theory and implementation. 2009. Diss.

355. ANI, ELISABETA-CRISTINA. Minimization of the experimental workload for the prediction of pollutants propagation in rivers. Mathematical modelling and knowledge re-use. 2009. Diss.

356. RÖYTTÄ, PEKKA. Study of a vapor-compression air-conditioning system for jetliners. 2009. Diss.

357. KÄRKI, TIMO. Factors affecting the usability of aspen (Populus tremula) wood dried at different temperature levels. 2009. Diss.

358. ALKKIOMÄKI, OLLI. Sensor fusion of proprioception, force and vision in estimation and robot control. 2009. Diss.

359. MATIKAINEN, MARKO. Development of beam and plate finite elements based on the absolute nodal coordinate formulation. 2009. Diss.

360. SIROLA, KATRI. Chelating adsorbents in purification of hydrometallurgical solutions. 2009. Diss.

361. HESAMPOUR, MEHRDAD. Treatment of oily wastewater by ultrafiltration: The effect of different operating and solution conditions. 2009. Diss.

362. SALKINOJA, HEIKKI. Optimizing of intelligence level in welding. 2009. Diss.

363. RÖNKKÖNEN, JANI. Continuous multimodal global optimization with differential evolution-based methods. 2009. Diss.

364. LINDQVIST, ANTTI. Engendering group support based foresight for capital intensive manufacturing industries – Case paper and steel industry scenarios by 2018. 2009. Diss.

365. POLESE, GIOVANNI. The detector control systems for the CMS resistive plate chamber at LHC. 2009. Diss.

366. KALENOVA, DIANA. Color and spectral image assessment using novel quality and fidelity techniques. 2009. Diss.

367. JALKALA, ANNE. Customer reference marketing in a business-to-business context. 2009. Diss.

368. HANNOLA, LEA. Challenges and means for the front end activities of software development. 2009. Diss.

369. PÄTÄRI, SATU. On value creation at an industrial intersection – Bioenergy in the forest and energy sectors. 2009. Diss.

370. HENTTONEN, KAISA. The effects of social networks on work-team effectiveness. 2009. Diss.

371. LASSILA, JUKKA. Strategic development of electricity distribution networks – Concept and methods. 2009. Diss.

372. PAAKKUNAINEN, MAARET. Sampling in chemical analysis. 2009. Diss.

373. LISUNOV, KONSTANTIN. Magnetic and transport properties of II-V diluted magnetic semiconductors doped with manganese and nickel. 2009. Diss.

374. JUSSILA, HANNE. Concentrated winding multiphase permanent magnet machine design and electromagnetic properties – Case axial flux machine. 2009. Diss.